AIIM

Association for Information and Image Management

1100 Wayne Avenue, Suite 1100
Silver Spring, Maryland 20910

301/587-8202

Centimeter

Inches

MANUFACTURED TO AIIM STANDARDS
BY APPLIED IMAGE, INC.

1 of 1

101/381-94JS(2)

SANDIA REPORT

SAND93—2275 • UC—523
Unlimited Release
Printed January 1994

VICTORIA-92 Pretest Analyses of PHEBUS-FPTO

N. E. Bixler, C. M. Erickson

Prepared by
Sandia National Laboratories
Albuquerque, New Mexico 87185 and Livermore, California 94550
for the United States Department of Energy
under Contract DE-AC04-94AL85000

DISTRIBUTION OF THIS DOCUMENT IS UNLIMITED

SF2900Q(8-81)

Issued by Sandia National Laboratories, operated for the United States Department of Energy by Sandia Corporation.

NOTICE: This report was prepared as an account of work sponsored by an agency of the United States Government. Neither the United States Government nor any agency thereof, nor any of their employees, nor any of their contractors, subcontractors, or their employees, makes any warranty, express or implied, or assumes any legal liability or responsibility for the accuracy, completeness, or usefulness of any information, apparatus, product, or process disclosed, or represents that its use would not infringe privately owned rights. Reference herein to any specific commercial product, process, or service by trade name, trademark, manufacturer, or otherwise, does not necessarily constitute or imply its endorsement, recommendation, or favoring by the United States Government, any agency thereof or any of their contractors or subcontractors. The views and opinions expressed herein do not necessarily state or reflect those of the United States Government, any agency thereof or any of their contractors.

Printed in the United States of America. This report has been reproduced directly from the best available copy.

Available to DOE and DOE contractors from
Office of Scientific and Technical Information
PO Box 62
Oak Ridge, TN 37831

Prices available from (615) 576-8401, FTS 626-8401

Available to the public from
National Technical Information Service
US Department of Commerce
5285 Port Royal Rd
Springfield, VA 22161

NTIS price codes
Printed copy: A04
Microfiche copy: A01

SAND93-2275
Unlimited Release
Printed January 1994

Distribution
Category UC-523

VICTORIA-92 Pretest Analyses of PHEBUS-FPT0

N. E. Bixler and C. M. Erickson
Severe Accident Phenomenology Department
Sandia National Laboratories
Albuquerque, New Mexico 87185-1137

Abstract

FPT0 is the first of six tests that are scheduled to be conducted in an experimental reactor in Cadarache, France. The test apparatus consists of an in-pile fuel bundle, an upper plenum, a hot leg, a steam generator, a cold leg, and a small containment. Thus, the test is integral in the sense that it attempts to simulate all of the processes that would be operative in a severe nuclear accident. In FPT0, the fuel will be trace irradiated; in subsequent tests high burn-up fuel will be used.

Separate pretest analyses of the FPT0 fuel bundle and primary circuit have been conducted using the USNRC's source term code, VICTORIA-92. Predictions for release of fission product, control rod, and structural elements from the test section are compared with those given by CORSOR-M. In general, the releases predicted by VICTORIA-92 occur earlier than those predicted by CORSOR-M. The other notable difference is that U release is predicted to be on a par with that of the control rod elements; CORSOR-M predicts U release to be about 2 orders of magnitude greater.

Predictions for the primary circuit indicate the size distribution of aerosols, deposition profiles and mechanisms, speciation of deposits, speciation of the bulk gases, and species that are delivered to containment. Retention of the condensable elements is in the range of 32% to 51%. Elements forming less volatile species tend to be retained in larger fraction than those forming more volatile species. The VICTORIA-92 predictions should be useful for guidance in on-line aerosol monitoring and in post-test chemical analyses.

Predictions indicate that revaporization should be important in FPT0. Volatile fission products continue to flow into containment long after the reactor has been shut down. The opportunity should not be missed to monitor this behavior; the PHEBUS test series offers a rare opportunity to observe revaporization where there is a prototypical mixture of elements.

Predictions of speciation in the colder portion of the FPT0 primary circuit, from the steam generator to the exit to containment, are suspect because of the assumption of thermodynamic equilibrium that is made in VICTORIA-92. In reality, chemical kinetics are limiting when temperatures fall below about 800 K, as they do in the steam generator of the FPT0 test. A "frozen chemistry" model would be a good approximation for gases that are rapidly quenched below this temperature. Such a model is slated for development in 1994, but is currently unavailable in VICTORIA-92.

DISTRIBUTION OF THIS DOCUMENT IS UNLIMITED

MASTER

Contents

		Page
Figures		vi
Tables		viii
Acknowledgments		ix
1.0	Introduction	1
1.1	VICTORIA-92	1
1.2	PHEBUS-FPT0	1
1.3	VICTORIA-92 Pretest Analyses of FPT0	1
2.0	Application of VICTORIA-92 to PHEBUS-FPT0	3
2.1	VICTORIA-92 Input for the FPT0 Fuel Bundle	3
2.2	VICTORIA-92 Input for the FPT0 Primary Circuit	5
3.0	Predictions for the FPT0 Fuel Bundle	14
4.0	Predictions for the FPT0 Primary Circuit	18
5.0	Conclusions	50
5.1	FPT0 Fuel Bundle	50
5.2	FPT0 Primary Circuit	50
6.0	References	52

Figures

Page

1. Schematic of the PHEBUS-FPT0 test configuration. 2
2. VICTORIA representation of the FPT0 fuel bundle. 4
3. Fuel temperature histories for cells 1 through 5. 6
4. Fuel temperature histories for cells 6 through 10. 6
5. Gas temperature histories for cells 1 through 6. 7
6. Gas temperature histories for cells 7 through 12. 7
7. Structure temperature histories for cells 1 through 6. 8
8. Structure temperature histories for cells 7 through 12. 8
9. Gas velocity histories for cells 1 through 6. 9
10. Gas velocity histories for cells 7 through 12. 9
11. VICTORIA-92 representation of the PHEBUS FPT0 circuit. 10
12. Gas temperatures in the FPT0 circuit for cells 1 through 7. 12
13. Gas temperatures in the FPT0 circuit for cells 13 through 19. 12
14. Structure temperatures in the FPT0 circuit for cells 1 through 5. 13
15. Inflow velocity for cell 1 of the FPT0 primary circuit. 13
16. Fractional release into the primary circuit for the volatile elements, Xe, Kr, I, Te, and Cs. 16
17. Fractional release into the primary circuit for Ba, Sr, and U. 16
18. Fractional release into the primary circuit for control rod and cladding elements, Ag, In, Cd, and Sn. 17
19. Locations and dominant mechanisms of aerosol deposition in the FPT0 primary circuit. 19
20. Aerosol mass mean diameter in the FPT0 primary circuit. 20
21. Aerosol standard deviation in the FPT0 primary circuit. 20
22. Aerosol mass concentration histories in the FPT0 circuit. 21
23. Aerosol particle concentration histories in the FPT0 circuit. 21
24. Hydrogen to steam ratio histories in the FPT0 circuit. 22
25. Iodine species at the inlet of the FPT0 circuit. 22
26. Iodine species at point C in the FPT0 circuit. 23
27. Iodine species at the steam generator in the FPT0 circuit. 23
28. Iodine species at point G in the FPT0 circuit. 24
29. Iodine species at the exit of the FPT0 circuit. 24
30. Cesium species at the inlet of the FPT0 circuit. 26
31. Cesium species at point C in the FPT0 circuit. 26
32. Cesium species at the steam generator in the FPT0 circuit. 27
33. Cesium species at point G in the FPT0 circuit. 27
34. Cesium species at the exit of the FPT0 circuit. 28
35. Tellurium species at the inlet of the FPT0 circuit. 28
36. Tellurium species at the point C in the FPT0 circuit. 29
37. Tellurium species at the steam generator in the FPT0 circuit. 29
38. Tellurium species at point G in the FPT0 circuit. 30
39. Tellurium species at the exit of the FPT0 circuit. 30
40. Total surface layer deposit density histories in the FPT0 circuit. 31
41. I surface deposit densities at the inlet of the FPT0 circuit. 31
42. I surface deposit densities at point C in the FPT0 circuit. 32
43. I surface deposit densities at the steam generator in the FPT0 circuit. 32
44. I surface deposit densities at point G in the FPT0 circuit. 33
45. I surface deposit densities at the exit of the FPT0 circuit. 33
46. Cs surface deposit densities at the inlet of the FPT0 circuit. 34
47. Cs surface deposit densities at point C in the FPT0 circuit. 34
48. Cs surface deposit densities at the steam generator in the FPT0 circuit. 35
49. Cs surface deposit densities at point G in the FPT0 circuit. 35

Figures

Page

50. Cs surface deposit densities at the exit of the FPT0 circuit. 36
51. Te surface deposit densities at the inlet of the FPT0 circuit. 36
52. Te surface deposit densities at point C in the FPT0 circuit. 37
53. Te surface deposit densities at the steam generator in the FPT0 circuit. 37
54. Te surface deposit densities at point G in the FPT0 circuit. 38
55. Te surface deposit densities at the exit of the FPT0 circuit. 38
56. U surface deposit densities at the inlet of the FPT0 circuit. 39
57. U surface deposit densities at point C in the FPT0 circuit. 39
58. U surface deposit densities at the steam generator in the FPT0 circuit. 40
59. U surface deposit densities at point G in the FPT0 circuit. 40
60. U surface deposit densities at the exit of the FPT0 circuit. 41
61. Ag surface deposit densities at the inlet of the FPT0 circuit. 41
62. Ag surface deposit densities at point C in the FPT0 circuit. 42
63. Ag surface deposit densities at the steam generator in the FPT0 circuit. 42
64. Ag surface deposit densities at point G in the FPT0 circuit. 43
65. Ag surface deposit densities at the exit of the FPT0 circuit. 43
66. In surface deposit densities at the inlet of the FPT0 circuit. 44
67. In surface deposit densities at point C in the FPT0 circuit. 44
68. In surface deposit densities at the steam generator in the FPT0 circuit. 45
69. In surface deposit densities at point G in the FPT0 circuit. 45
70. In surface deposit densities at the exit of the FPT0 circuit. 46
71. Cd surface deposit densities at the inlet of the FPT0 circuit. 46
72. Cd surface deposit densities at point C in the FPT0 circuit. 48
73. Cd surface deposit densities at the steam generator in the FPT0 circuit. 48
74. Cd surface deposit densities at point G in the FPT0 circuit. 49
75. Cd surface deposit densities at the exit of the FPT0 circuit. 49

Tables

Page

1. Initial Fission Product Inventory (g-mol/m^3) 3
2. Cell Radii and Heights Used to Represent the FPT0 Primary Circuit 5
3. Floor, Wall, and Ceiling Areas in Each Cell (cm^2) 11
4. Integral Releases Predicted by VICTORIA and CORSOR-M 15
5. Summary of Retention in and Release from the FPT0 Primary Circuit 47

Acknowledgments

The authors wish to thank D. A. Powers and T. J. Heames for their helpful comments. Thanks also go to the United States Nuclear Regulatory Commission for their support of this work through FIN A1837.

1.0 Introduction

1.1 VICTORIA-92

The consequences of a severe nuclear reactor accident depend on the quantity, characteristics, and timing of the release of radionuclides from the containment, which is often referred to as the source term. The behavior of the radionuclides within the reactor coolant system (RCS) will have a significant effect on determining the quantity of radionuclides within the containment during an accident, and thus on the potential release into the atmosphere. VICTORIA-92 [1] is a mechanistic code for predicting fission product release from fuel, chemical speciation and interactions, aerosol physics, transport, and decay heating within the RCS under severe accident conditions.

VICTORIA-92 follows the evolution of 26 elements, including those from fuel and control rods, major RCS materials, and the coolant, as they interact under the influence of varying temperatures, pressures, and velocities. Local chemical equilibrium is assumed for the 288 chemical species in the database. Species that reach the coolant channel may condense onto structural surfaces or form aerosols that grow and agglomerate, which may in turn deposit onto structural surfaces, reheat, revaporize, resuspend, or chemically interact with other materials on the surface.

1.2 PHEBUS-FPT0

PHEBUS is an experimental reactor located in Cadarache, France. A series of six tests, the FPT series, is scheduled to be conducted there. The first test, FPT0, was run in December, 1993.

The FPT tests are integral in nature, i.e., they attempt to represent all of the processes that would take place during a severe nuclear accident. A schematic of the apparatus to be used in FPT0 is shown in Figure 1. It consists of an in-pile fuel bundle containing 20 fuel rods and 1 control rod, an upper plenum, a hot leg, a steam generator tube, a cold leg, and a containment vessel. In FPT0, the fuel will be trace irradiated; current plans are to perform subsequent FPT tests with high burn-up fuel.

Ideally, the experimental data from PHEBUS should contain enough information to construct a complete mass balance as a function of time. This would require detailed data on the transient release of fission products from the fuel, of transport into the containment, and of accumulation along the length of the test section. Such data, if it were possible to obtain, would allow VICTORIA, which does produce a complete mass balance of the initial fuel inventory, to be validated with the confidence that any disagreement between prediction and measurement was due to the code itself. Obviously, it is not possible to measure a complete and accurate mass balance with available instrumentation and techniques. However, the goal should be to quantify the inflow, outflow and deposition of fission products in the test section as accurately as possible. These measurements should capture the transient nature of the deposition as well as the spatial distribution. Furthermore, they should capture differences between interactions with Inconel and with the stainless steel liner that is to reside in a portion of the primary circuit. These types of data will generally be useful for validating VICTORIA.

1.3 VICTORIA-92 Pretest Analyses of FPT0

VICTORIA-92 [1] analyses of PHEBUS-FPT0 were performed in two parts: (1) the fuel bundle and a portion of the upper plenum and (2) the upper plenum and primary circuit leading to containment. The reasons for the subdivision of the domain were as follows: (1) to allow comparisons with CORSOR-M calculations on fission product releases from the fuel bundle; (2) to diminish the CPU time required for the individual calculations; and (3) allow sensitivity studies to be conducted separately on the two subdomains. The separate results of these two analyses are presented in Sections 3.0 and 4.0. Section 2.0 describes the modeling details used in the two analyses.

The analyses reported here are pre-test: no experimental data were available at the time these analyses were conducted. This work is the first part of an ongoing participation in the PHEBUS program.

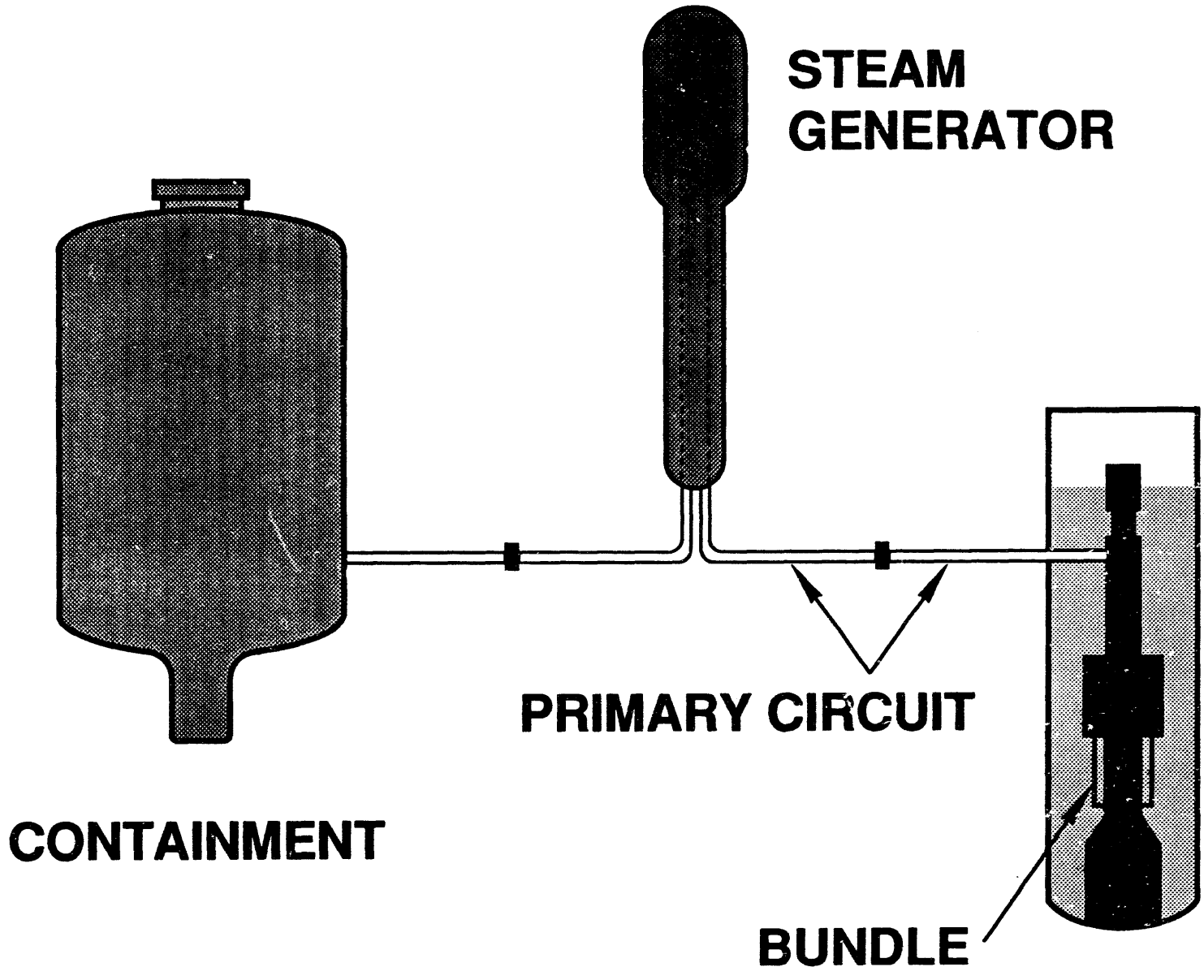

Figure 1. Schematic of the PHEBUS-FPT0 test configuration.

2.0 Application of VICTORIA-92 to PHEBUS-FPT0

As described in Section 1.0, VICTORIA-92 analyses of FPT0 were performed separately on the fuel bundle and on the primary circuit. Both input decks are modifications of ones provided by Y. Drossinos at ISPRA [2,3]. Because the input parameters needed to specify the fuel bundle region are somewhat different than those to specify the circuit, they are described separately in the following two subsections.

2.1 VICTORIA-92 Input for the FPT0 Fuel Bundle

The input data for the fuel bundle calculations are discussed in the order that they occur in the input deck.

The VICTORIA representation of the fuel bundle is shown schematically in Figure 2. The bottom 10 cells (fueled) are each 3.65 cm in radius and 10 cm high. The top two cells (unfueled) were each chosen to be a full meter in height. This choice was made to ensure that thermodynamic equilibrium would be established by the time the gas reached the outlet. Making these heights artificially large should not have significantly affected the predictions of fission product release.

Input was chosen so that no chemistry was performed within fuel grains but interactions between fission products and UO_2 at the fuel grain surface were modeled. This option was chosen because it gave the best agreement with HI, VI, and ACRR ST data in another study [4].

Data for the fuel were chosen as follows. The pellet diameter, gap thickness, cladding thickness, helium fill pressure, and fraction of theoretical density were 8.19 mm, 85 microns, 0.57 mm, 28 bars, and 0.9582, respectively. Each fueled cell contained 20 fuel rods. Permeabilities were chosen based on simple estimates to be 10^{-14} m^2 in the fuel pellets and 10^{-12} m^2 in the gap, clad, and fuel film.

The initial fission product inventory in the stoichiometric UO_2 fuel is given in Table 1. Grain diameters were taken, in the absence of any data, to be 10 microns. No sensitivity calculations were conducted to determine the effect of grain size on releases. Varying this parameter would have affected release rates more than integral release fractions. Diffusion coefficients for each of the fission products were represented by the expression

$$D = 5 \times 10^{-5} e^{-50000/T}. \qquad (1)$$

where T is the local temperature in K and D is in units of m^2/s. The coefficients are ones recommended by Matzke [5].

One control rod was present in the bottom 10 cells. The alloy diameter, alloy length, inner and outer diameter of the stainless steel cladding, and rod length were 8.66 mm, 1 m, 8.7 mm, 9.7 mm, and 1.1 m, respectively. The alloy molar composition was 80% Ag, 15% In, and 5% Cd. The He fill pressure was 4 bars.

The settling flags were all set to -1.0 to allow downward, inter-cell, gravitational settling. Axial flow areas were set to 27.7 cm^2 for the fueled cells and to 41.9 cm^2 for the unfueled cells; radial flow areas were all set to 0. Hydraulic diameters were set to 1.34 cm for the fueled cells and to 7.30 cm for the unfueled cells. Cell floor areas for aerosol settling were chosen to be 10^{-6} m^2 for the bottom cell, 0.0 for the others; wall areas were chosen to be 229 cm^2 for the fueled cells and to be 91.7 cm^2 for the unfueled cells; ceiling areas were chosen to be 0.0 for all cells. Structural materials were chosen to be inert in all the cells to represent the ZrO_2 sheath.

Twelve mass bins were used to represent the aerosol size distributions. In VICTORIA-92, each mass bin represents all of the aerosol particles whose individual

Table 1: Initial Fission Product Inventory (g-mol/m^3)

Element	Cs	Ba	I	Sr	Zr	Sn	Te	Kr	Xe	Mo	Ru	Sb	Eu
Concentration	1.027	1.027	0.269	1.225	2.920	0.020	0.352	0.372	2.465	1.822	1.423	0.010	0.019

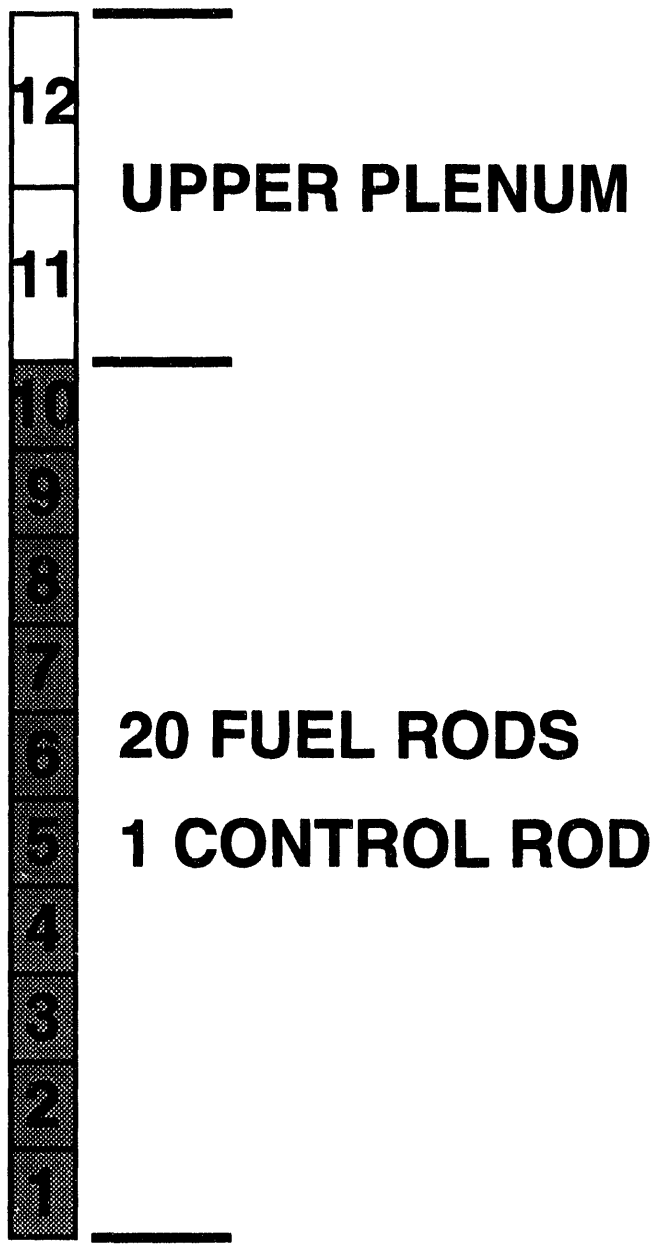

Figure 2. VICTORIA representation of the FPT0 fuel bundle.

masses are approximated by the mass corresponding to that bin. In this calculation, the mass bins ranged from 10^{-21} to 10^{-10} kg by decade. The parameters affecting aerosol physics and numerics were chosen to be the usual values used in most VICTORIA-92 calculations [1].

Because the gas velocities were relatively large and the cell lengths relatively small in this calculation, the time steps had to be kept small. The time step chosen was 0.1 s. Even this choice resulted in the Courant condition being exceeded by almost a factor of 10 in the fueled (shorter) cells. The top cells were chosen to be artificially large so that the Courant condition would be slightly less than unity there. This allowed equilibrium thermodynamics to be reached before the gas exited from the domain. Calculations were run from 10,000 to 18,000 s. However, in FPT0 the reactor will be shut down at 16,000 s (see Figures 3 and 4), so negligible release occurs after this time. Thus, most of the results for the fuel bundle are shown from 10,000 to 16,000 s.

Thermal-hydraulic input for the fuel bundle were taken from calculations done by Shepherd et al. using the code, CATHARE [2]. Fuel centerline, fuel perimeter, and cladding temperatures were prescribed to be the same in a given cell. The temperature histories for the fuel in each of the fueled cells are shown in Figures 3 and 4; gas temperature histories are shown in Figures 5 and 6; structure temperatures are shown in Figures 7 and 8; gas pressures were chosen to be uniformly 2.2 bars; and axial velocities are shown in Figures 9 and 10. Radial velocities were all set to 0. The mass rate of steam into the bottom cell was held at 3 g/s until 12,000 s, ramped down to 1.5 g/s between 12,000 and 14,000 s, then held at that value for the remainder of the calculation.

2.2 VICTORIA-92 Input for the FPT0 Primary Circuit

The VICTORIA-92 representation of the FPT0 primary circuit is shown schematically in Figure 11. (The containment is on the right side in this figure; whereas, it is on the left side in Figure 1.) Cell radii and lengths are given in Table 2. The cells with 90° bends shown in Figure 11 were treated by using the standard bend deposition model in VICTORIA-92 [1]. Downward inter-cell settling was modeled in each of the vertically oriented cells. Points C and G, shown in Figure 11, are referenced in Section 4.0.

Axial flow areas were chosen to be the cross sectional areas of each cell; radial flow areas were chosen to be 0. Each hydraulic diameter was chosen to be the true diameter of the cell. Floor, ceiling, and wall areas were set as shown in Table 3. The structural material in the first cell was taken to be inert (ZrO_2); the structural material in each of the other cells was taken to be oxidized inconel.

Ten aerosol mass bins were used, which represented particles ranging from 10^{-21} to 10^{-9} kg. This range was chosen to be smaller than normal because of the relatively low fission product source rates in FPT0. Other parameters affecting aerosol physics and numerics were chosen to be the normal values used in most VICTORIA-92 calculations.

Calculations were run from 10,000 to 18,000 s using 0.1 s time steps. The Courant limit for this calculation is about 0.01 s. CPU requirements would have been pro-

Table 2: Cell Radii and Heights Used to Represent the FPT0 Primary Circuit

Cell	1	2	3	4	5	6	7	8	9	10	11	12	13	14	15
R (cm)	3.65	3.05	2.40	1.97	1.50	1.50	1.50	2.04	1.80	1.50	1.50	1.50	1.26	1.00	1.00
H (cm)	13.7	9.80	78.5	7.00	222.	11.8	513.	76.1	3.00	298.	13.1	4.00	3.55	148.	148.

Cell	16	17	18	19	20	21	22	23	24	25	26	27	28	29	30
R (cm)	1.00	1.00	1.00	1.00	1.26	1.50	1.50	1.50	1.50	1.50	1.50	1.50	1.50	1.50	1.50
H (cm)	148.	15.7	15.7	443.	3.50	15.8	31.4	159.	19.2	91.7	31.4	25.0	31.4	85.0	31.4

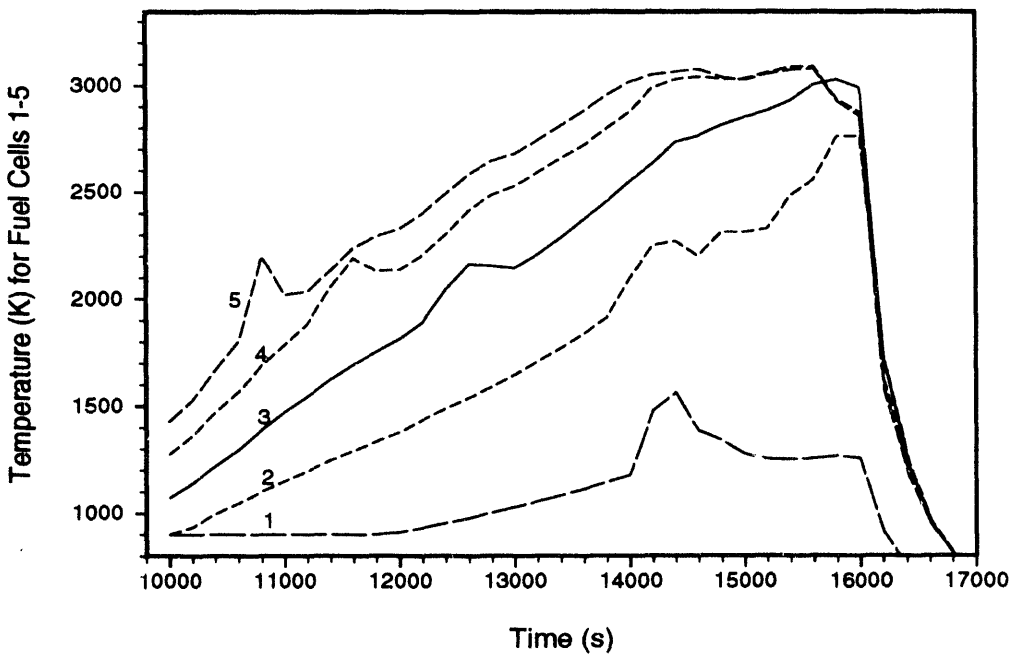

Figure 3. Fuel temperature histories for cells 1 through 5.

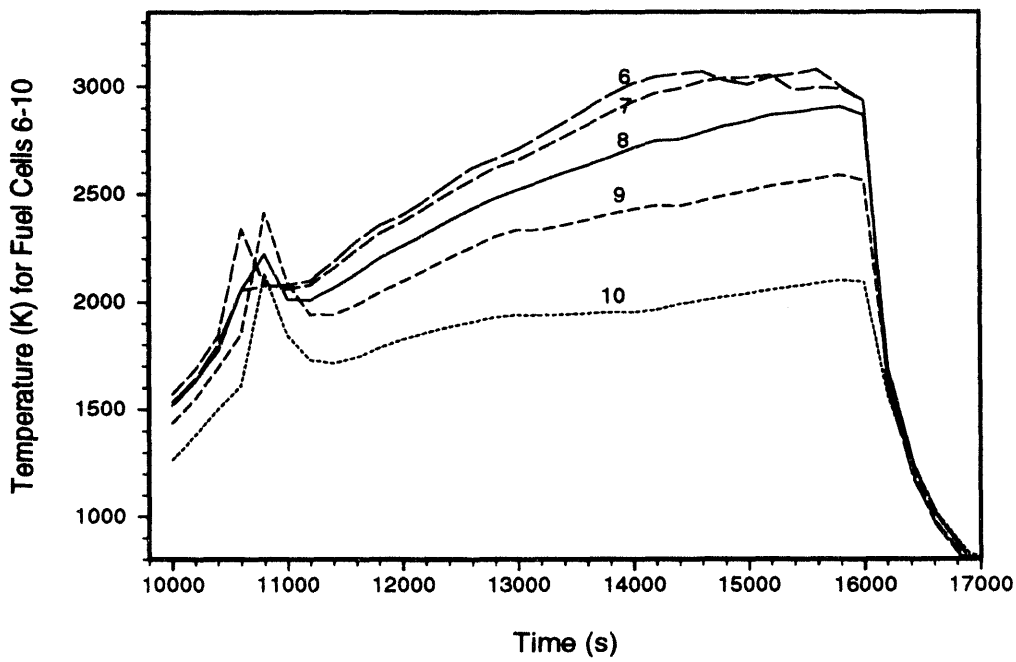

Figure 4. Fuel temperature histories for cells 6 through 10.

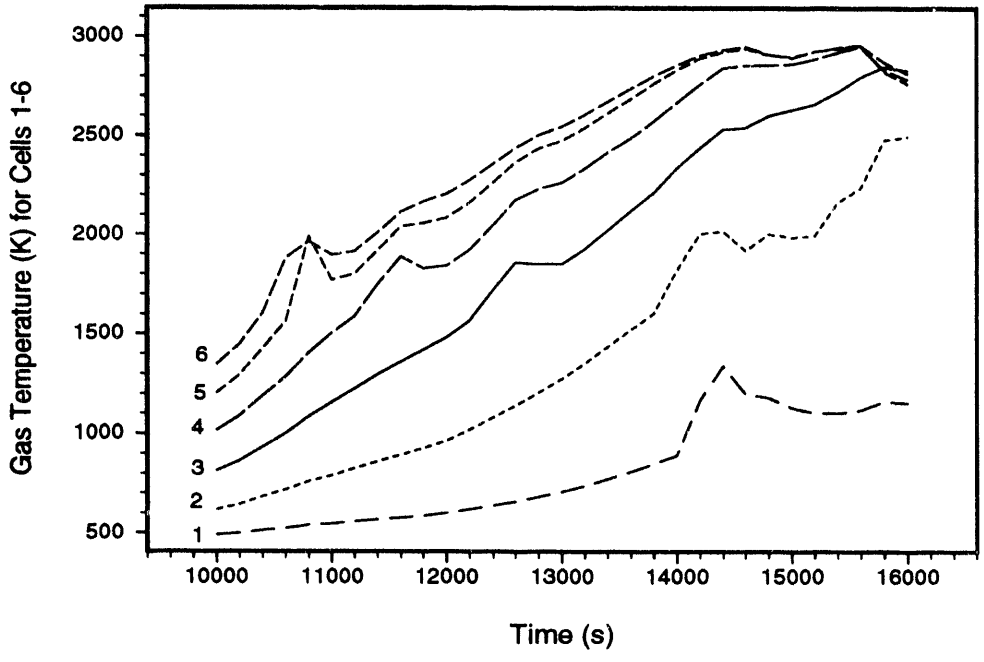

Figure 5. Gas temperature histories for cells 1 through 6.

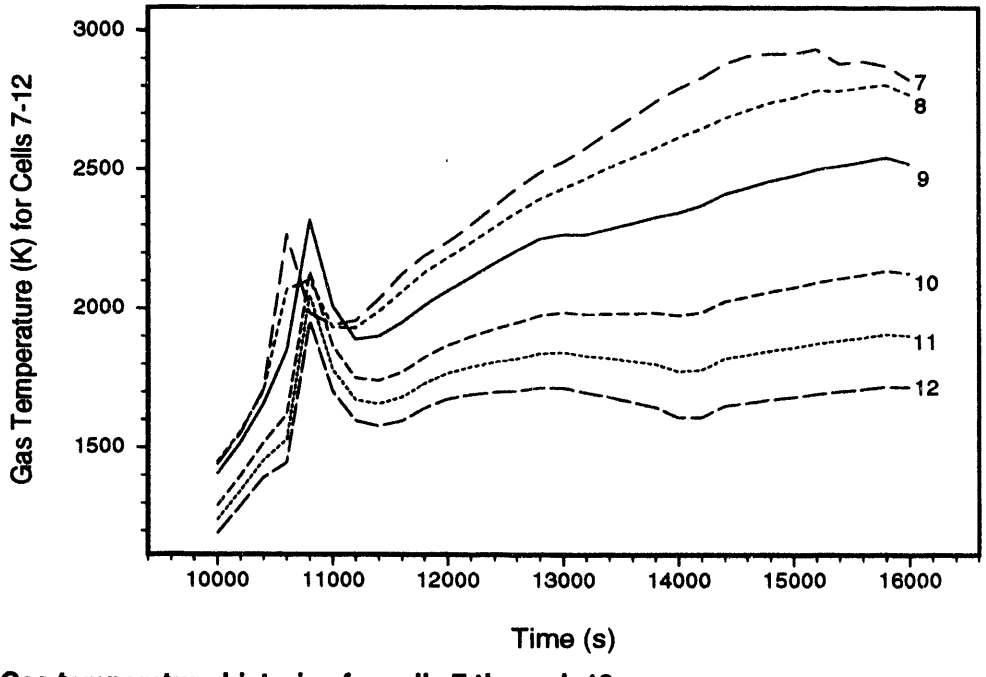

Figure 6. Gas temperature histories for cells 7 through 12.

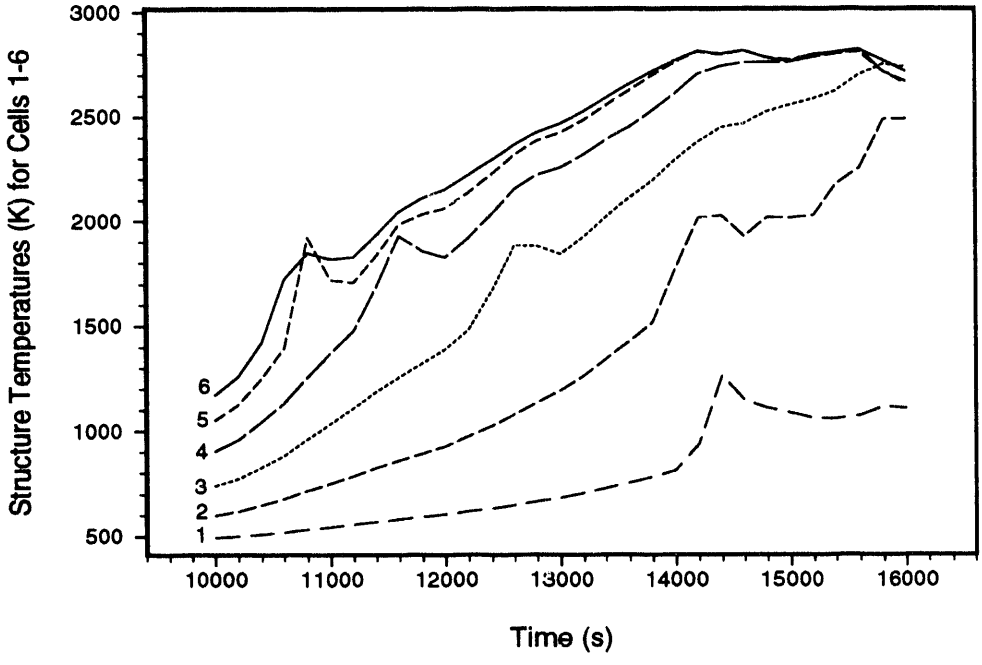

Figure 7. Structure temperature histories for cells 1 through 6.

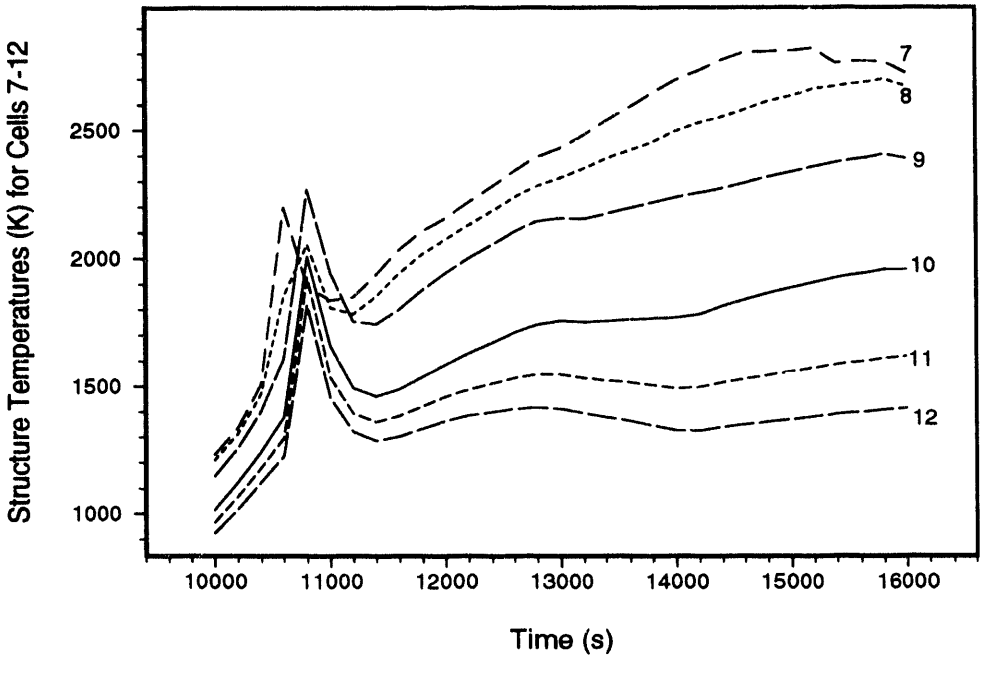

Figure 8. Structure temperature histories for cells 7 through 12.

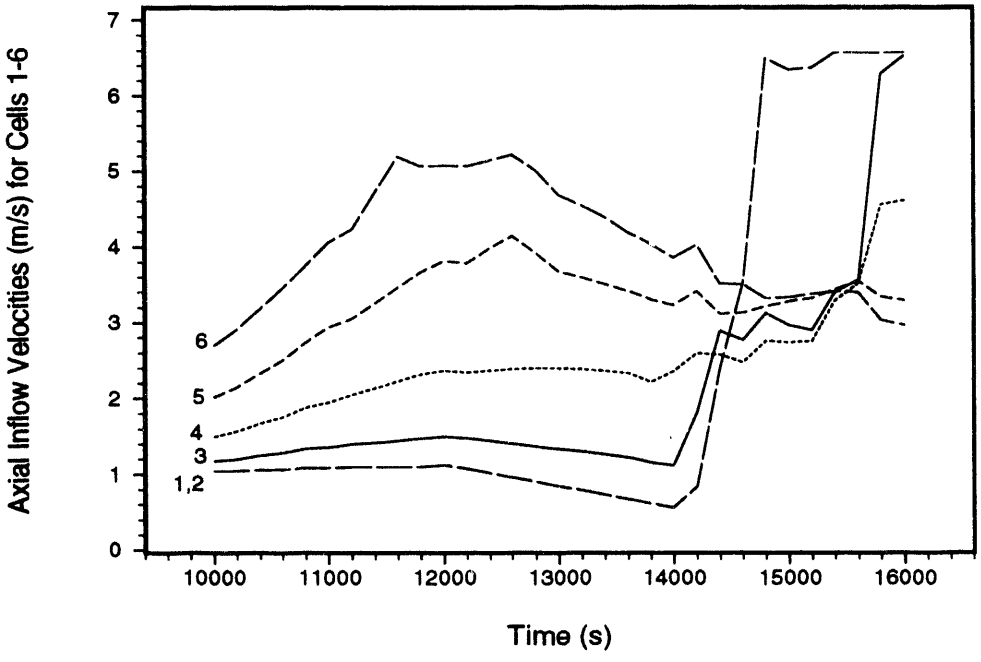

Figure 9. Gas velocity histories for cells 1 through 6.

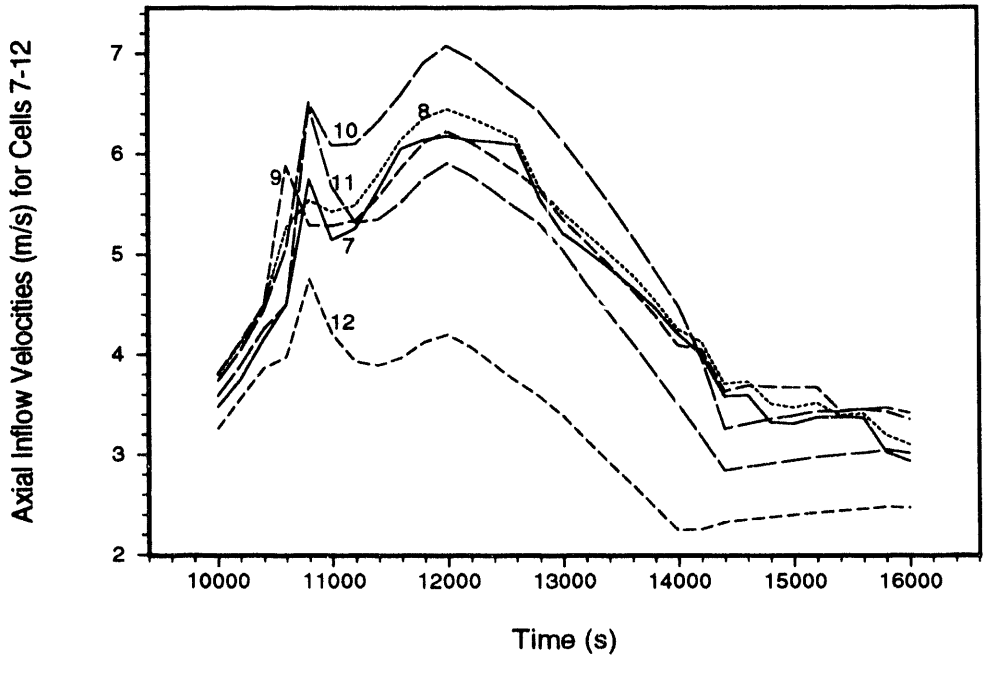

Figure 10. Gas velocity histories for cells 7 through 12.

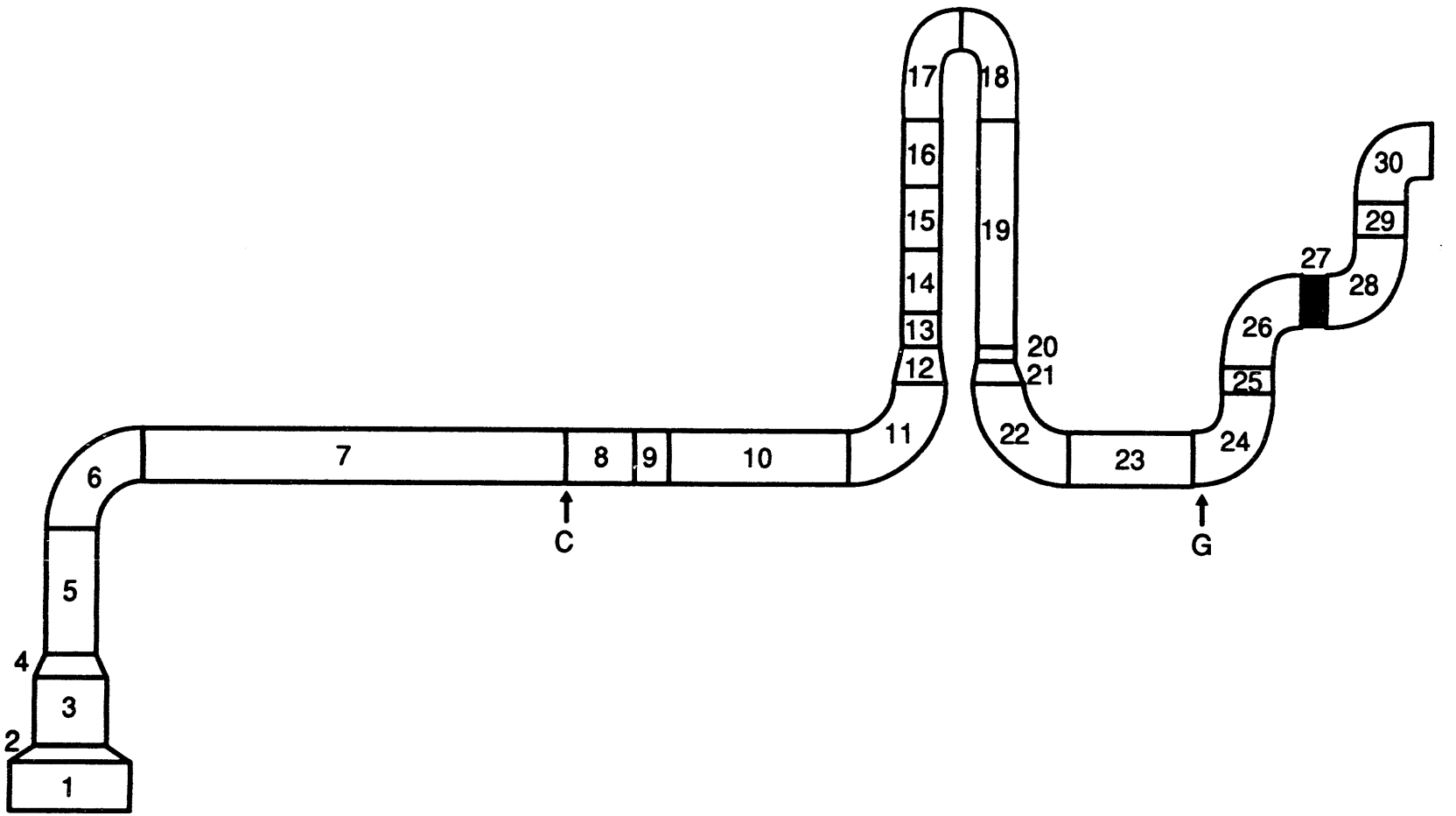

Figure 11. VICTORIA-92 representation of the PHEBUS FPT0 circuit.

hibitive if the Courant limit had been adhered to. Instead, tests were done to show that the results did not change appreciably if 0.1 s time steps were used instead of 0.01 s time steps [6].

Calculations made with the French code CATHARE [3] were used as the basis for the thermal-hydraulic input needed by VICTORIA-92. The data are summarized in the following paragraphs.

The thermal histories for the gas in cells 1 through 7 are shown in Figure 12. The temperatures for cells 8 through 12 were held uniformly at 973. K. The thermal histories for the gas in cells 13 through 19 are shown in Figure 13. The temperatures for cells 20 through 30 were held uniformly at 423. K.

The structural surfaces in cells 1 through 5 are shown in Figure 14. The surface temperatures for cells 6 through 30 are to be regulated in the FPT0 test and so were calculated to be nearly constant over the FPT0 test. The values used in the VICTORIA-92 analysis were as follows: the surface temperatures for cells 6 through 12 were held uniformly at 973 K; cell 13 was held at about 681 K; cell 14 was held at about 425 K; cell 15 was held at about 424 K; and cells 16 through 30 were held uniformly at 423 K.

Gas pressures varied slightly during the calculation; they were nearly uniform at 2.2 bars. The lowest pressure was 2.199 bars and the greatest was 2.210 bars.

Radial flow velocities were uniformly zero for the entire transient. Axial flow velocities were spatially and temporally variable. Figure 15 shows the inflow velocities into cell 1. Velocities through the remainder of the domain were those required in order to conserve mass.

One aerosol, UO_2, and 18 vapor sources, including H_2 and H_2O, were used to input each of the elements into the circuit. The release rates used by VICTORIA-92 were those predicted by CORSOR-M (using the Petti correlation for release of the volatiles [7]) for the fuel and control rod elements and ICARE [3] for steam and hydrogen. The CORSOR-M predicted releases are compared in the following section with those of VICTORIA-92. It would be desirable, for reasons outlined below, to perform calculations using VICTORIA-92 predictions for the releases from the fuel bundle as input to the FPT0 primary circuit.

Table 3: Floor, Wall, and Ceiling Areas in Each Cell (cm^2)

Cell	1	2	3	4	5	6	7	8	9	10	11	12	13	14	15
Floor, Ceiling	0.01	0.	0.	0.	0.	0.	1539.	311.	10.8	895.	0.	0.	0.	0.	0.
Wall	313.	188.	1184.	86.5	2088.	111.	1757.	355.	12.3	1022.	123.	37.7	28.2	928.	928.

Cell	16	17	18	19	20	21	22	23	24	25	26	27	28	29	30
Floor, Ceiling	0.	0.	0.	0.	0.	0.	0.	478.	0.	275.	0.	0.	0.	255.	0.
Wall	928.	98.6	98.6	2784.	27.8	148.	296.	546.	181.	314.	296.	236.	296.	291.	296.

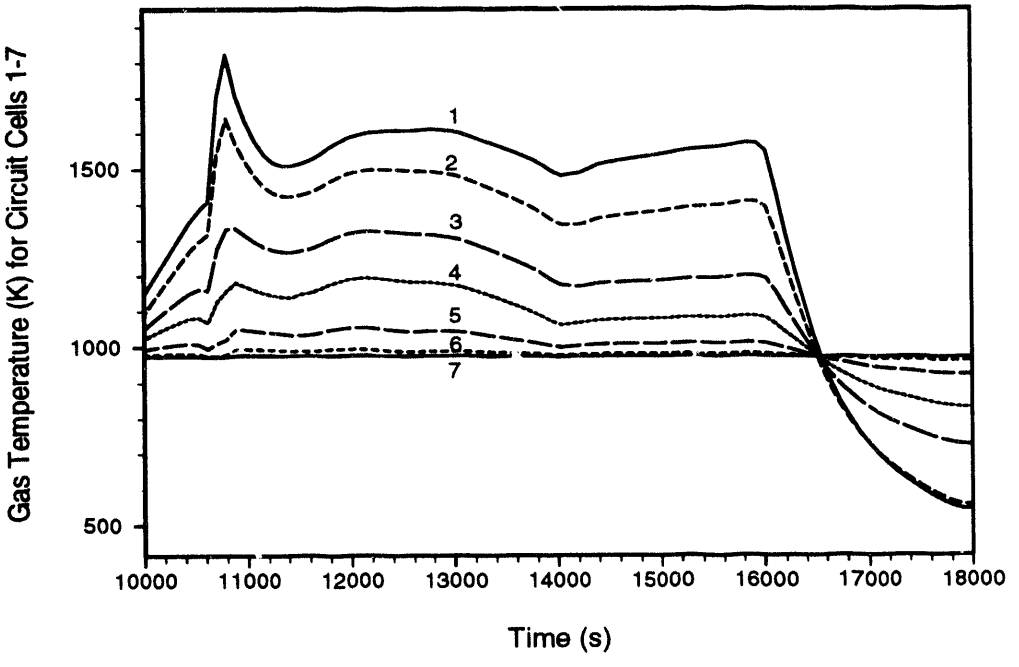

Figure 12. Gas temperatures in the FPT0 circuit for cells 1 through 7.

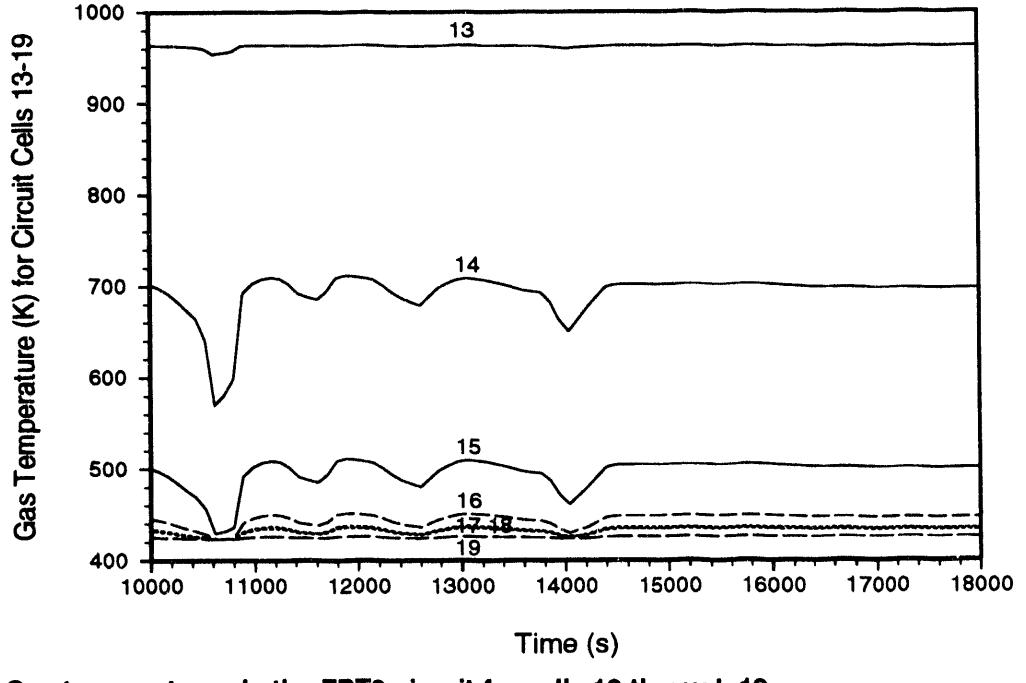

Figure 13. Gas temperatures in the FPT0 circuit for cells 13 through 19.

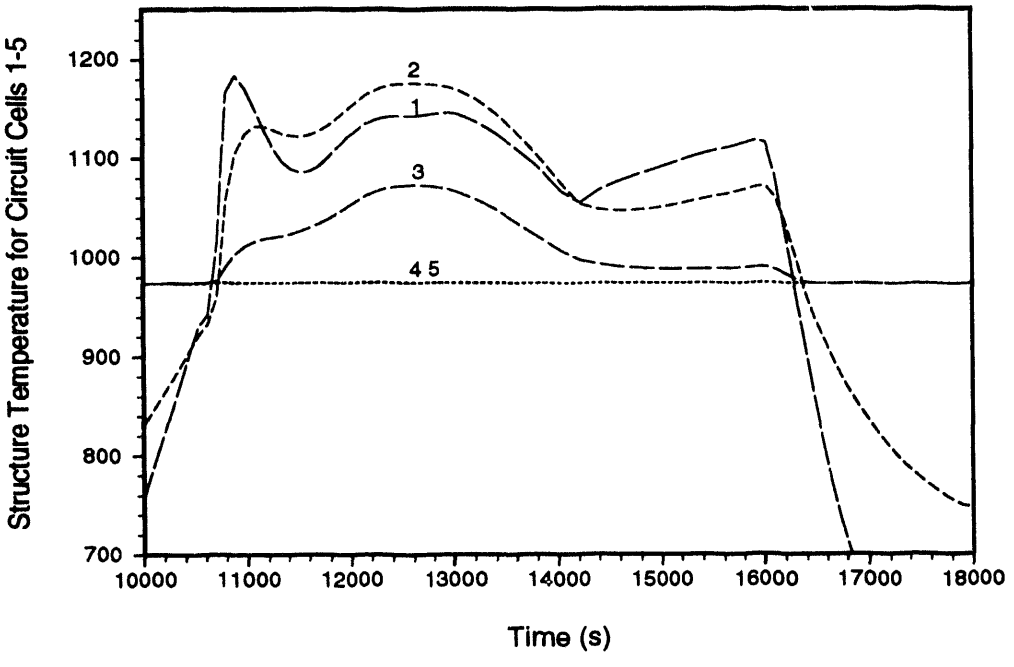

Figure 14. Structure temperatures in the FPT0 circuit for cells 1 through 5.

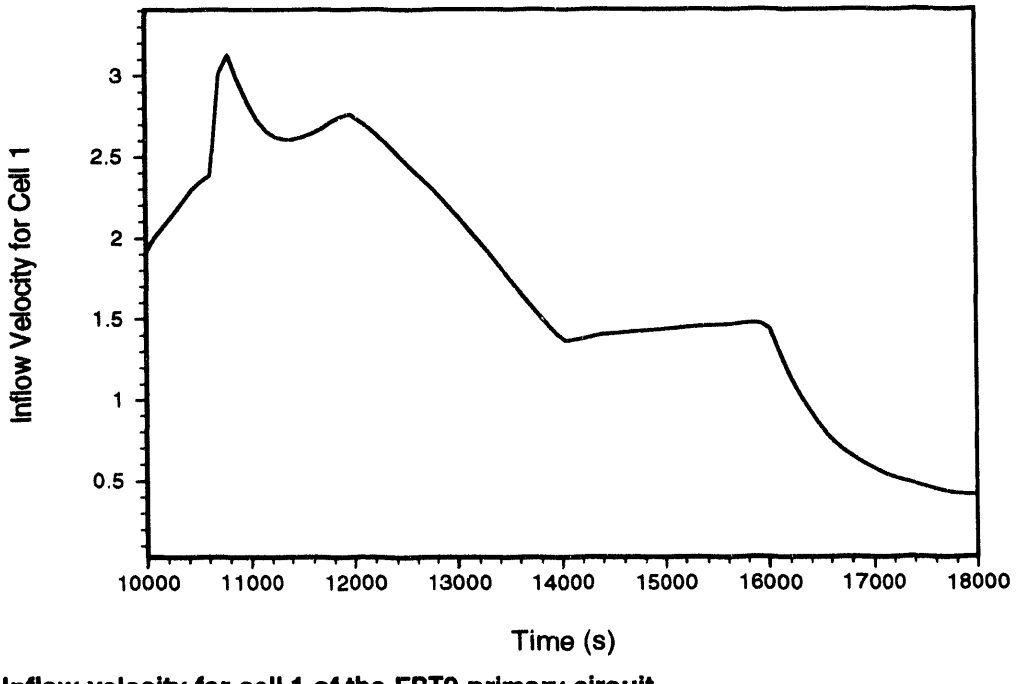

Figure 15. Inflow velocity for cell 1 of the FPT0 primary circuit.

3.0 Predictions for the FPT0 Fuel Bundle

This section compares VICTORIA-92 predictions for release of fission products and structural materials from the fuel bundle region with those of CORSOR-M, which are used as the basis for the analysis of the primary circuit given in Section 4.0.

Table 4 compares the integral releases predicted by VICTORIA-92 with those predicted by CORSOR-M. Figures 16 through 18 compare the relative timing of release. In general, VICTORIA-92 predicts that releases occur earlier than does CORSOR-M.

Total release fractions for four of the elements, I, Te, Xe, and Kr, are predicted to be within a factor of two by the two codes. However, VICTORIA-92 allows a significant fraction of the Te to interact with the zircaloy cladding while CORSOR-M does not. This is a low concentration effect due to the trace irradiated fuel used in FPT0. If more Te had been available for release, a smaller fraction of it would have been able to interact with the cladding and, thus, a larger fraction would have been released.

VICTORIA-92 predicts substantially lower releases of U, Cs, Ba, Sr, Cd, Sn, and Zr than does CORSOR-M. The U, Ba, and Zr releases predicted by CORSOR-M are larger than have been observed in other tests. VICTORIA-92 predicts that a substantial fraction of the Cs gets bound up in the pores as $Cs_2U_2O_7$, which reduces the fraction of Cs that can be released. This effect undoubtedly results from the low fission product inventory for FPT0; if more Cs were present in the fuel, only a small fraction would be able to interact with the UO_2 at the grain surfaces. The Sr releases predicted by the two codes agree reasonably well. The VICTORIA-92 prediction for release of Cd is based on a model that allows most of the alloy to relocate to colder regions of the test section after failure. If this assumption is valid for the experiment, then the VICTORIA-92 prediction should be reasonable; if the Cd remains in hotter regions of the test section, then the CORSOR-M prediction should be more accurate. It is difficult to anticipate which assumption will prevail in the FPT0 test. Sn release in VICTORIA-92 can occur once the cladding melts. However, the cladding was not allowed to melt in this calculation in order to better represent the interactions of Te with the cladding. This is because the cladding failure model in VICTORIA-92 assumes that melted cladding is entirely removed and is unavailable for further interaction. The choice to retain the cladding in this analysis allowed Te-cladding interactions to occur, but did not allow much of the Sn in the cladding to be released. For this reason, the CORSOR-M prediction for Sn release is probably more realistic than the VICTORIA-92 prediction.

VICTORIA-92 predicts substantially higher releases of Ag and In than does CORSOR-M. This may be due to a VICTORIA-92 model in which 2% of the alloy is converted into aerosol upon burst of the control rod, as was measured by Bowsher et al. [8]. The conversion of control rod alloy to aerosol is not modeled by CORSOR-M.

Release of the control rod cladding elements, Fe, Cr, Mn, and Ni, was not modeled in the VICTORIA-92 calculation. Thus, the releases of these elements were null. A model for this type of release should be added to the code.

Based on the above discussion, it is obvious that some of the differences between the two sets of predictions will have to await execution of FPT0 for resolution. This is especially true of the U release, which according to CORSOR-M should dominate the elements released into the circuit. On the other hand, VICTORIA-92 predicts U release to be similar to that of the control rod elements. Even so, release of U and the control rod elements is predicted by VICTORIA-92 to dominate those of the fission products for FPT0. This will not be the case for the later FPT tests, because they will use high burn-up fuel.

Table 4: Integral Releases Predicted by VICTORIA and CORSOR-M

Element	Initial Inventory (g)	CORSOR-M Mass Release (g)	CORSOR-M Fraction Release (%)	VICTORIA Mass Release (g)	VICTORIA Fraction Release (%)
U	9183	140	1.5	2.5	0.03
Cs	0.1378	0.12	87	0.050	37
I	0.03446	0.030	87	0.028	81
Te	0.04532	0.040	88	0.022	49
Ba	0.1424	0.049	34	0.0072	5.1
Sr	0.1083	0.0041	3.8	0.0011	1.0
Xe	0.3268	0.28	86	0.27	83
Kr	0.03143	0.027	86	0.026	83
Ag	471.2	3.9	0.83	19	4.0
In	88.35	0.50	0.57	2.5	2.8
Cd	29.45	10.	34	1.1	3.7
Sn	39.25	24.	61	0.0016	0.00
Zr	2062	0.35	0.02	0.0040	0.00
Fe	76.64	1.7	2.2		
Cr	24.77	1.6	6.1		
Mn	2.18	0.0019	0.09		
Ni	13.10	0.00013	0.00		

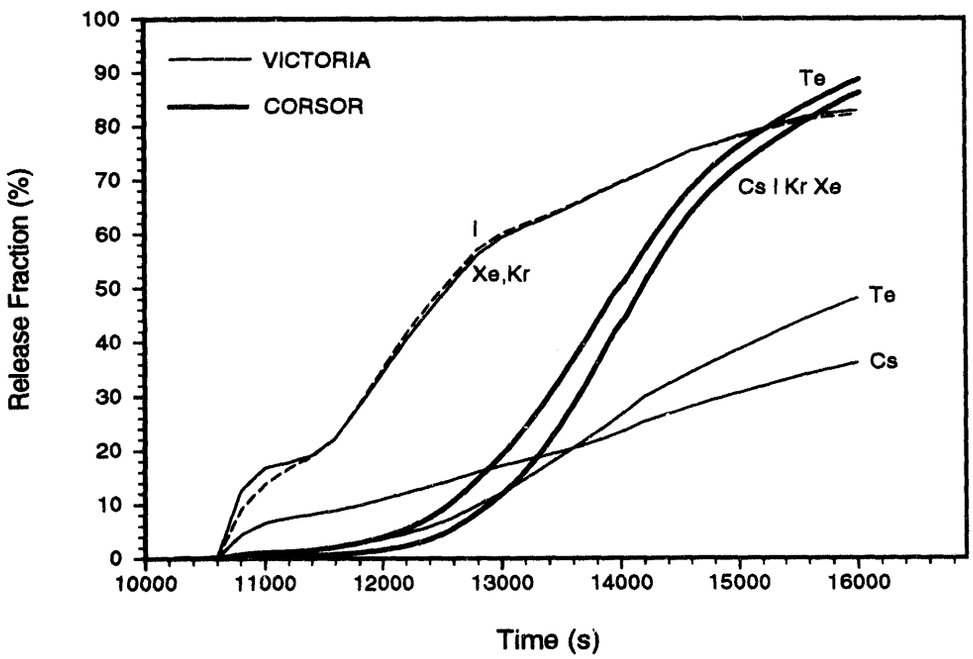

Figure 16. Fractional release into the primary circuit for the volatile elements, Xe, Kr, I, Te, and Cs.

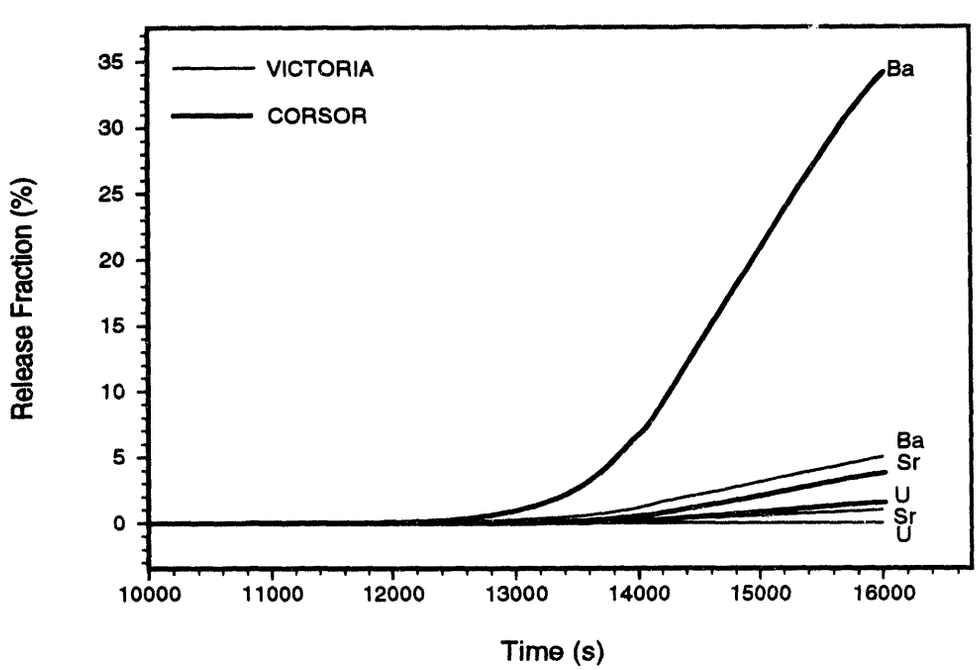

Figure 17. Fractional release into the primary circuit for Ba, Sr, and U.

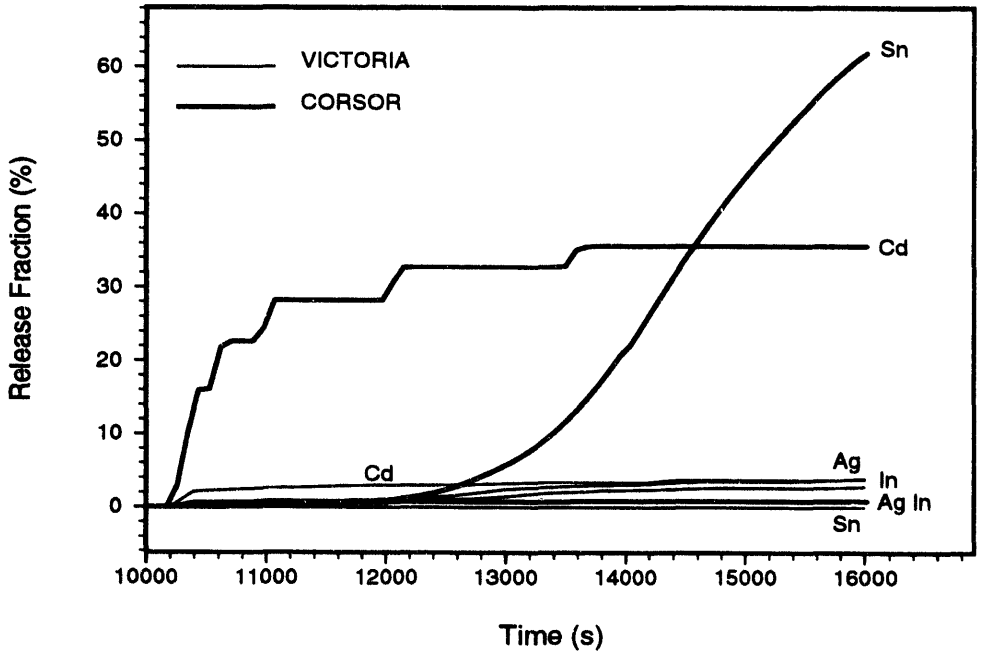

Figure 18. Fractional release into the primary circuit for control rod and cladding elements, Ag, In, Cd, and Sn.

4.0 Predictions for the FPT0 Primary Circuit

Release data from CORSOR-M using the Petti correlation [7] for volatile release, given in Table 4 and shown in Figures 16 through 18, were used as input in the analysis of the FPT0 primary circuit. A future calculation using VICTORIA-92 release predictions as input to the primary circuit should be performed. Other input data are discussed in Subsection 2.2.

Figure 19 shows the locations and mechanisms of aerosol deposition. The largest aerosol deposits occur in the vertical section above the fuel bundle and in the first half of the steam generator. The primary deposition mechanism in these regions is thermophoretic deposition, which occurs because the gas stream is significantly hotter than the surfaces (see Figures 12 through 15). Aerosol deposition also occurs along the straight horizontal section near point C. The dominant deposition mechanism there is gravitational settling.

Figure 20 shows the aerosol mass mean diameter at point C, the steam generator, point G, and the exit to containment. The mass mean diameter changes significantly over the transient, depending on the rate of release from the test section. Several early peaks occur as material is expelled from the control rod. The relatively small aerosol sizes prior to about 13,000 s will be difficult to quantify with on-line impactors. The broad peak from 13,000 to 16,000 s corresponds to release from the fuel rods. On-line impactors should be effective for measuring aerosol size distributions during this period. Differences in mass mean diameter from point to point within the primary circuit tend not to be great.

The multiplicity of peaks in the mass mean diameter of the aerosol during the period between 10,000 and 12,000 s, corresponding to multiple failures of a single control rod, is an artifact of the way that the CORSOR-M calculation was applied to FPT0. Therefore, redoing the calculation using VICTORIA-92 release data would be worthwhile. Furthermore, the smaller total mass release predicted by VICTORIA-92 should produce somewhat smaller aerosols, an effect that should be quantified.

Aerosol standard deviations are shown in Figure 21. These range in value from 1 to 3. They are around 2 over most of the transient. Again, the variation from point to point within the primary circuit is not great.

Aerosol mass and particle concentrations are shown at four locations in Figures 22 and 23, respectively. During the period when the reactor is operating, the mass concentrations generally range from 10^{-5} to 10^{-1} kg/m^3 and the particle concentrations from 10^{12} to 10^{14} particles/m^3. Again the temporal variation of these quantities is much greater than the spatial variation.

Idaho National Engineering Laboratory has supplied an on-line aerosol monitor (OLAM) for measuring particle concentrations during the FPT transients. It operates by attenuation of an optical beam. Predictions for particle concentrations are well within the range for which the OLAM was calibrated [9], which indicates that this device should prove useful for observing the onset of control and fuel rod releases. However, predictions for both aerosol mass and particle concentrations would have been somewhat lower had the releases from the test section predicted by VICTORIA-92 been used as input to the primary circuit.

The hydrogen/steam ratio is shown in Figure 24 at four points in the FPT0 primary circuit. As might be expected, there is no significant variation from point to point because only a small fraction of the steam reacts with the fuel and structural materials as it flows through the circuit. There is, however, a large variation in time; the ratio is small over most of the transient, except at around 10,300 s when ICARE predicts cladding oxidation to occur rapidly.

Figures 25 through 29 show the dominant iodine species at the inlet, point C, the steam generator, point G, and at the exit, respectively. At the inlet, the dominant species are I(g), HI(g), and CsI(g), in that order over most of the transient. By point C the temperature has cooled to 700°C, which is low enough that the dominant forms are CsI(c) followed by CsI(g) over most of the transient. In the steam generator and beyond, the dominant form is CsI(c) over the entire transient until reactor shutdown. After reactor shutdown, CdI_2(c), CdI_2(g), and other species compete for dominance. This set of plots, as well as ones to follow, make it clear that revaporization is important in the FPT0 primary cir-

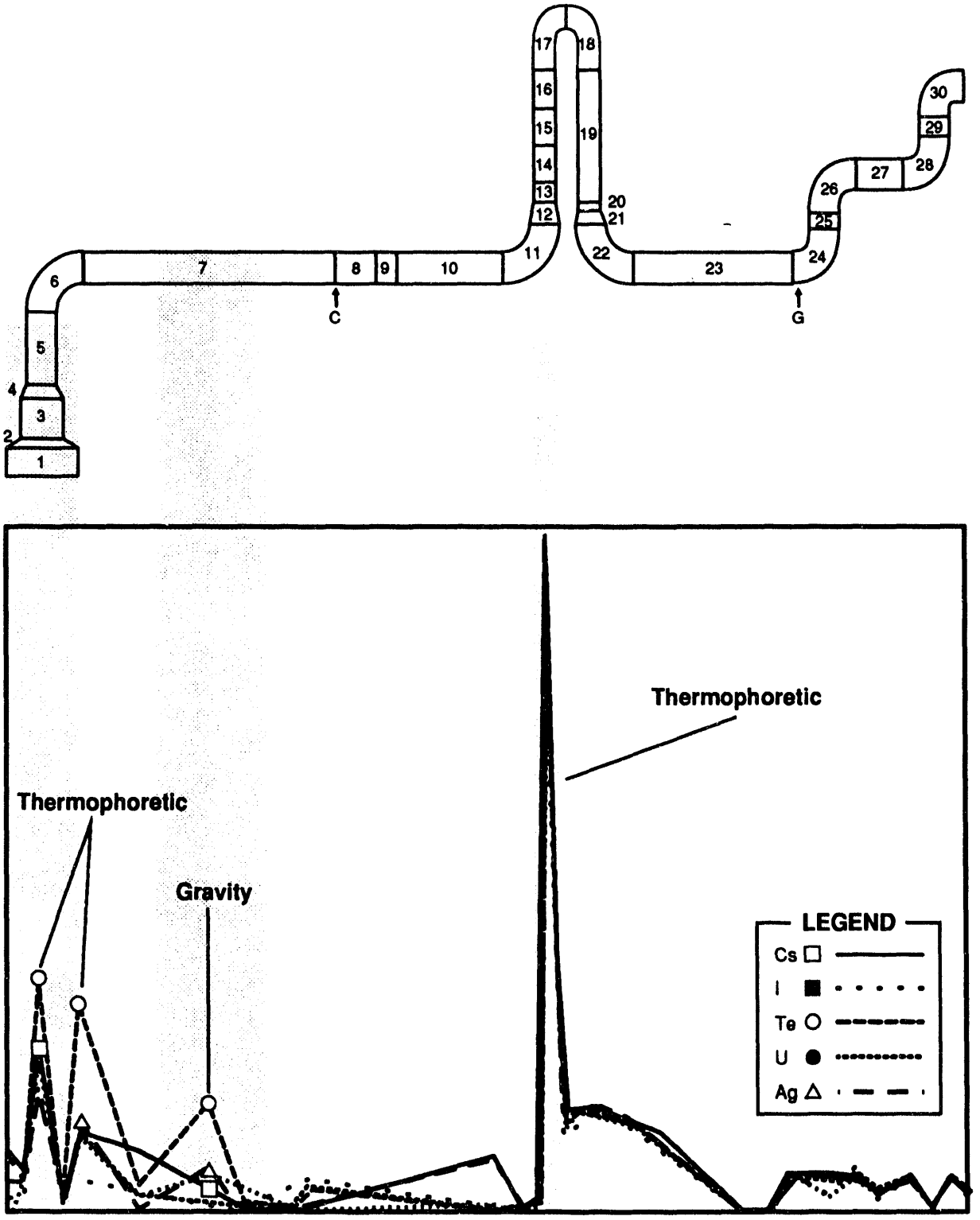

Figure 19. Locations and dominant mechanisms of aerosol deposition in the FPT0 primary circuit.

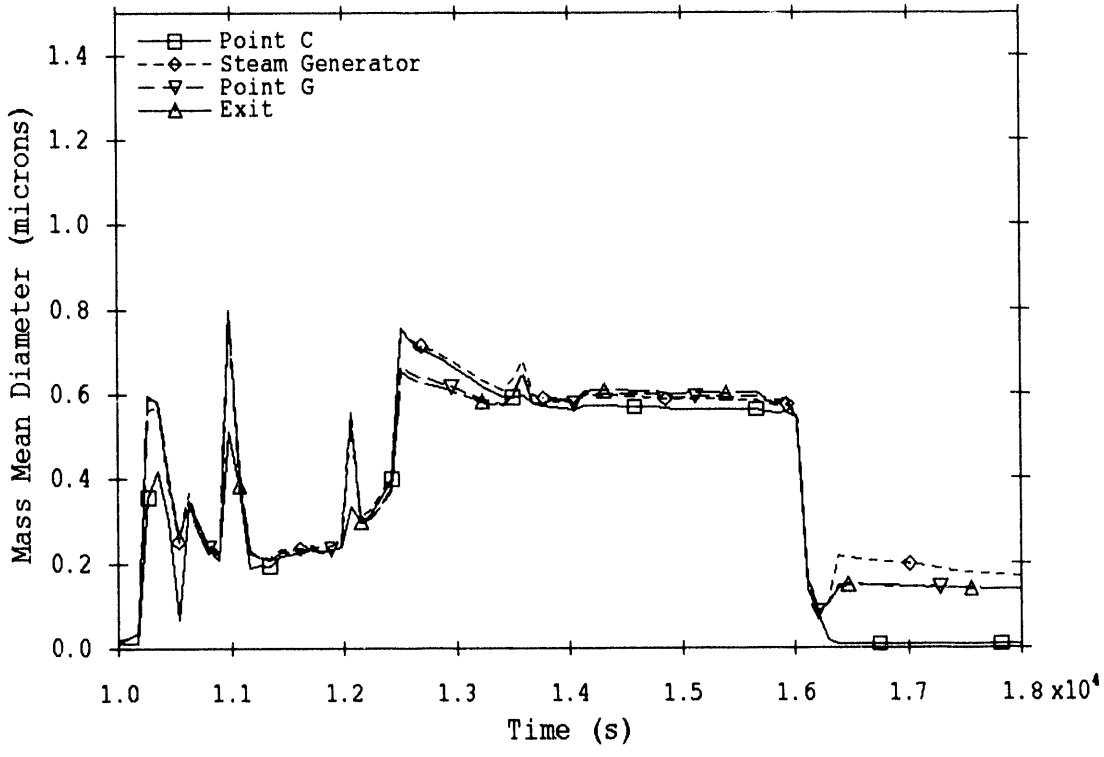

Figure 20. Aerosol mass mean diameter in the FPT0 primary circuit.

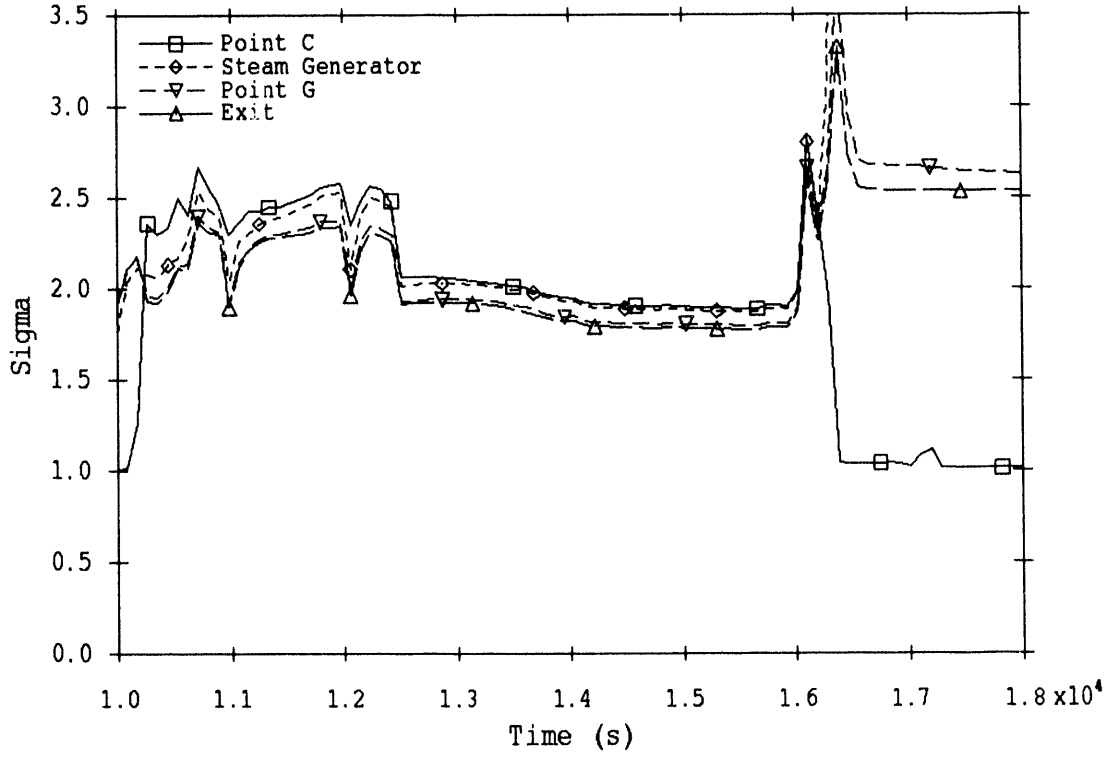

Figure 21. Aerosol standard deviation in the FPT0 primary circuit.

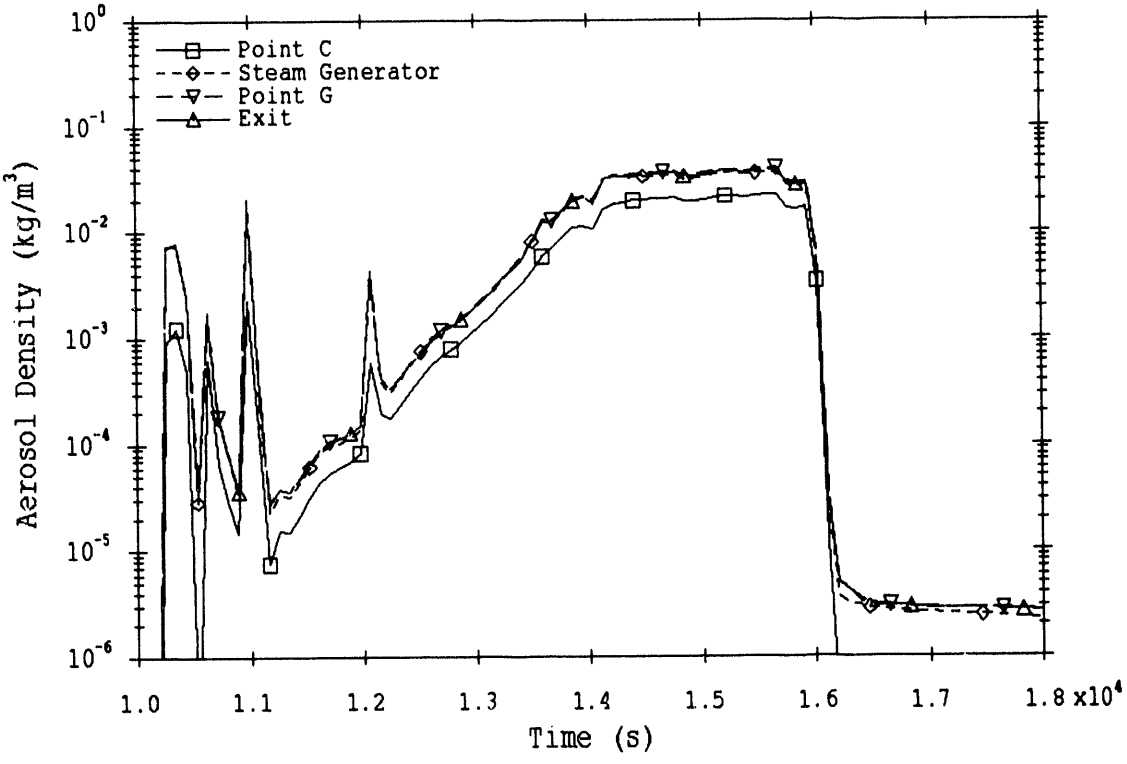

Figure 22. Aerosol mass concentration histories in the FPT0 circuit.

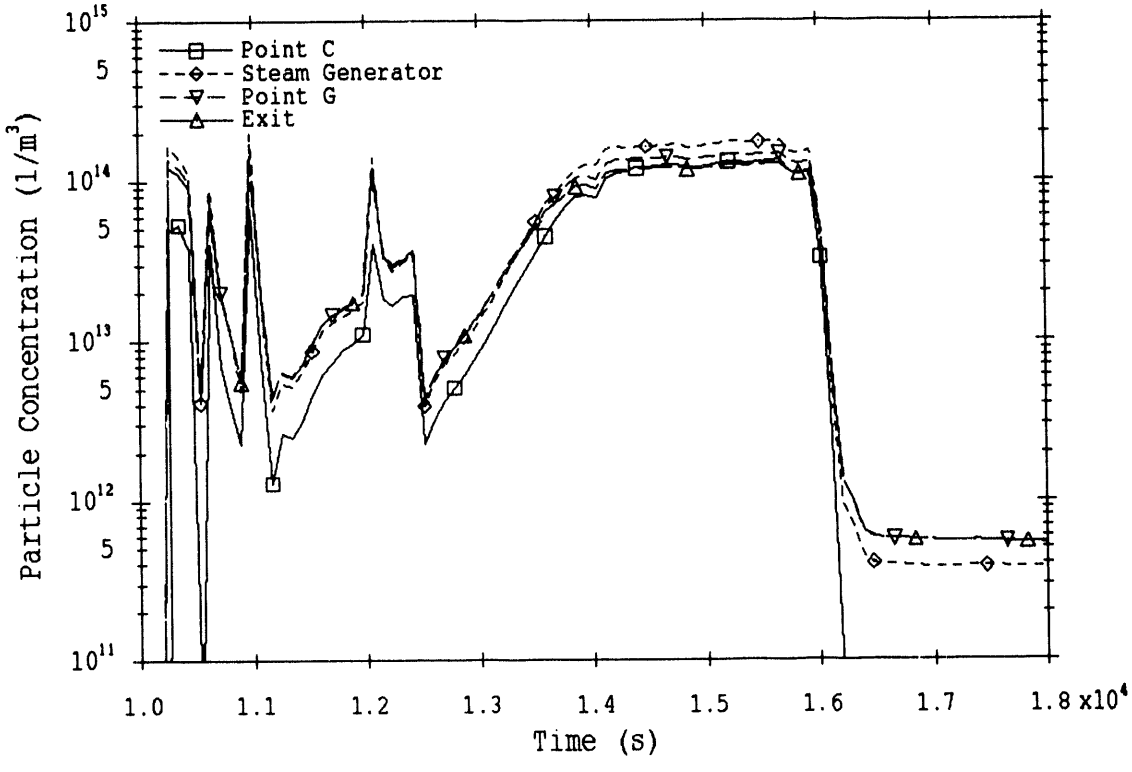

Figure 23. Aerosol particle concentration histories in the FPT0 circuit.

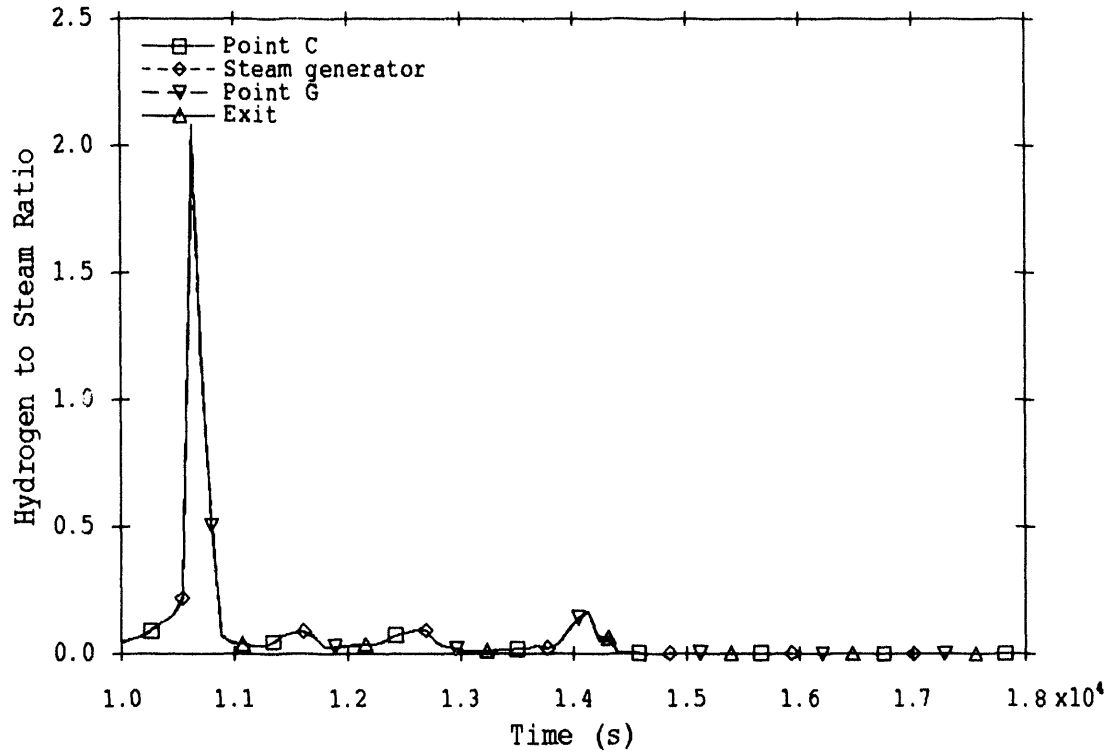

Figure 24. Hydrogen to steam ratio histories in the FPT0 circuit.

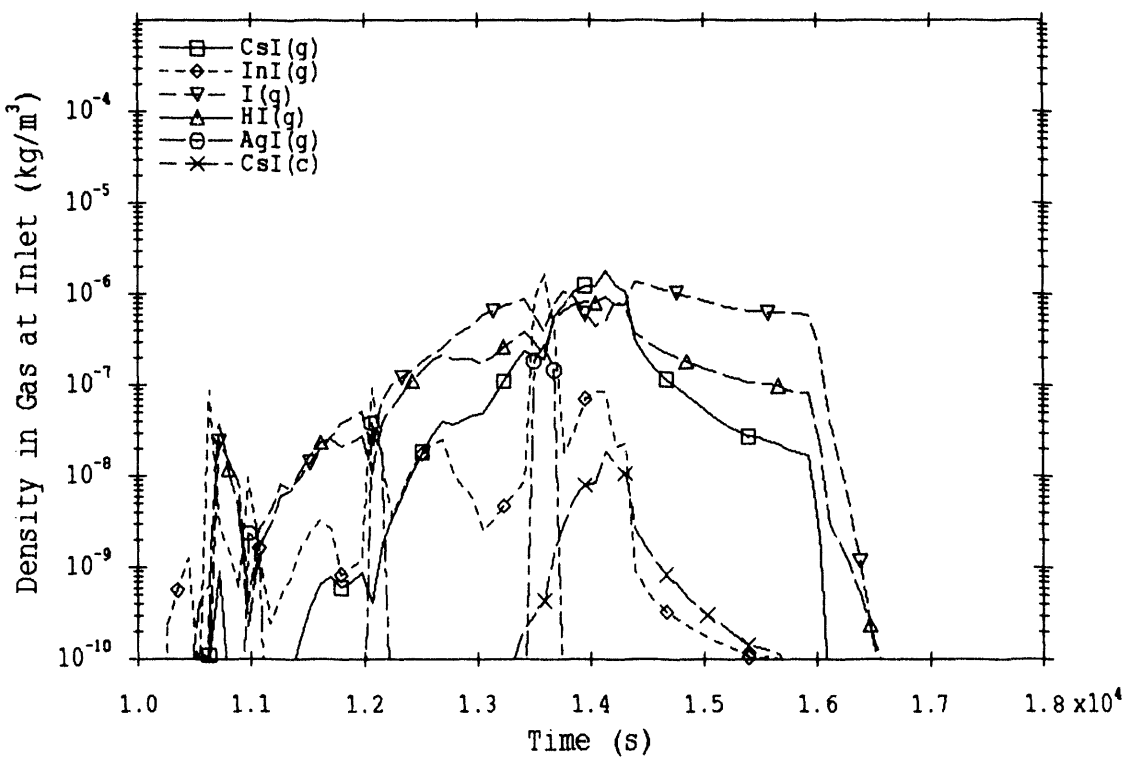

Figure 25. Iodine species at the inlet of the FPT0 circuit.

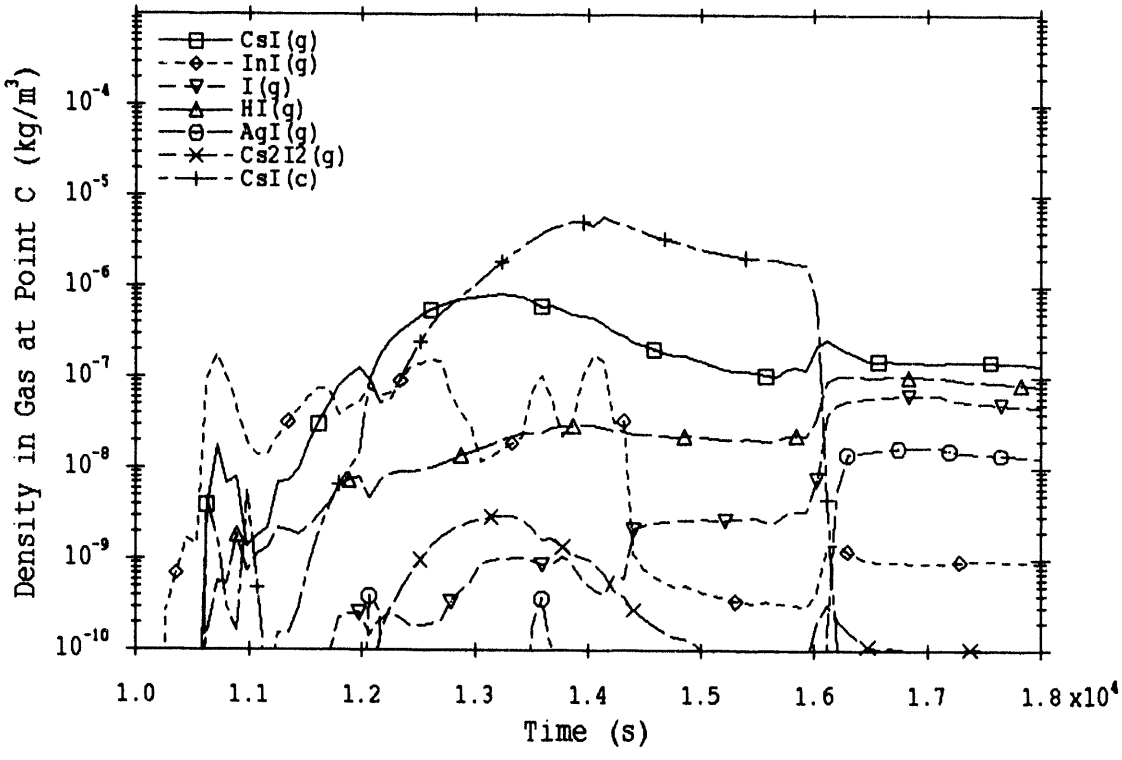

Figure 26. Iodine species at point C in the FPT0 circuit.

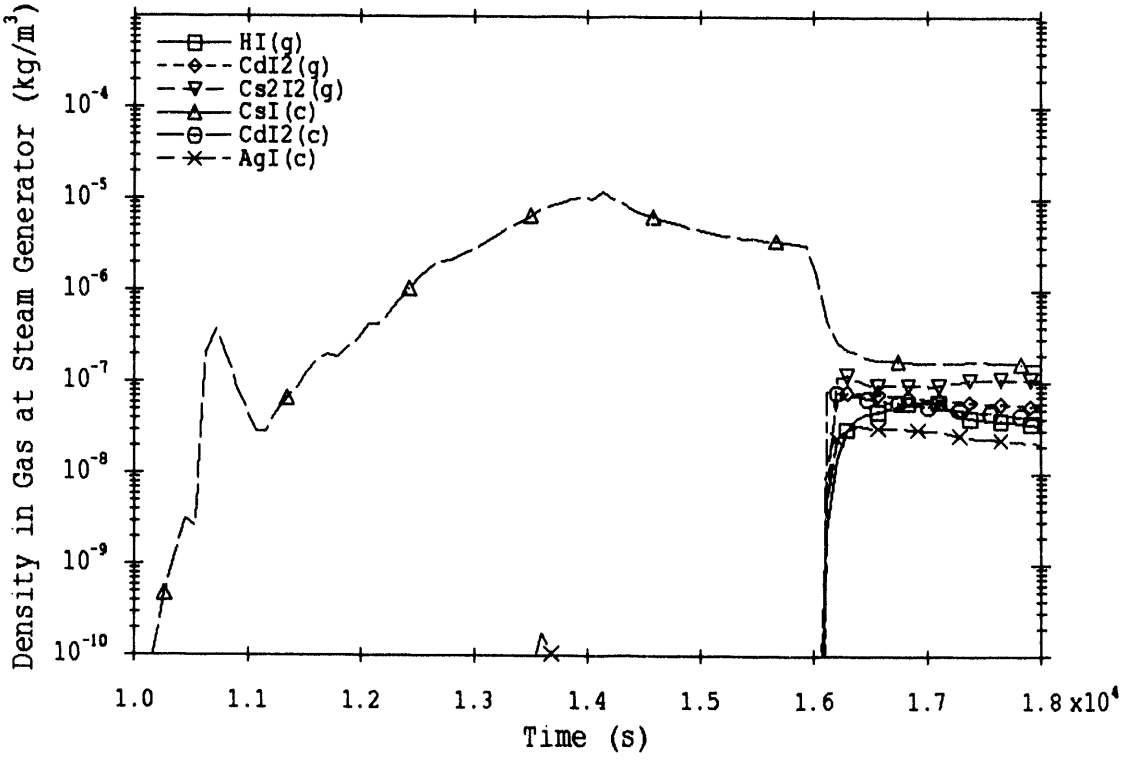

Figure 27. Iodine species at the steam generator in the FPT0 circuit.

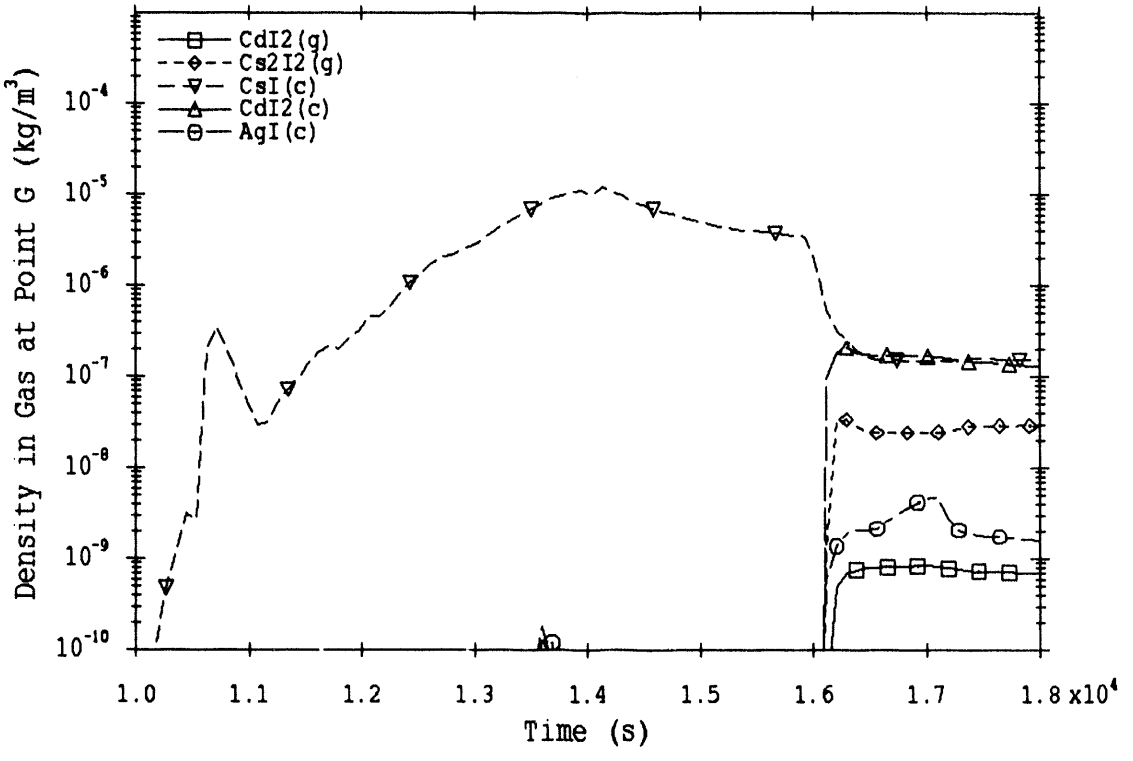

Figure 28. Iodine species at point G in the FPT0 circuit.

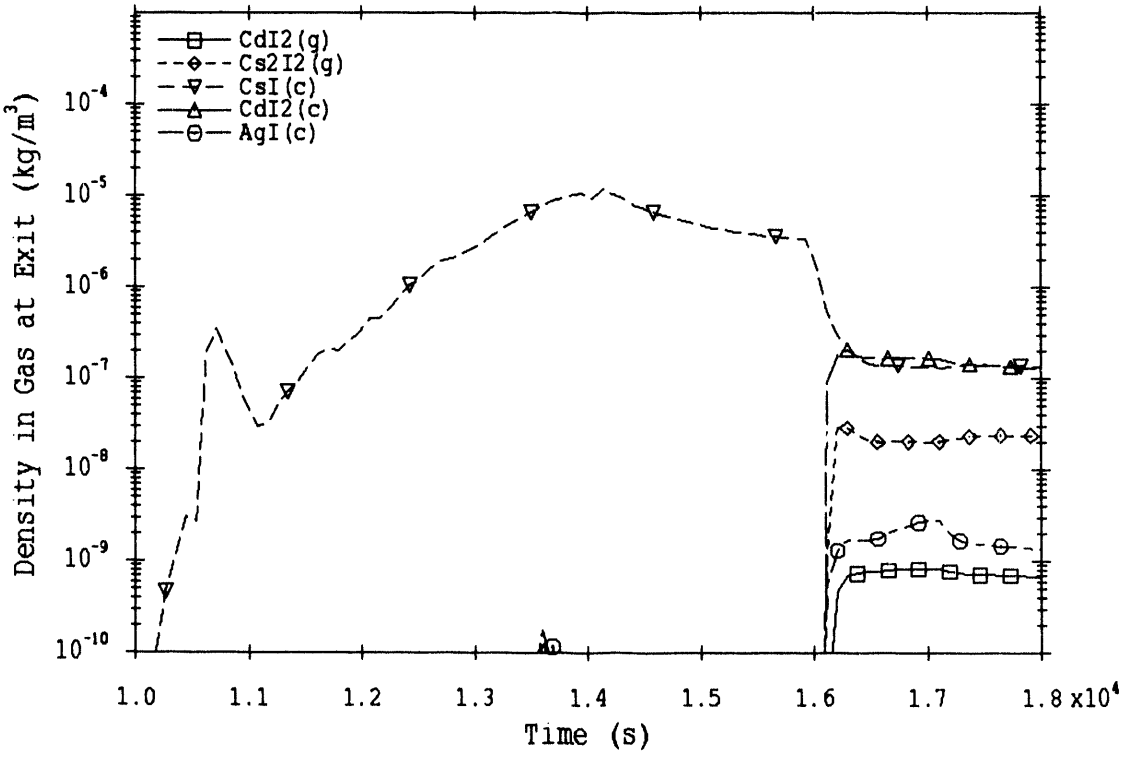

Figure 29. Iodine species at the exit of the FPT0 circuit.

cuit, becoming apparent after reactor shutdown when fission product release from the fuel is negligible.

Figures 30 through 34 show the dominant cesium species at the same set of locations. At the inlet, $Cs_2Zr_2O_5$(c) dominates over the entire transient. CsOH(g) and $Cs_2Zr_3O_7$(c) are next in dominance during the early and intermediate portions of the transient, respectively. The Cs species at the inlet all die out quickly after the reactor is shut down at 16,000 s. At point C, $Cs_2Zr_2O_5$(c) followed by CsOH(g) are the dominant species early in the transient; $Cs_2Zr_2O_5$(c) followed by Cs_2ZrO_3(c) are dominant in the intermediate portion of the transient, and CsI(g) followed by CsOH(g) are dominant after reactor shutdown. In the steam generator, temperatures are cool enough (about 200°C) that only condensed phase species are important. CsI(c) dominates over most of the transient. CsOH(c), $Cs_2Zr_2O_5$(c), and Cs_2ZrO_3(c) also compete for dominance during the first half of the transient. Similar trends are found at point G and the exit.

SnTe(g) and Te(g) are the dominant tellurium species at the inlet, as shown in Figure 35. At point C (Figure 36), the number of species has increased and many of them dominate over short periods of the transient. By the steam generator (Figure 37), the number of significant tellurium species has decreased to eight. Of these CdTe(c) is dominant early and late in the transient and Te(c) in the intermediate portion. Cs_2Te(c) also plays a significant role. Similar trends are predicted at point G (Figure 38) and the exit (Figure 39).

It should be noted, however, that some of the predictions of speciation in and beyond the steam generator are suspect because of the assumption of thermodynamic equilibrium that is made in VICTORIA-92. In reality, thermodynamic equilibrium is an excellent assumption at temperatures above 1000 K; at temperatures below 800 K it may be a poor assumption. Temperatures between the inlet to the circuit and the steam generator are about 973 K, but fall to well below 800 K in the steam generator. A better approximation to the chemical speciation in the steam generator and beyond would be that the speciation is "frozen," i.e., that the speciation does not continue to change once temperatures fall below 800 K. Rather, only phase change should be allowed below this cutoff. This "frozen chemistry" model is not yet available in VICTORIA-92, and so was not used in this analysis of FPT0. It is planned as a future development to the code.

Figure 40 shows the build-up of surface layer deposits at the inlet, point C, the steam generator, and the exit. By the end of the transient, the total deposits are about 0.02 g/cm^2 at all of the points except point C, where the deposits are only about 0.0009 g/cm^2. Thermophoresis is the dominant deposition mechanism at each of these points except point C, where gravitational settling is dominant. This difference in deposition mechanisms probably accounts for the difference in surface deposit density.

Figures 41 through 45 show the dominant I species deposited at the inlet, point C, the steam generator, point G, and the exit, respectively. CsI(c) dominates over the others and is predicted to be the only measurable form of iodine deposit in the primary circuit.

Figures 46 through 50 show the dominant deposited Cs species at the same locations. $Cs_2U_2O_7$(c) and $Cs_2Zr_3O_7$(c) are the dominant deposits at the inlet; Cs_2ZrO_3(c), CsI(c), and $Cs_2U_2O_7$(c) are important at point C; CsI(c) and Cs_2ZrO_3(c) dominate in the steam generator and at point G; and $Cs_2Zr_2O_5$(c), CsI(c), and Cs_2ZrO_3(c) are important at the exit into containment.

Figures 51 through 55 show the dominant Te species deposited at the inlet, point C, the steam generator, and point G, respectively. Te(c) followed by SnTe(c) dominate at the inlet; the same two species plus CdTe(c) are important at point C; at the steam generator, at point G, and at the exit to containment, Te(c) and CdTe(c) dominate. Again, predictions of speciation of deposits in the steam generator and at point G are suspect.

Uranium surface deposit densities are shown in Figures 56 through 60. UO_2 is the dominant U species throughout the primary circuit. The surface deposits of UO_2 are 10^{-3} to 10^{-2} g/cm^2, which is several orders of magnitude greater than any of the fission product surface deposits. However, if the VICTORIA-92 predictions for U release from the fuel are more realistic than those of CORSOR-M, the U deposits would be about two orders of magnitude less than is shown in these figures. Other important U species deposits include U_4O_9 at the inlet and point C and $BaUO_4$ and $SrUO_4$ from the steam generator to the exit into containment.

Silver deposits are shown in Figures 61 through 65. Ag(c) is the dominant Ag species throughout the primary circuit. Indium surface deposit densities are shown in Figures 66 through 70. In(c) and In_2O_3 are

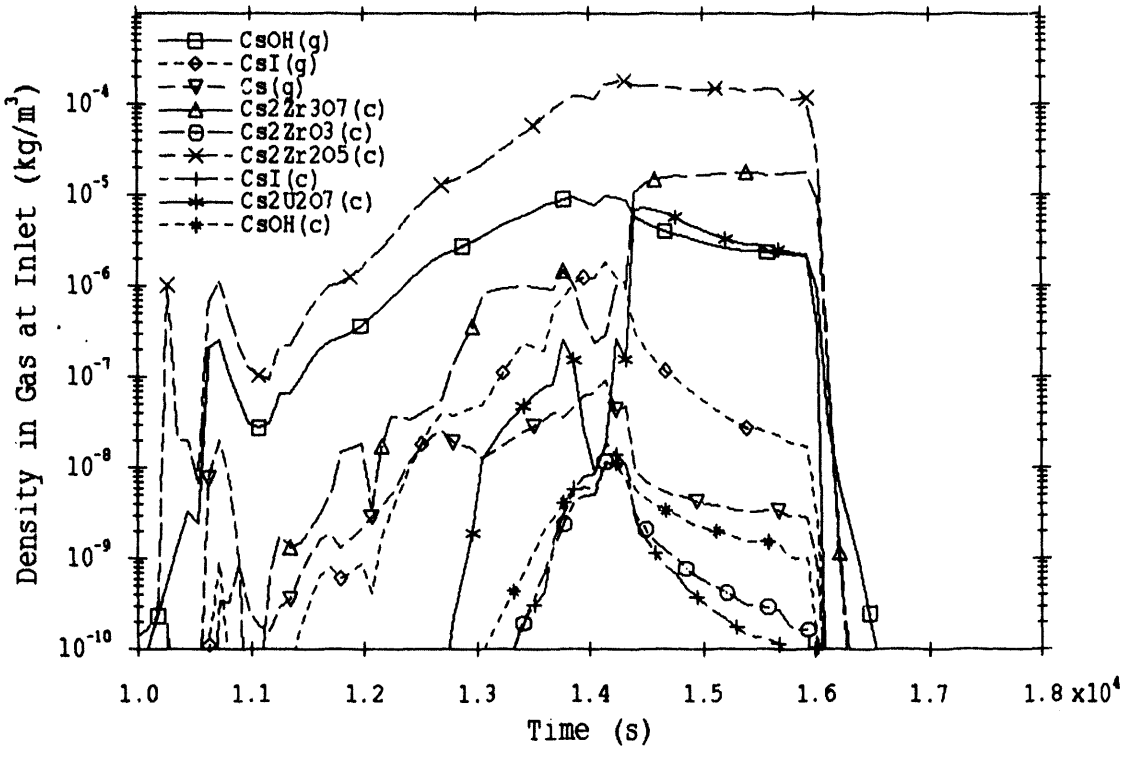

Figure 30. Cesium species at the inlet of the FPT0 circuit.

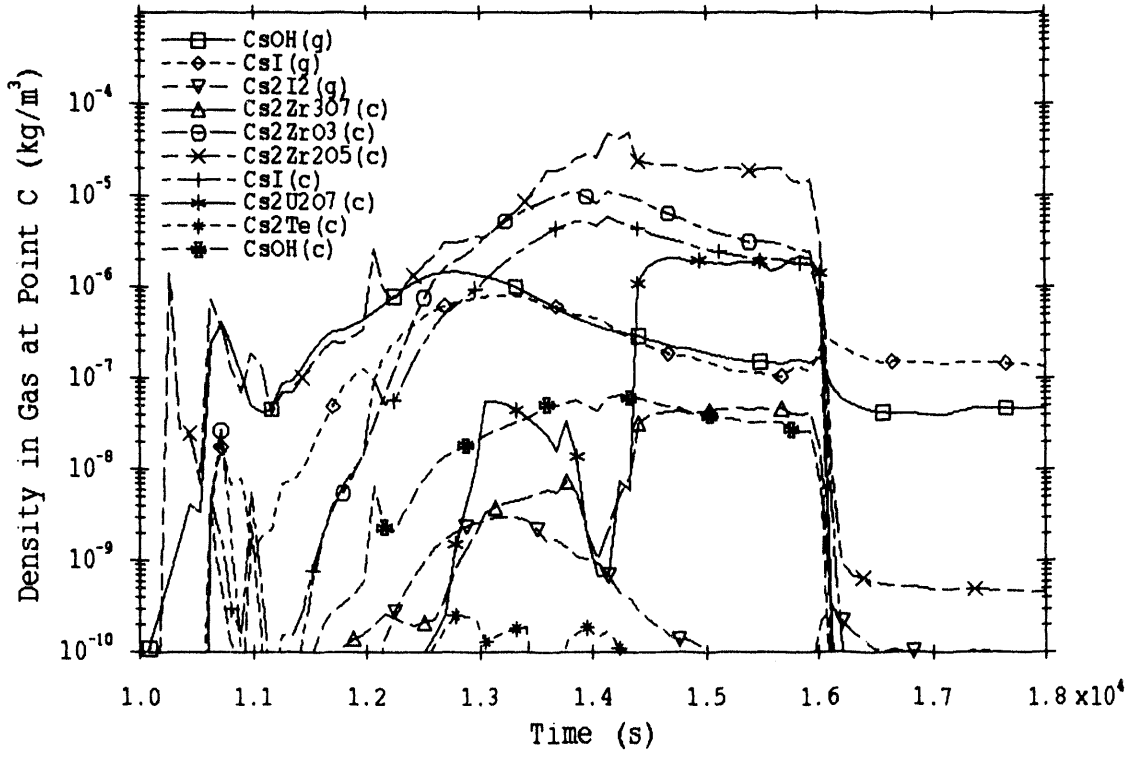

Figure 31. Cesium species at point C in the FPT0 circuit.

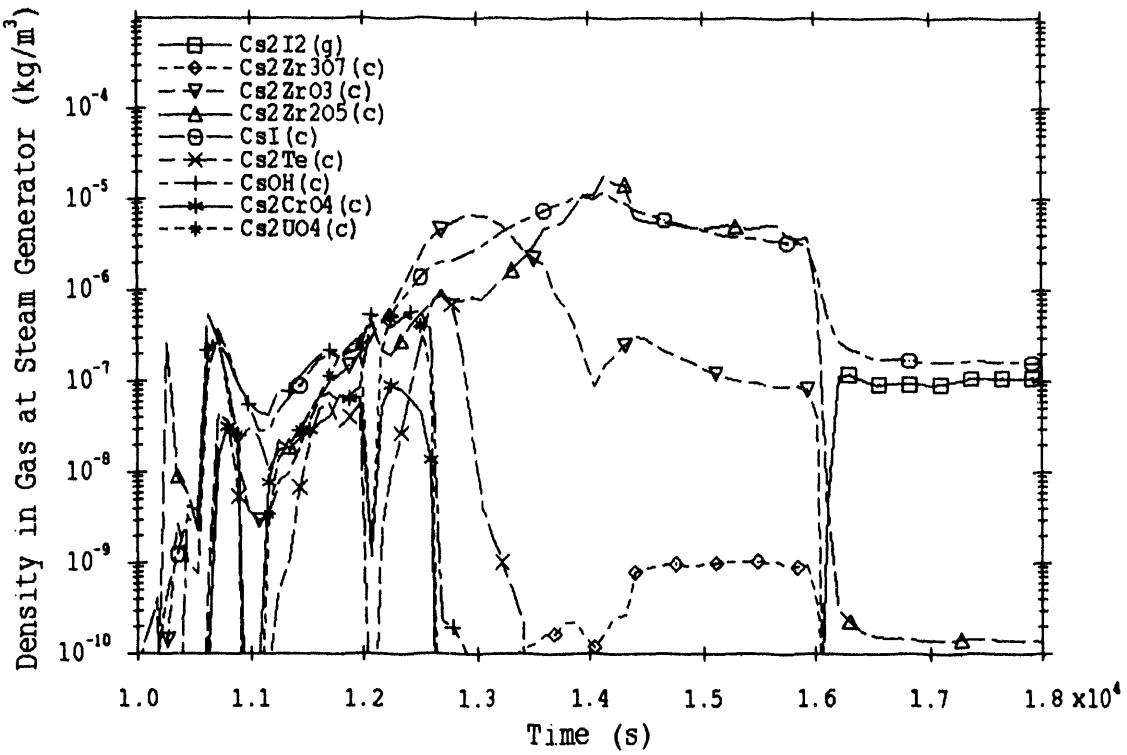

Figure 32. Cesium species at the steam generator in the FPT0 circuit.

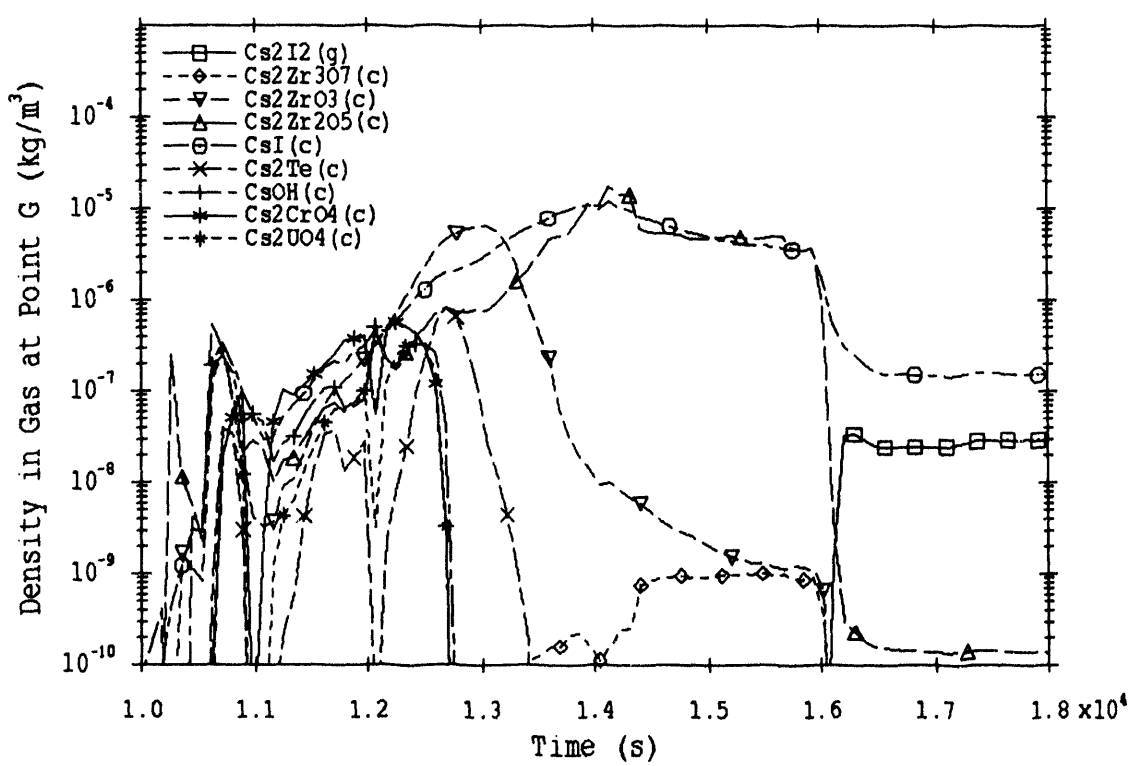

Figure 33. Cesium species at point G in the FPT0 circuit.

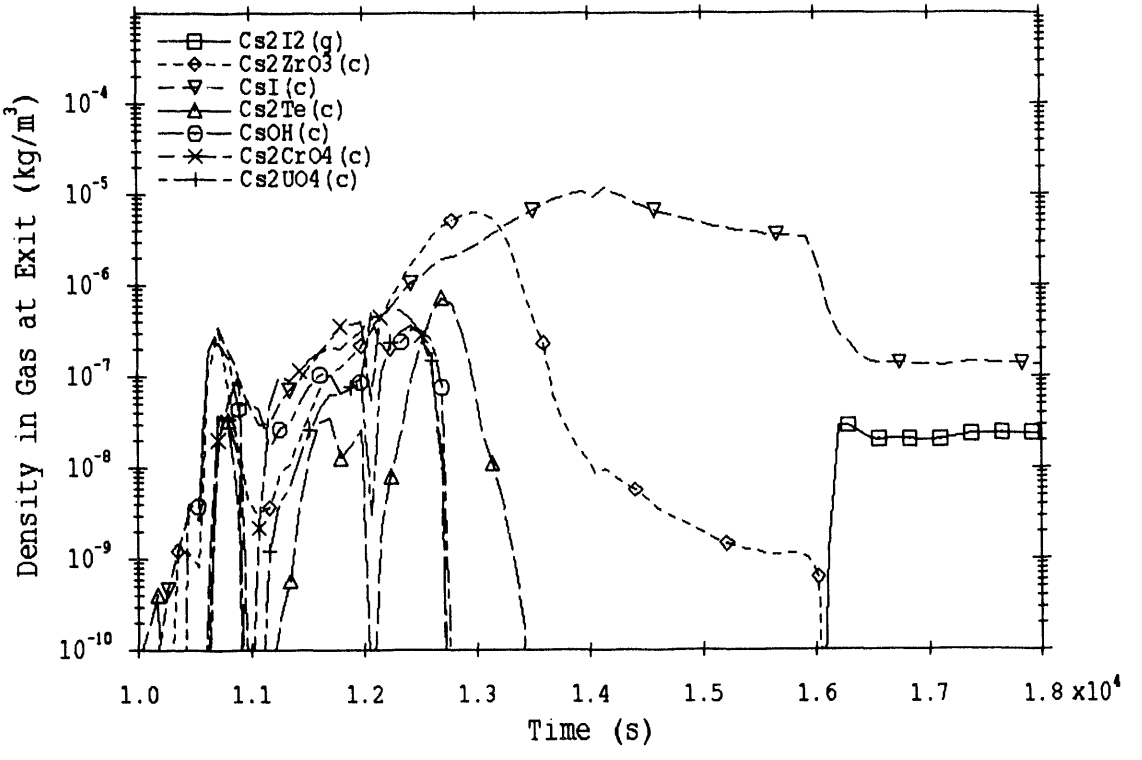

Figure 34. Cesium species at the exit of the FPTO circuit.

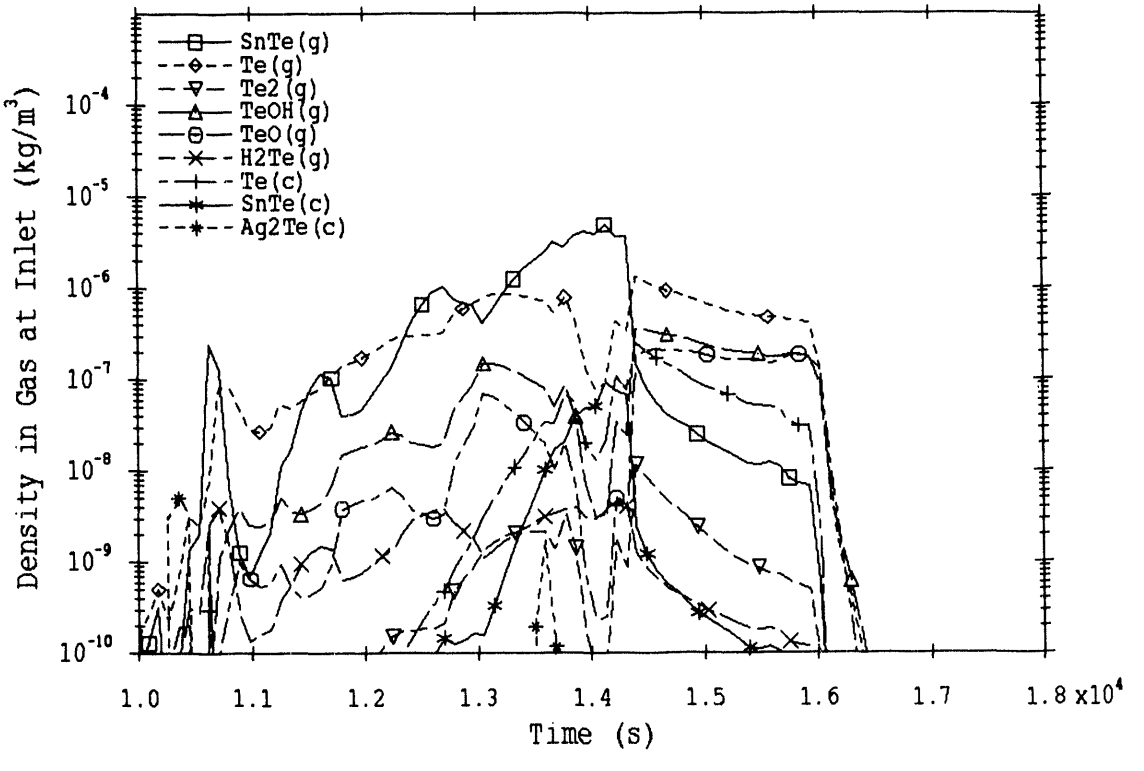

Figure 35. Tellurium species at the inlet of the FPTO circuit.

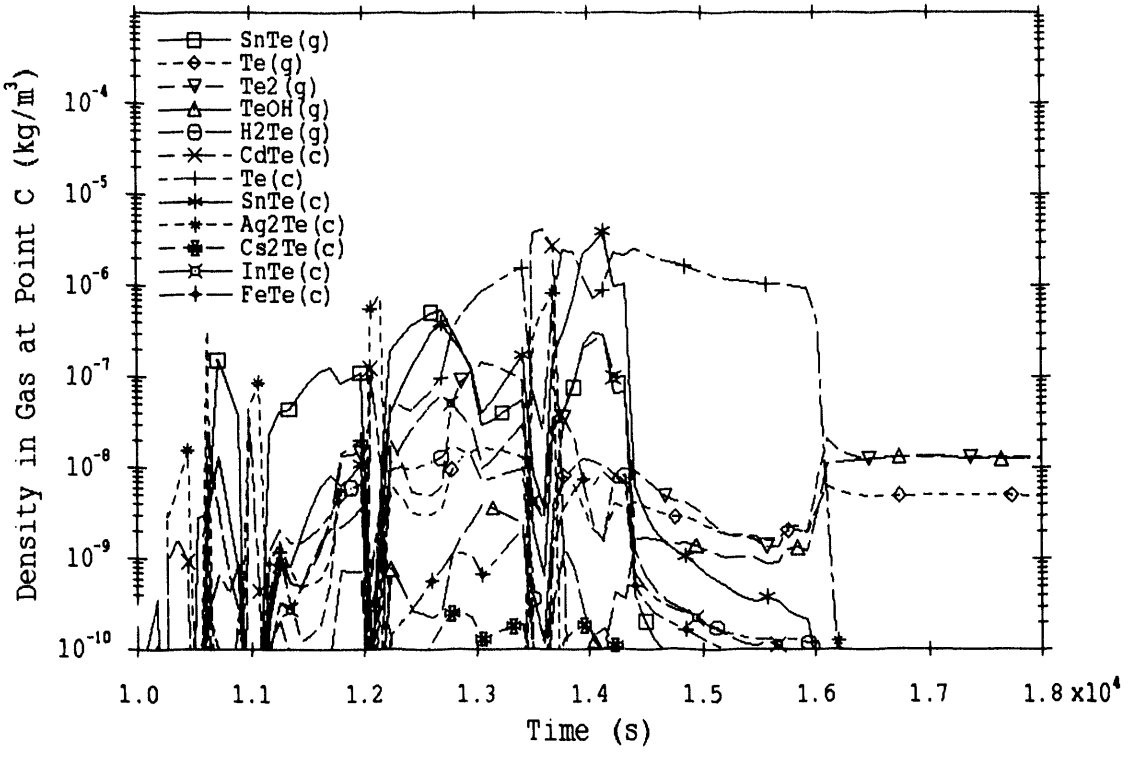

Figure 36. Tellurium species at the point C in the FPT0 circuit.

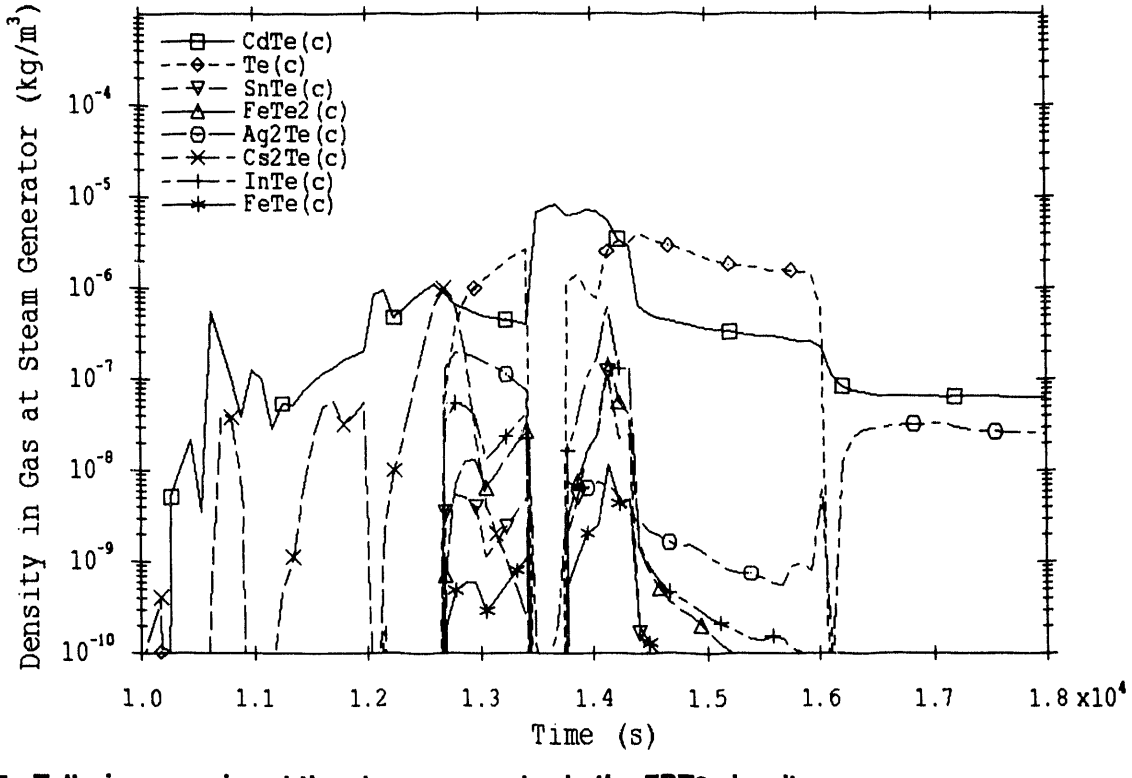

Figure 37. Tellurium species at the steam generator in the FPT0 circuit.

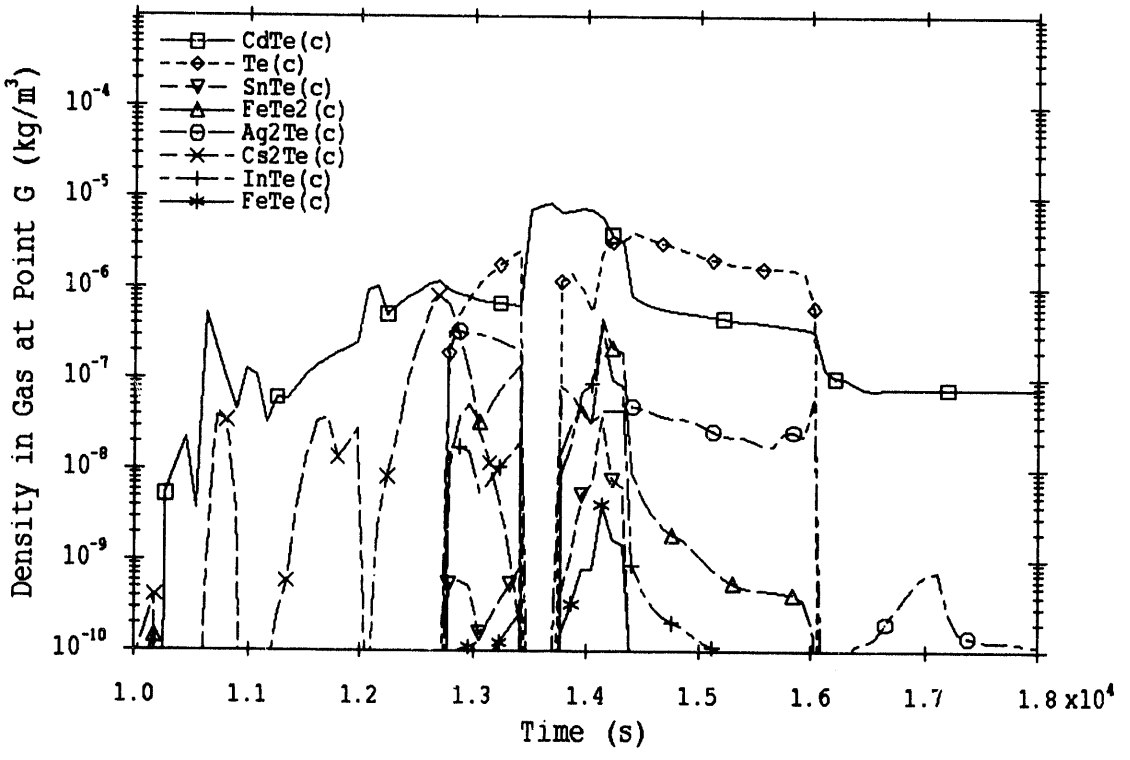

Figure 38. Tellurium species at point G in the FPT0 circuit.

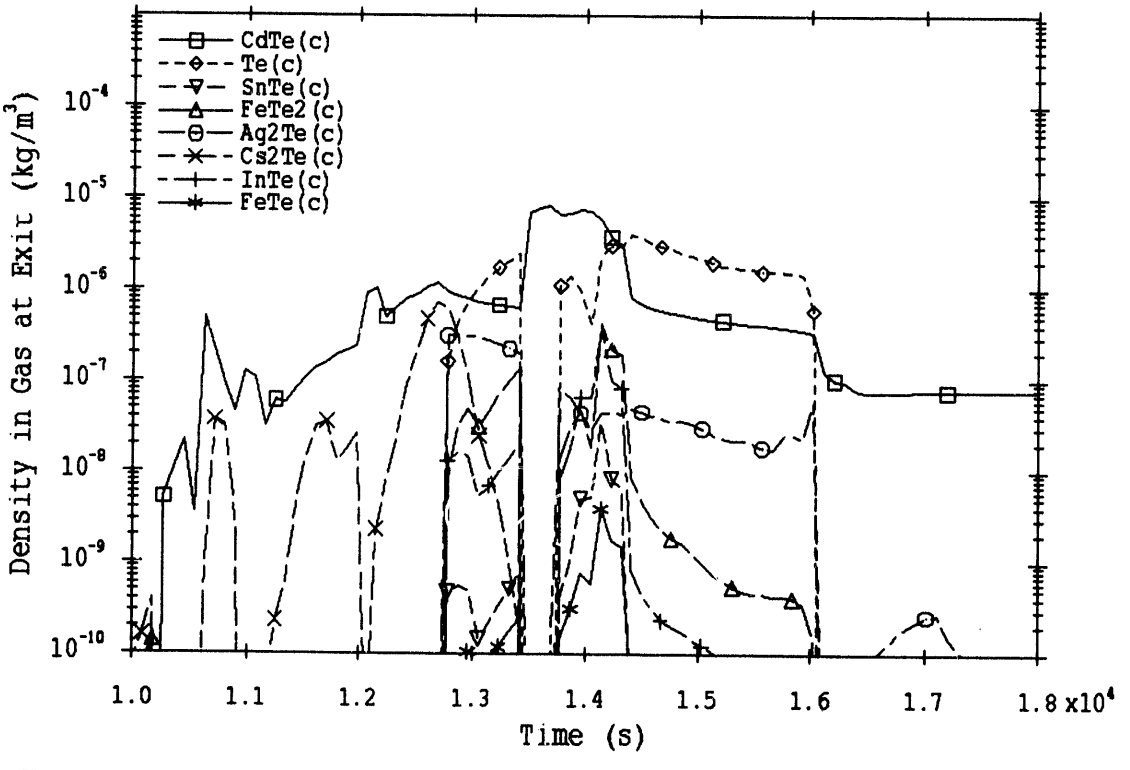

Figure 39. Tellurium species at the exit of the FPT0 circuit.

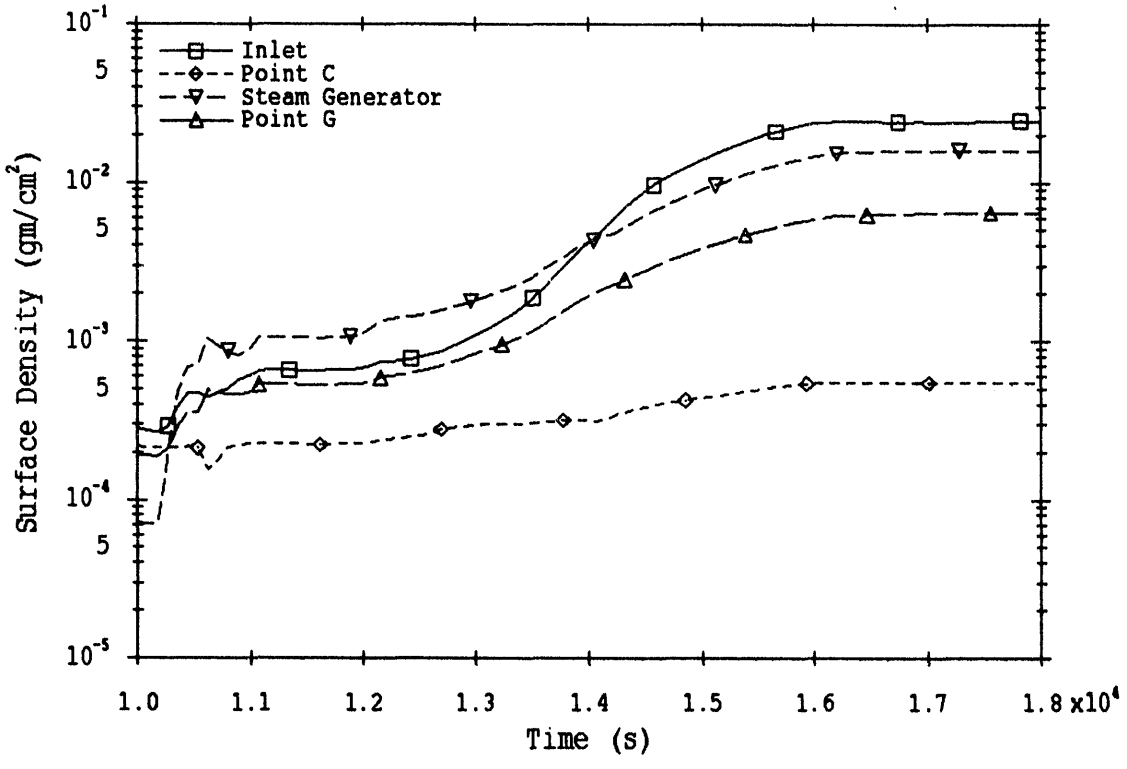

Figure 40. Total surface layer deposit density histories in the FPT0 circuit.

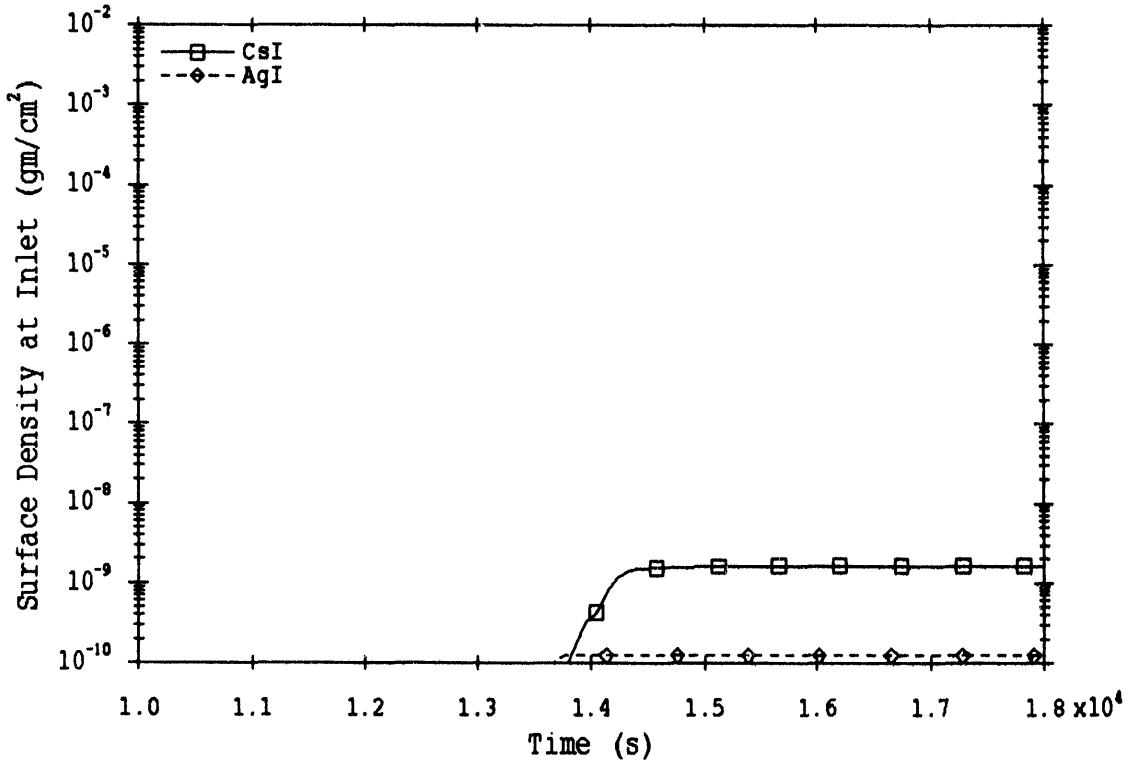

Figure 41. I surface deposit densities at the inlet of the FPT0 circuit.

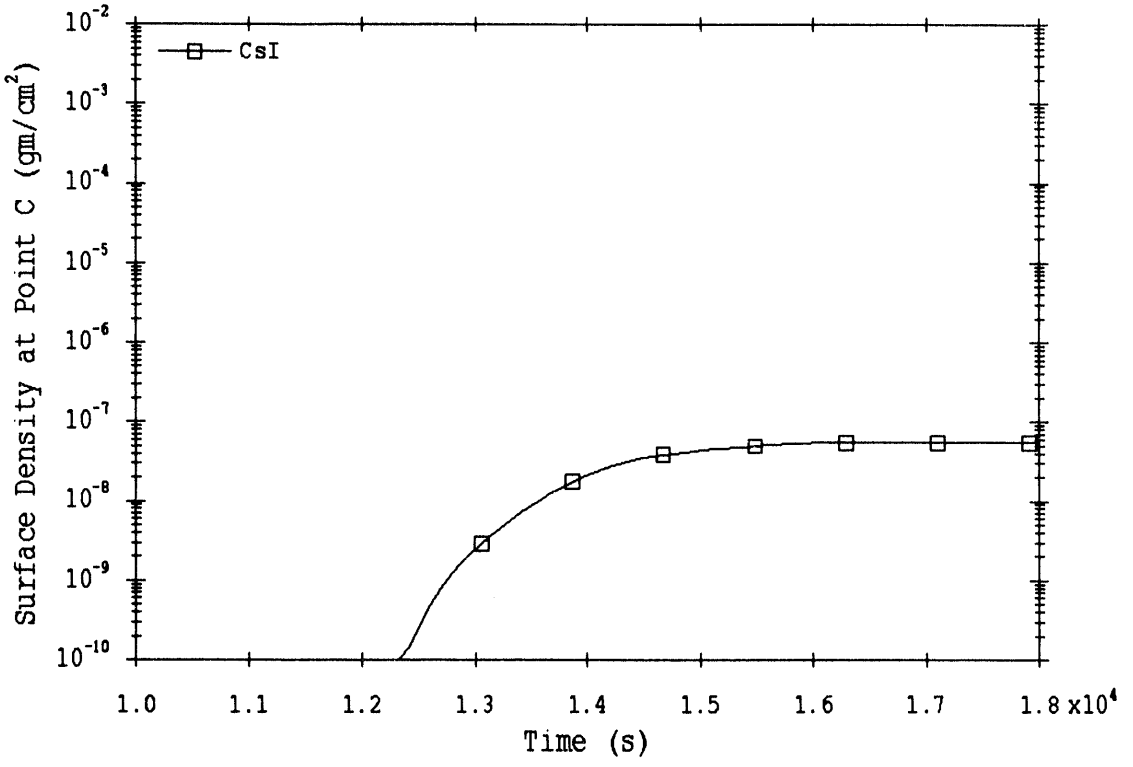

Figure 42. I surface deposit densities at point C in the FPT0 circuit.

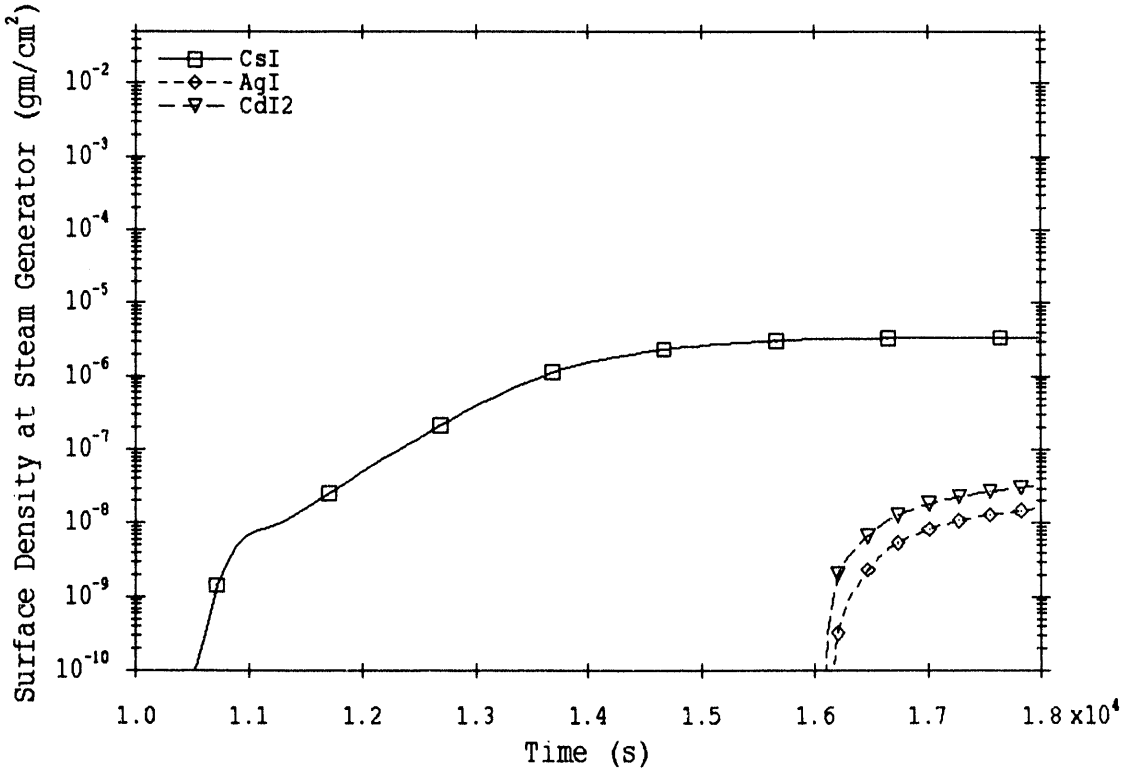

Figure 43. I surface deposit densities at the steam generator in the FPT0 circuit.

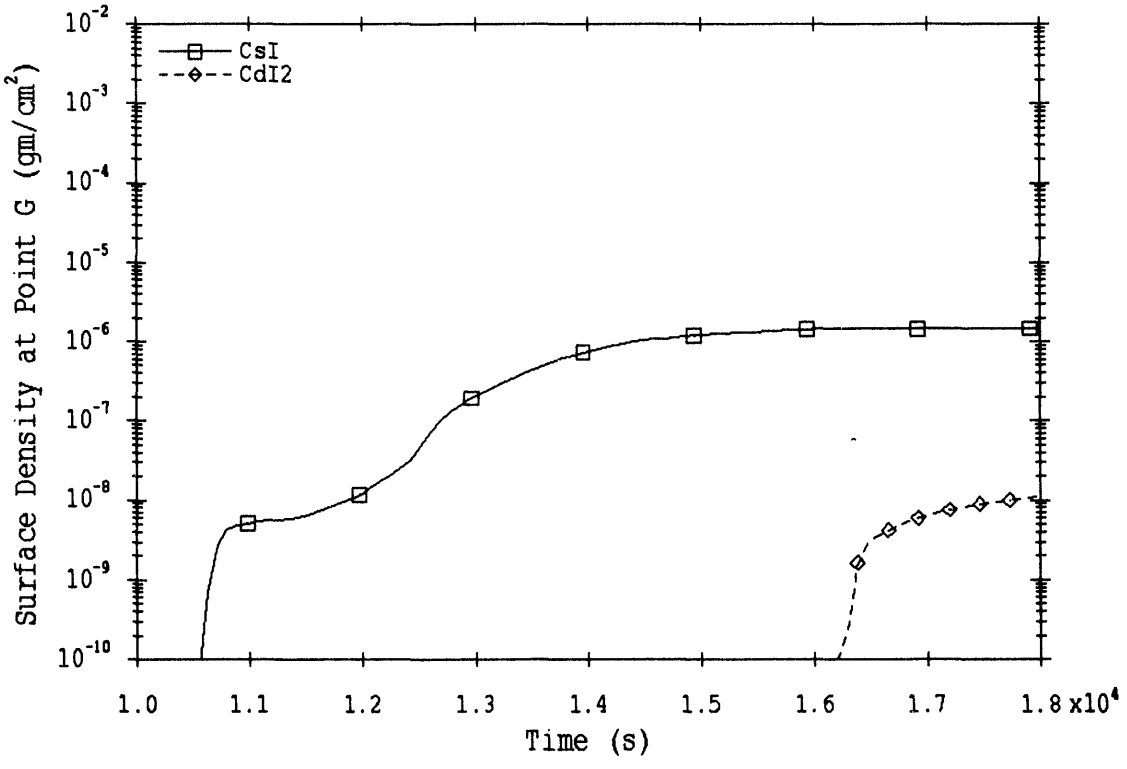

Figure 44. I surface deposit densities at point G in the FPT0 circuit.

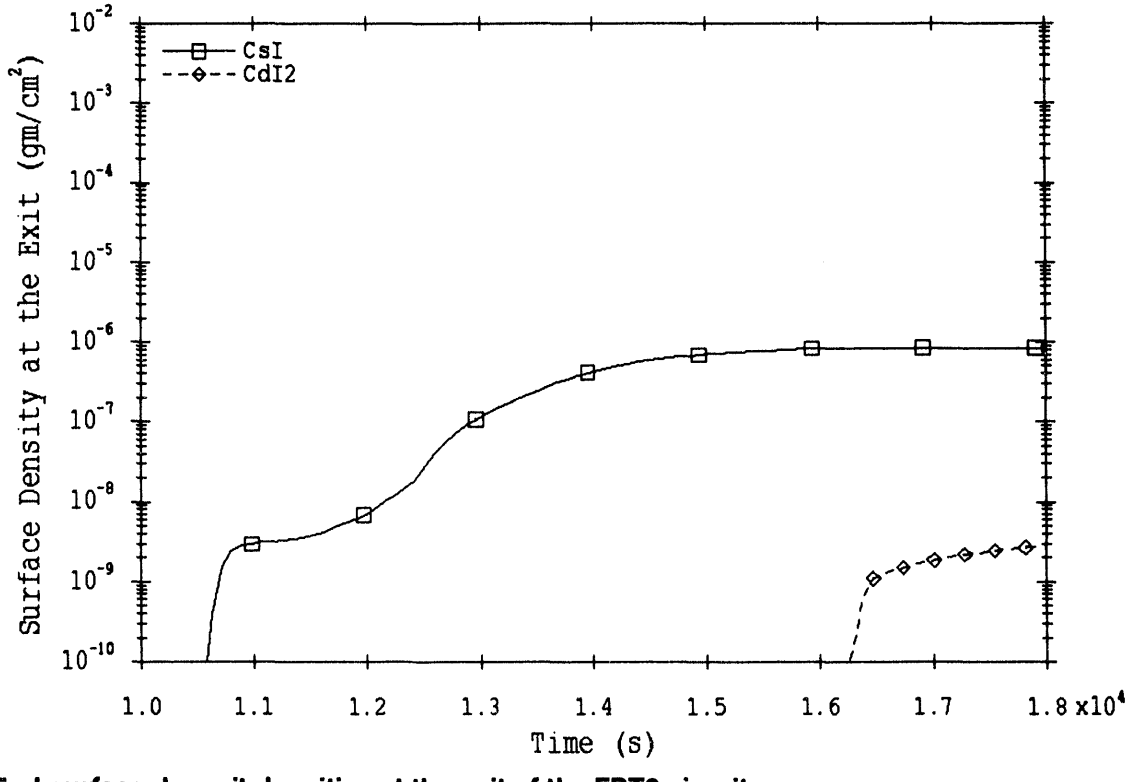

Figure 45. I surface deposit densities at the exit of the FPT0 circuit.

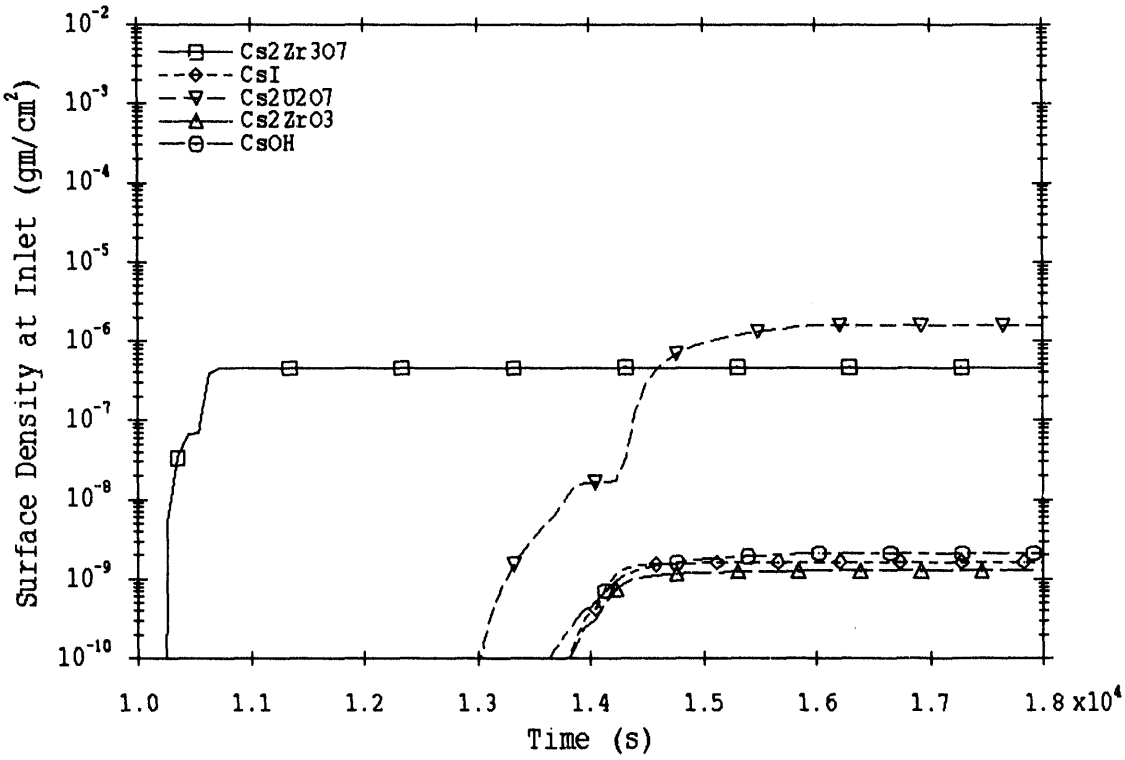

Figure 46. Cs surface deposit densities at the inlet of the FPT0 circuit.

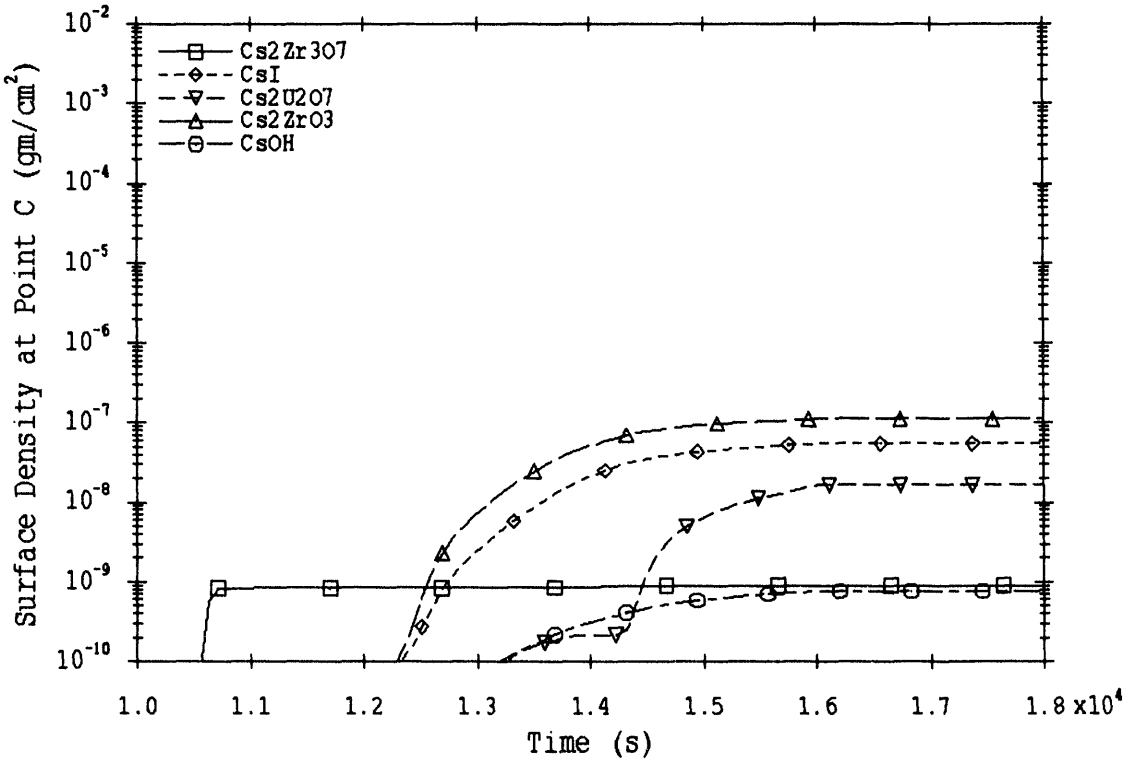

Figure 47. Cs surface deposit densities at point C in the FPT0 circuit.

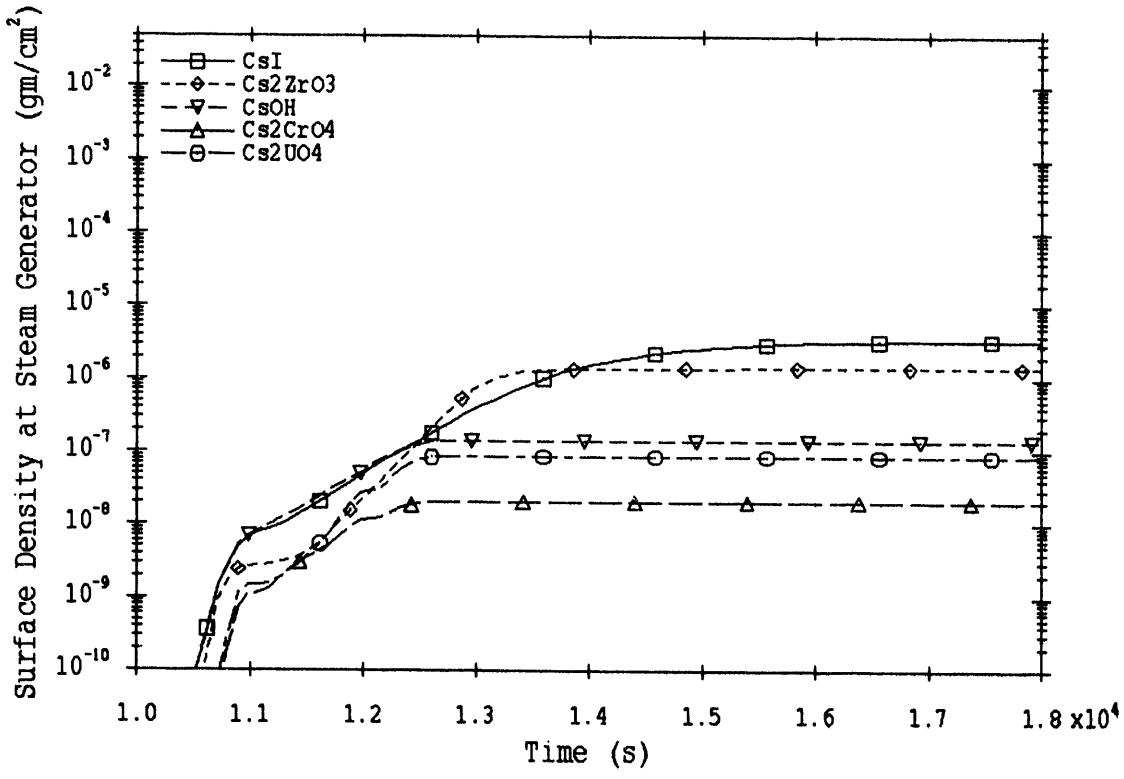

Figure 48. Cs surface deposit densities at the steam generator in the FPT0 circuit.

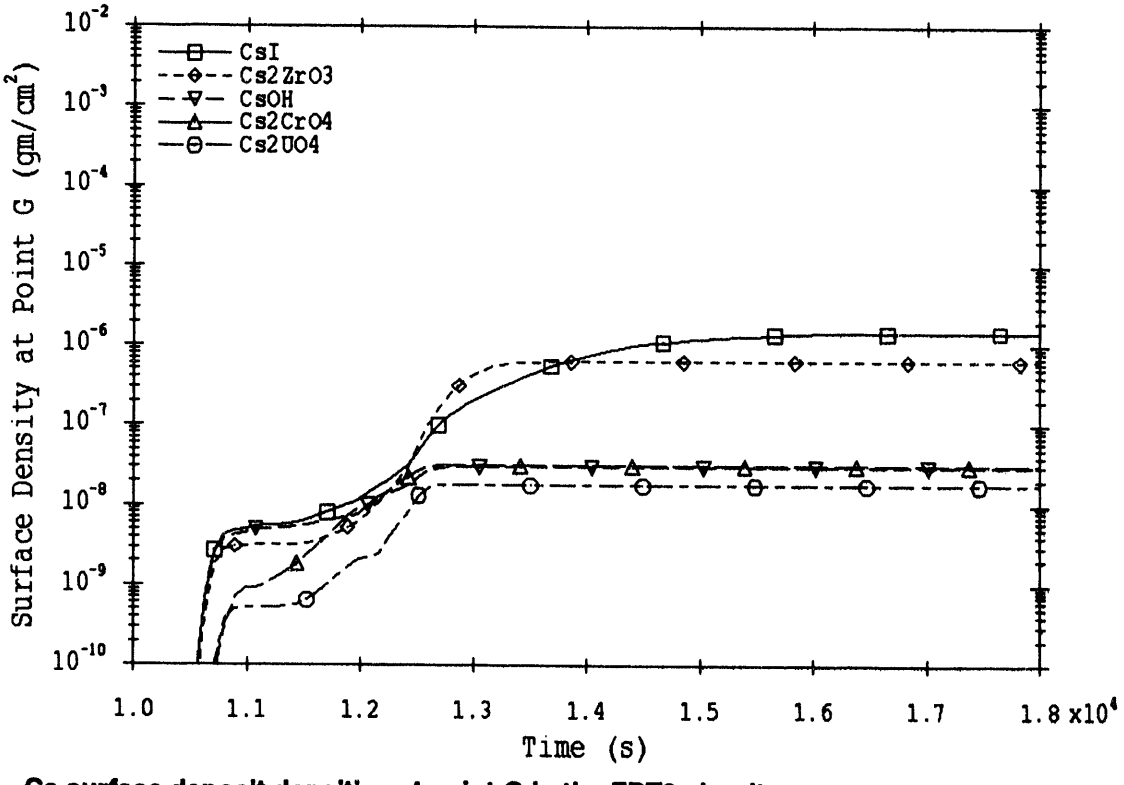

Figure 49. Cs surface deposit densities at point G in the FPT0 circuit.

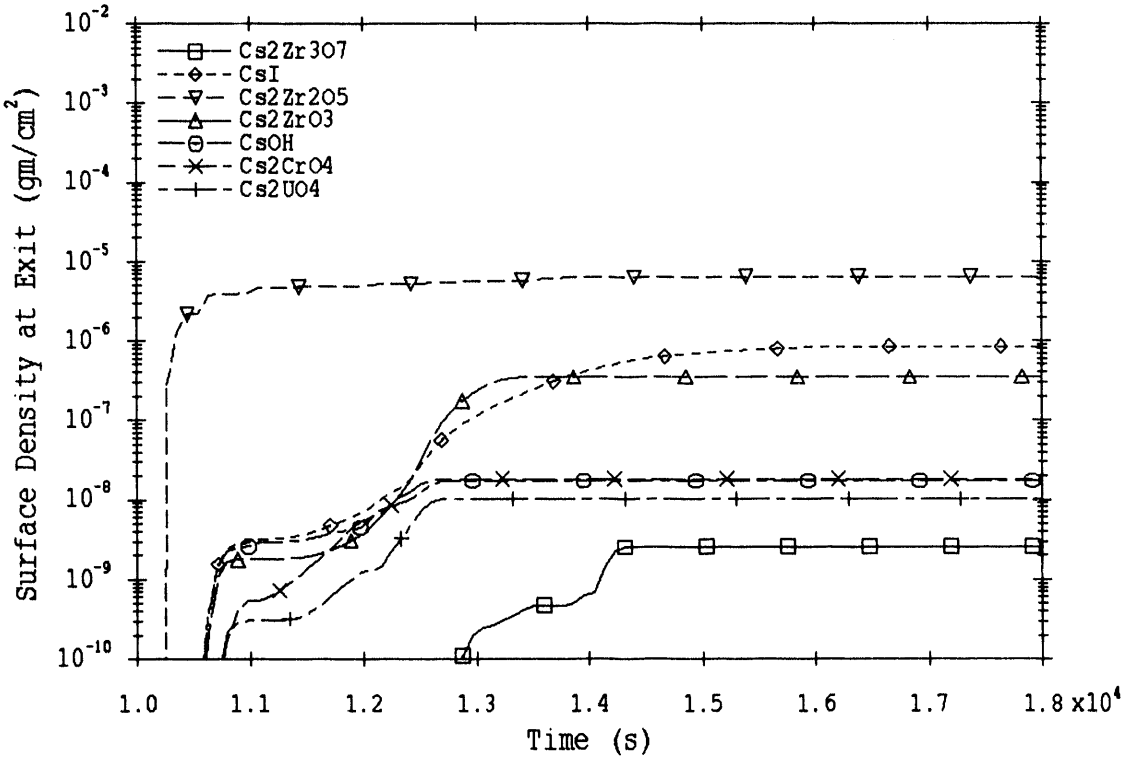

Figure 50. Cs surface deposit densities at the exit of the FPT0 circuit.

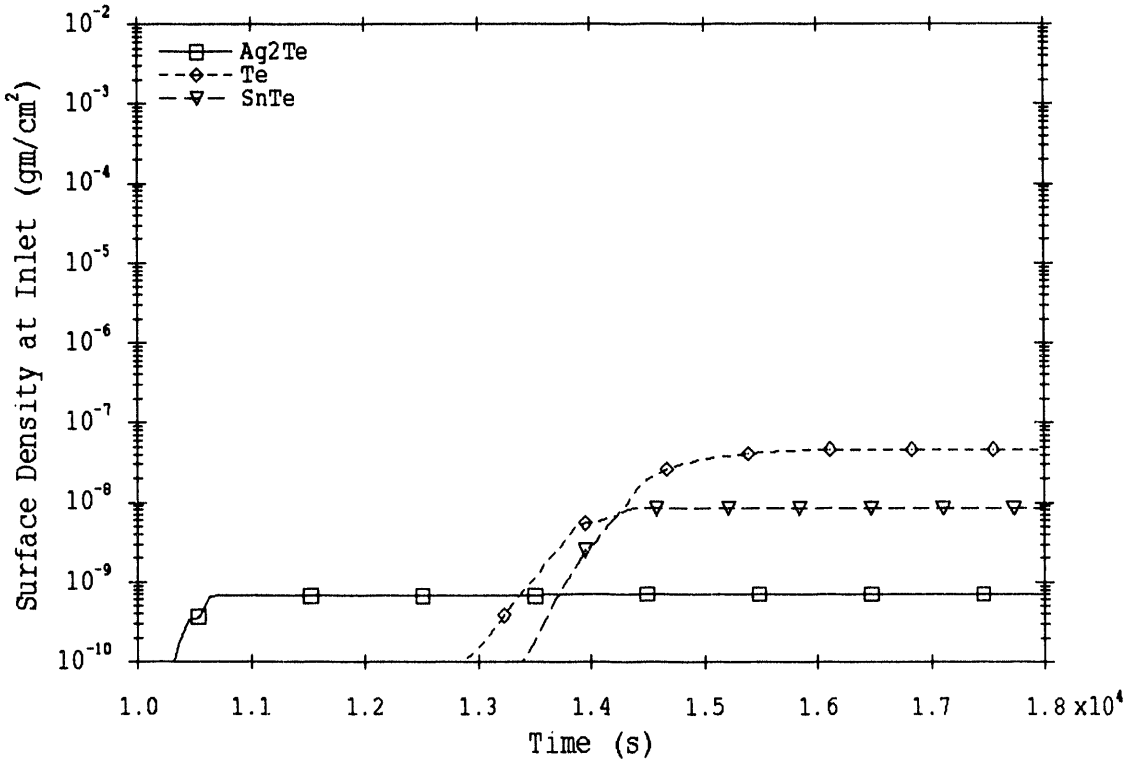

Figure 51. Te surface deposit densities at the inlet of the FPT0 circuit.

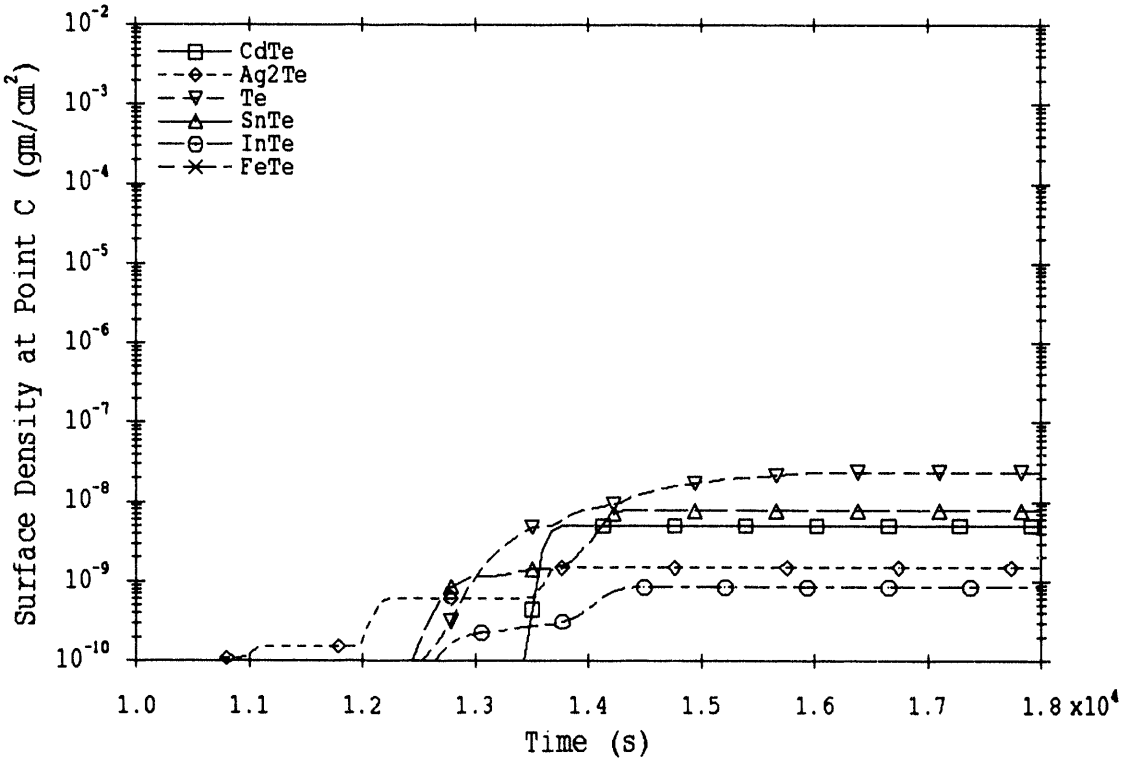

Figure 52. Te surface deposit densities at point C in the FPT0 circuit.

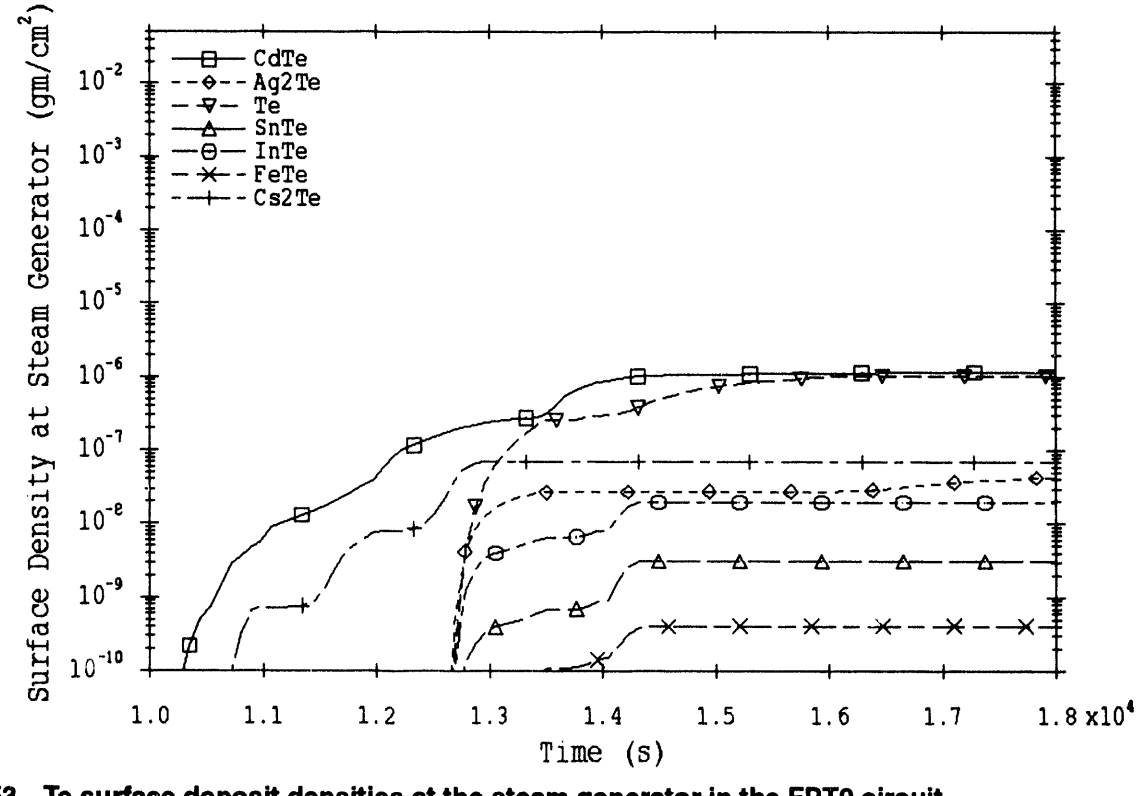

Figure 53. Te surface deposit densities at the steam generator in the FPT0 circuit.

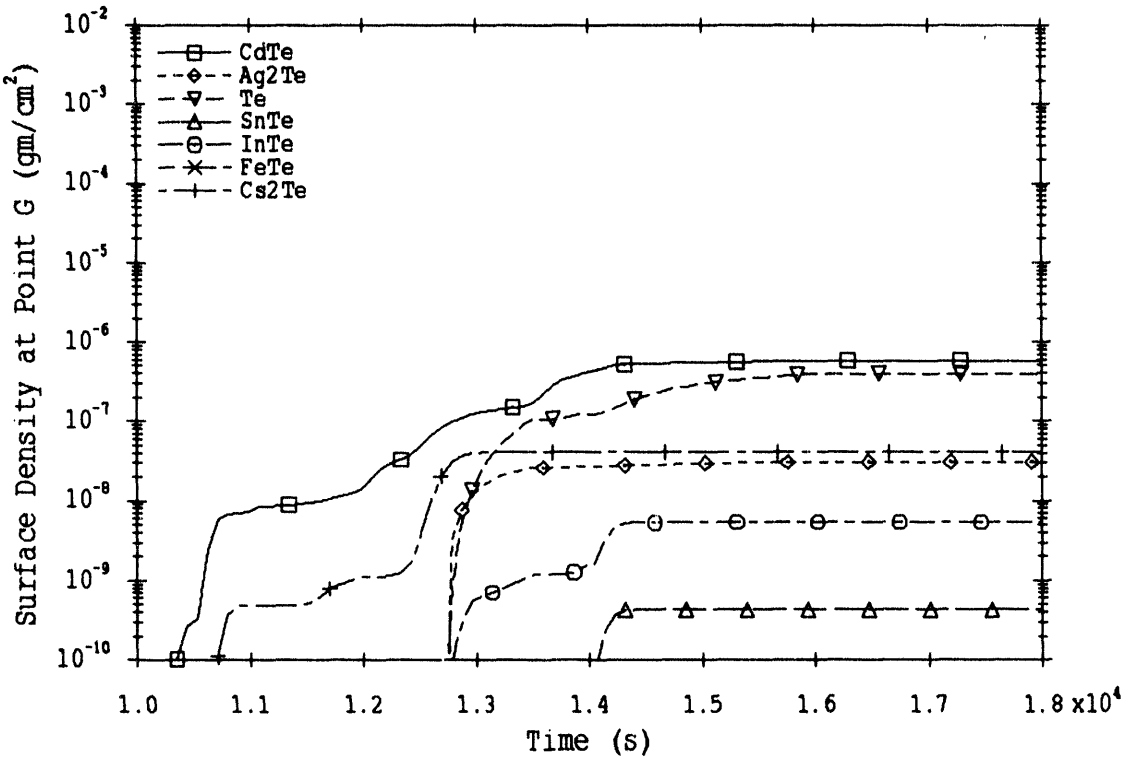

Figure 54. Te surface deposit densities at point G in the FPTO circuit.

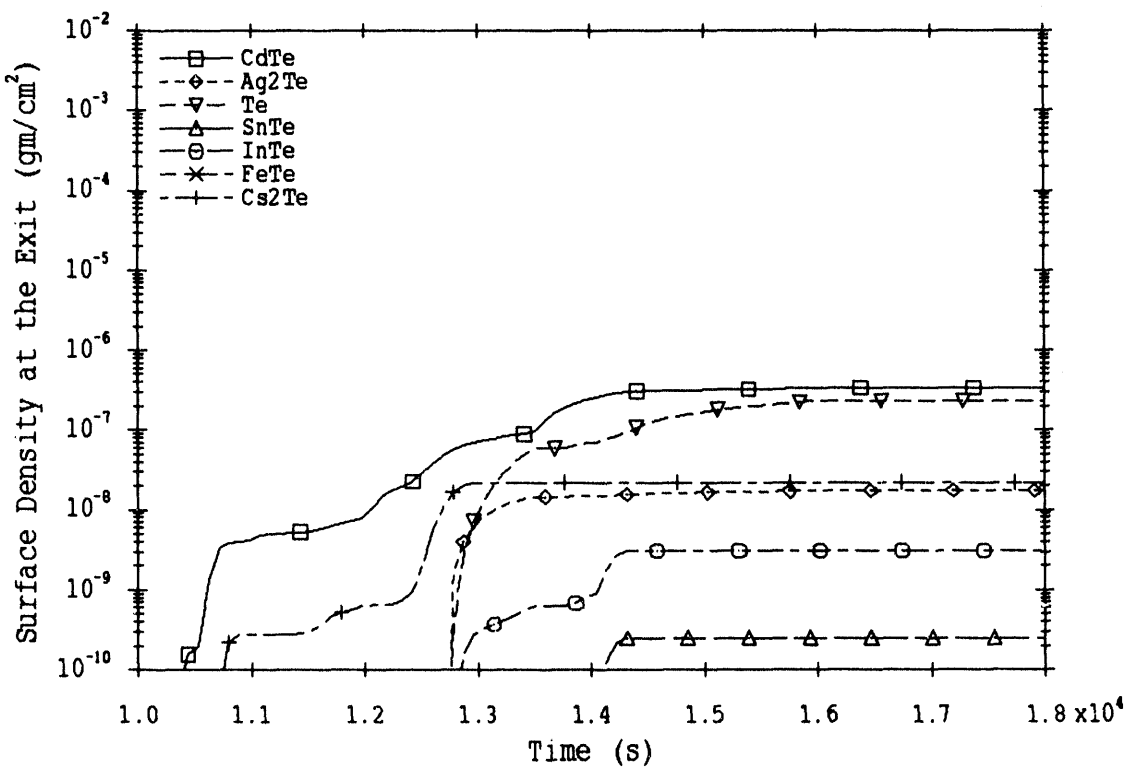

Figure 55. Te surface deposit densities at the exit of the FPTO circuit.

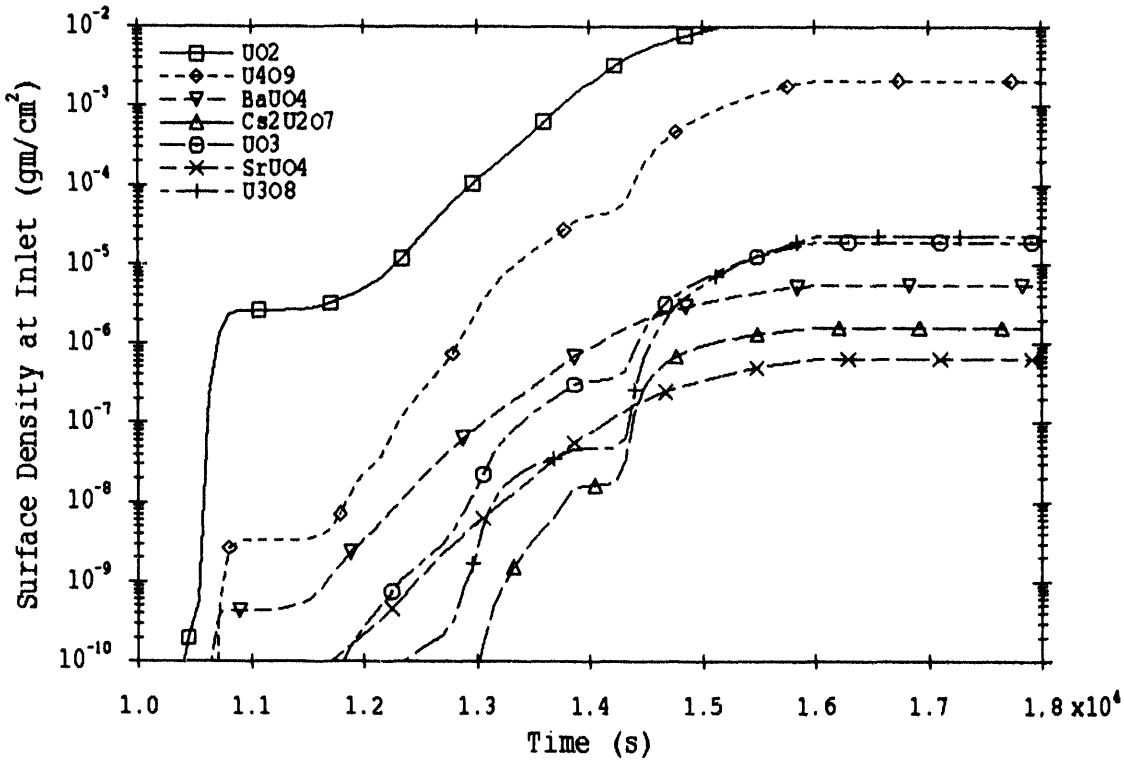

Figure 56. U surface deposit densities at the inlet of the FPTO circuit.

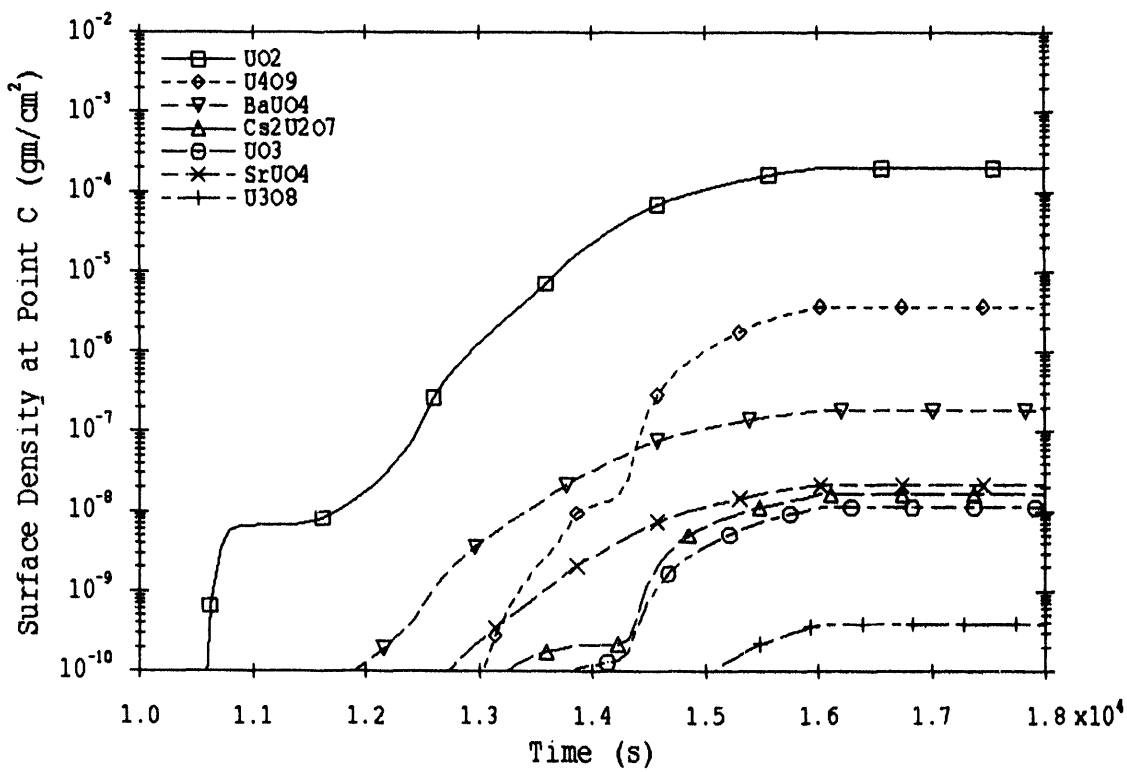

Figure 57. U surface deposit densities at point C in the FPTO circuit.

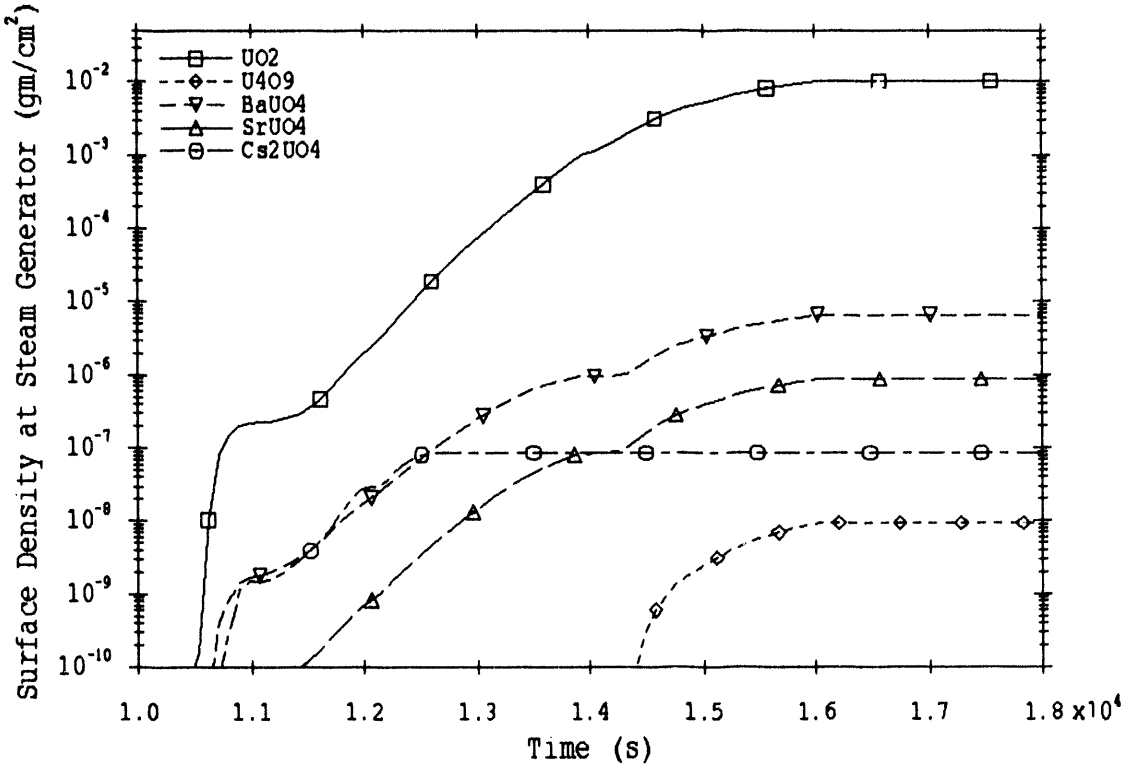

Figure 58. U surface deposit densities at the steam generator in the FPTO circuit.

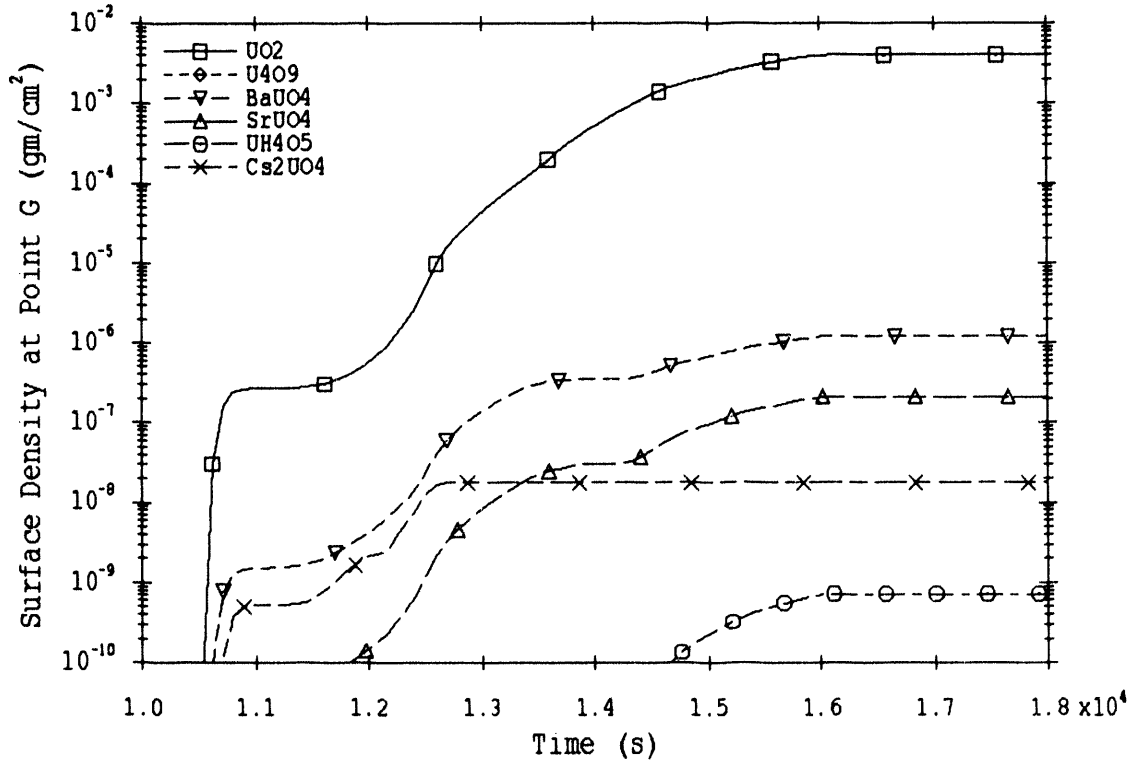

Figure 59. U surface deposit densities at point G in the FPTO circuit.

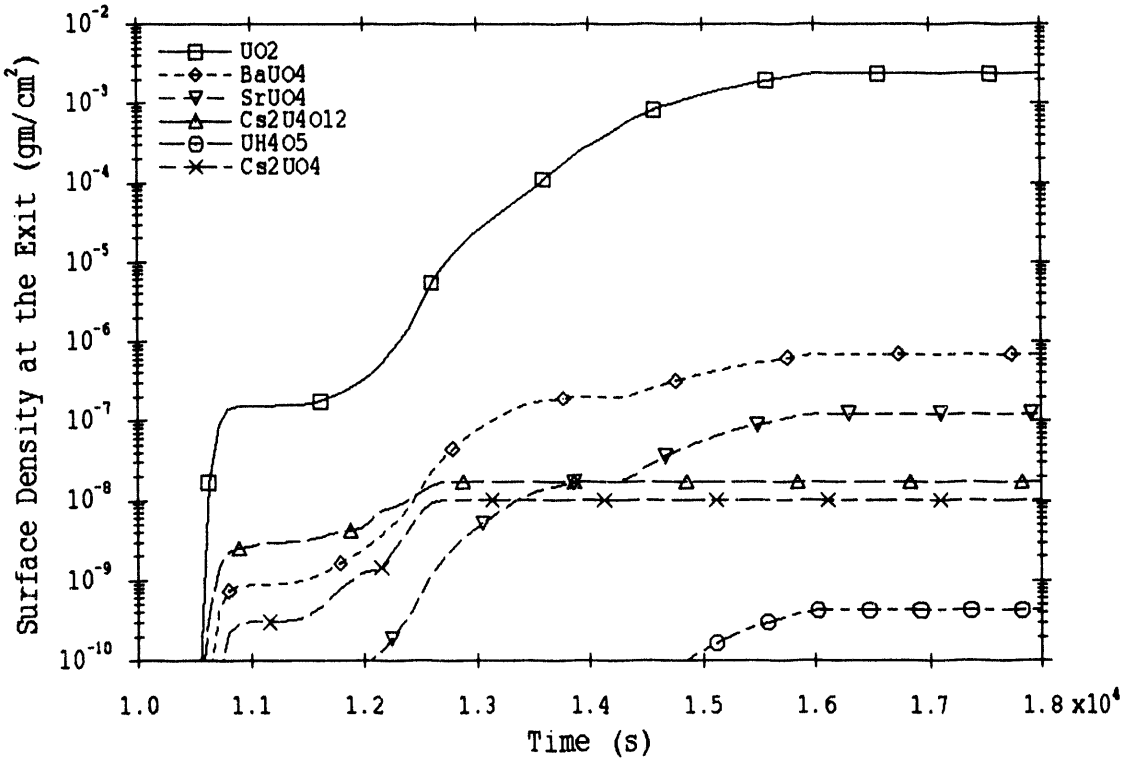

Figure 60. U surface deposit densities at the exit of the FPT0 circuit.

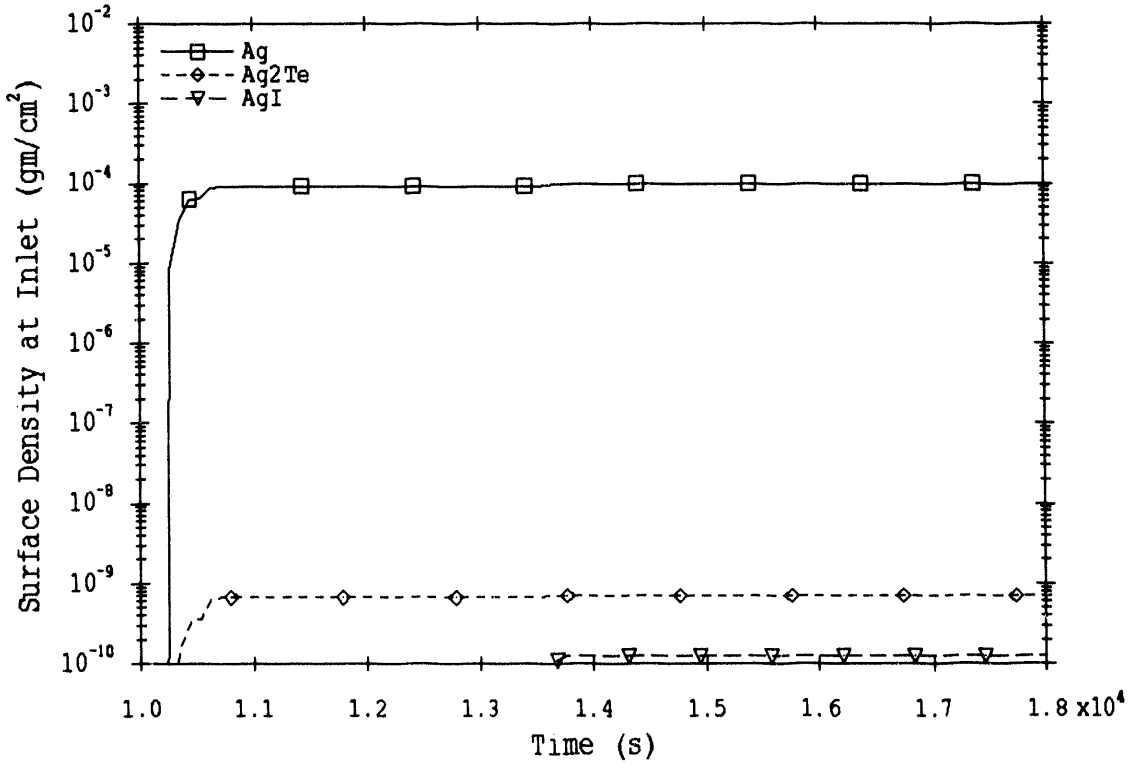

Figure 61. Ag surface deposit densities at the inlet of the FPT0 circuit.

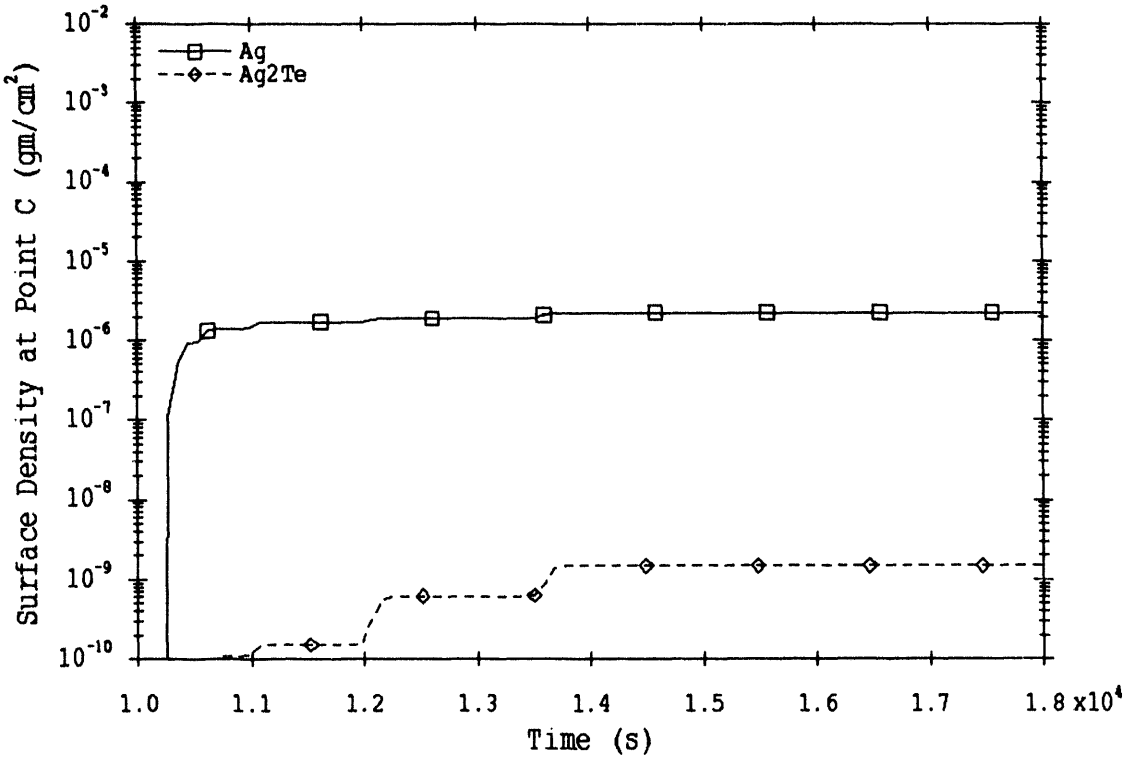

Figure 62. Ag surface deposit densities at point C in the FPT0 circuit.

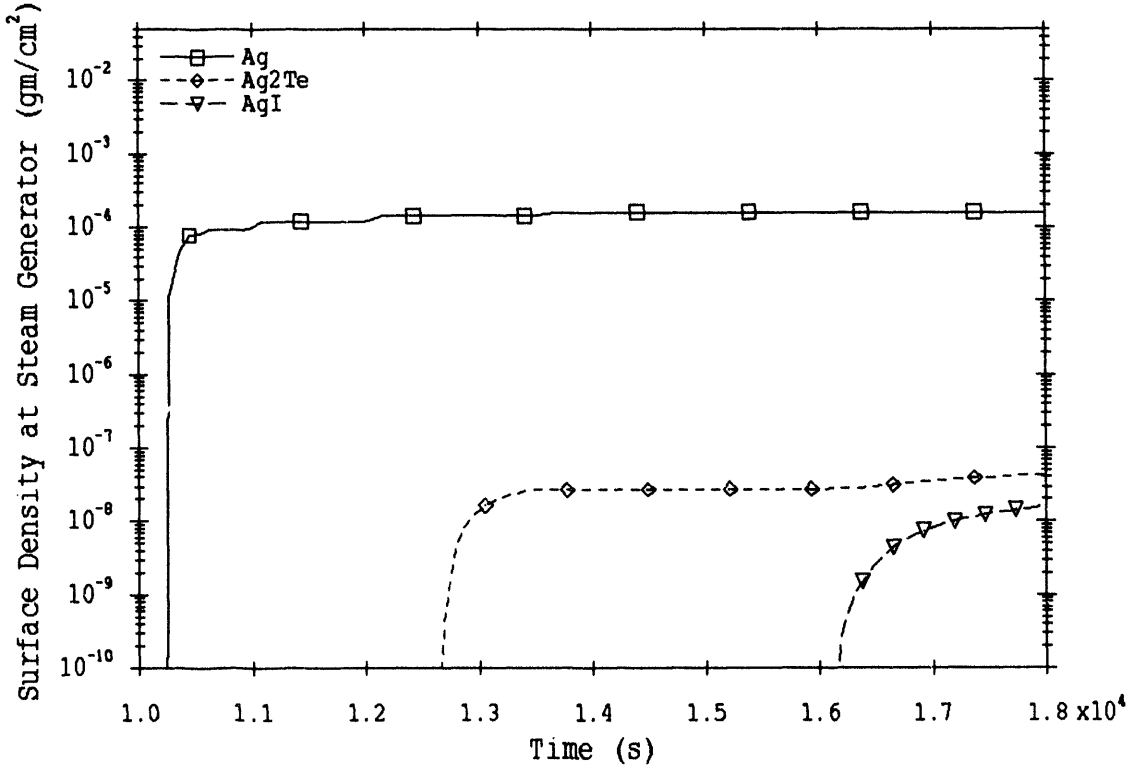

Figure 63. Ag surface deposit densities at the steam generator in the FPT0 circuit.

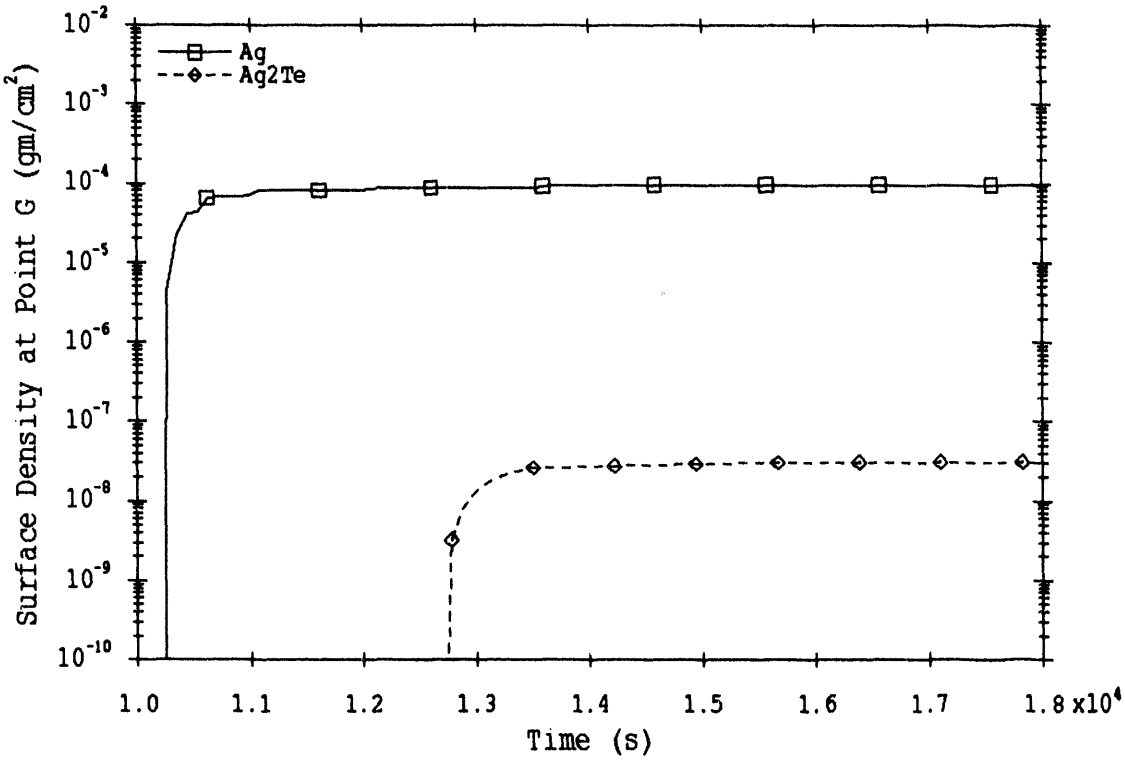

Figure 64. Ag surface deposit densities at point G in the FPTO circuit.

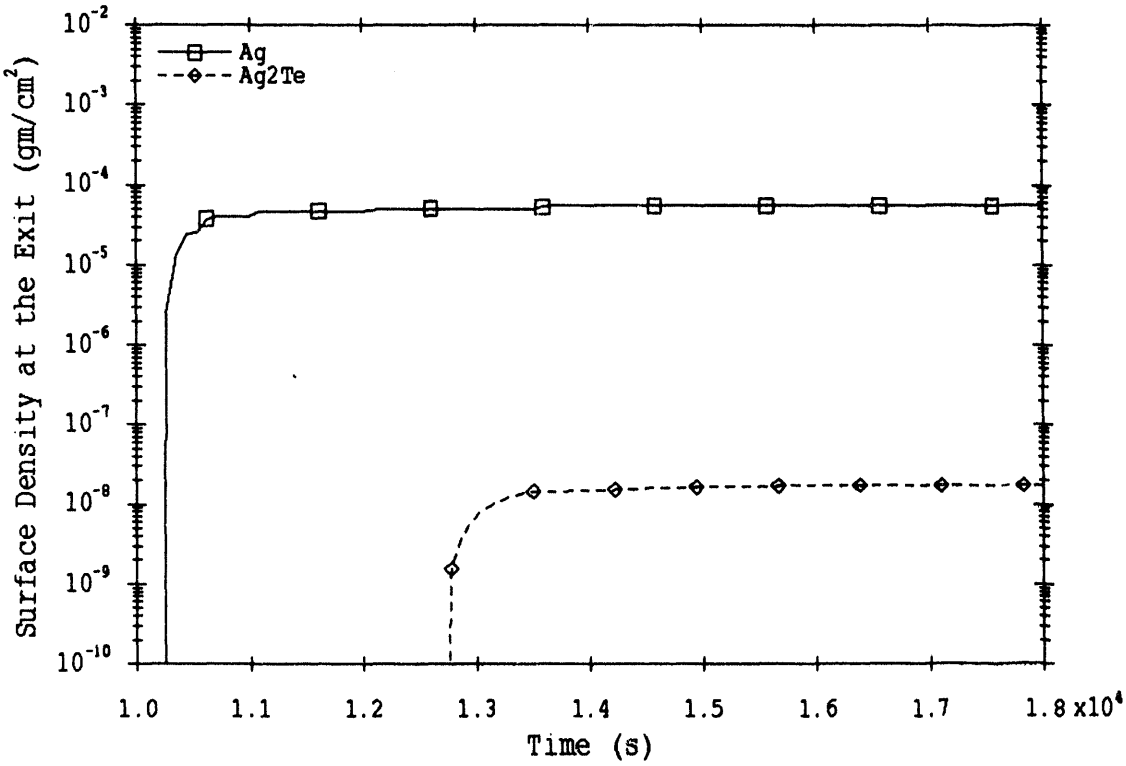

Figure 65. Ag surface deposit densities at the exit of the FPTO circuit.

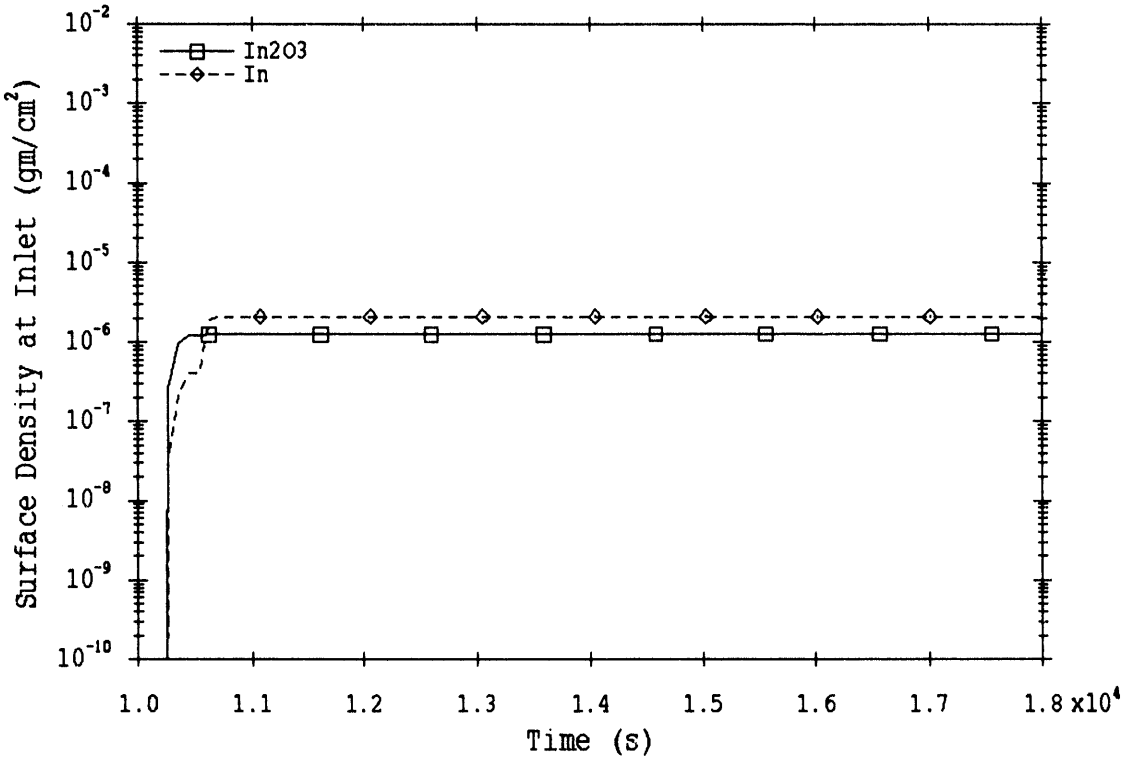

Figure 66. In surface deposit densities at the inlet of the FPT0 circuit.

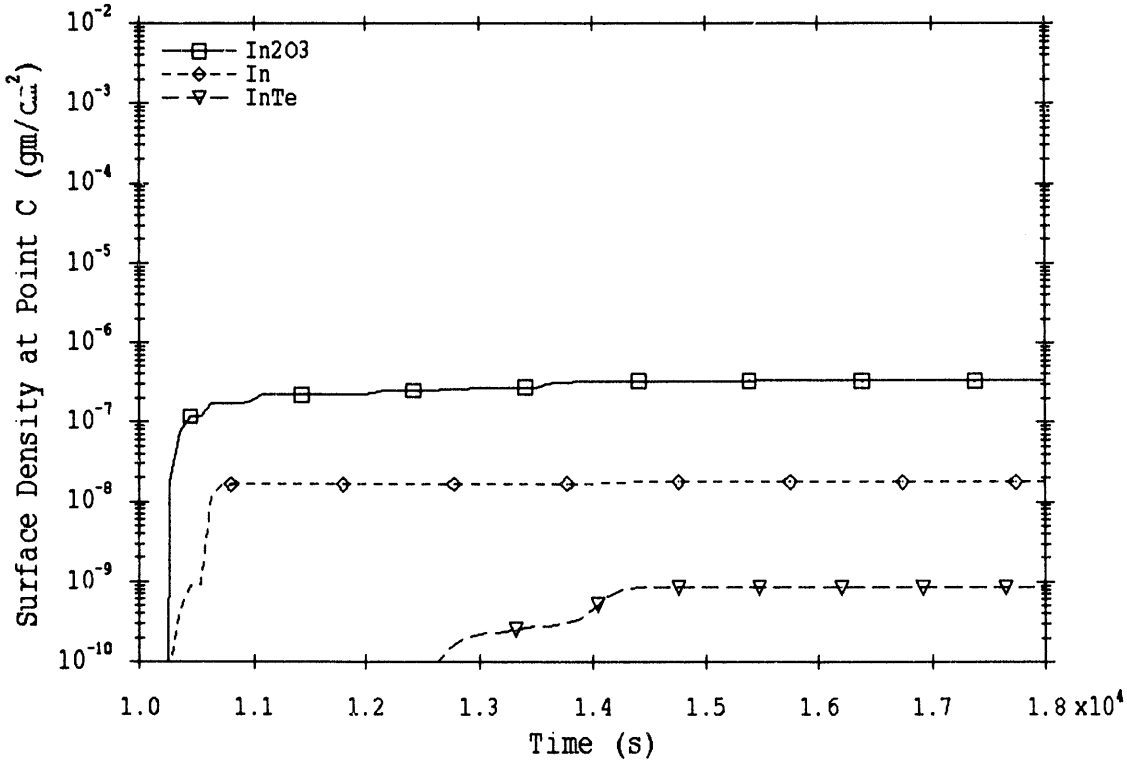

Figure 67. In surface deposit densities at point C in the FPT0 circuit.

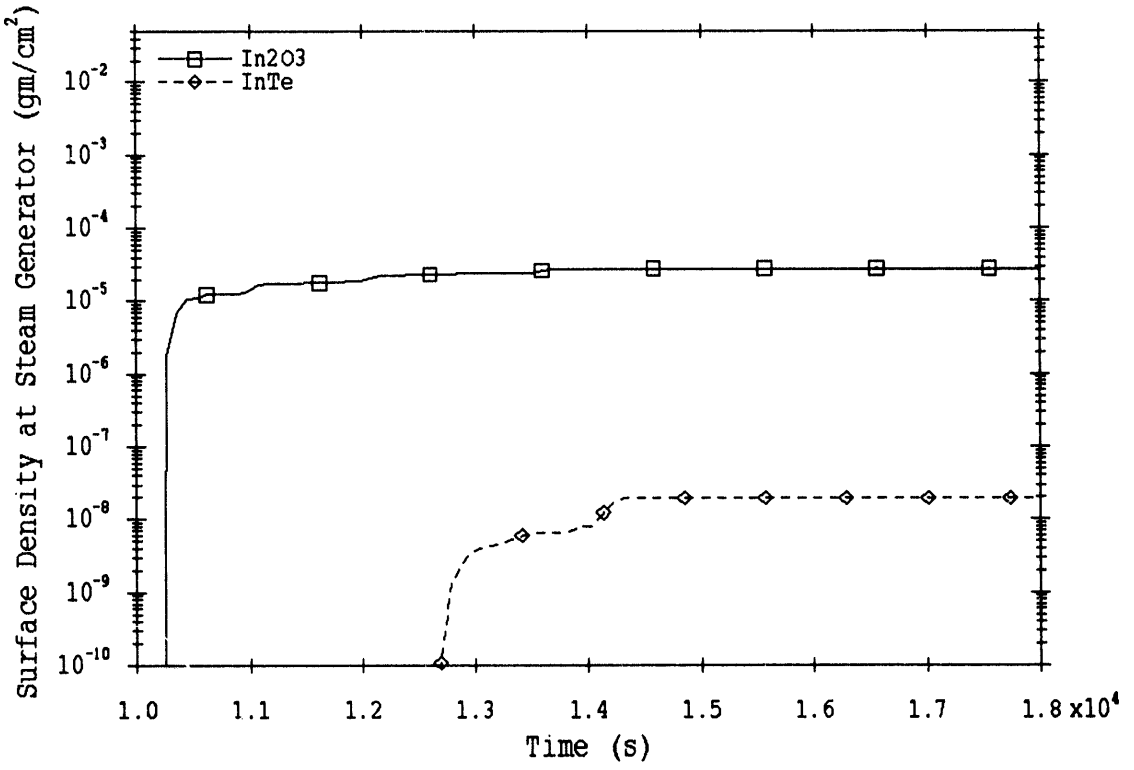

Figure 68. In surface deposit densities at the steam generator in the FPT0 circuit.

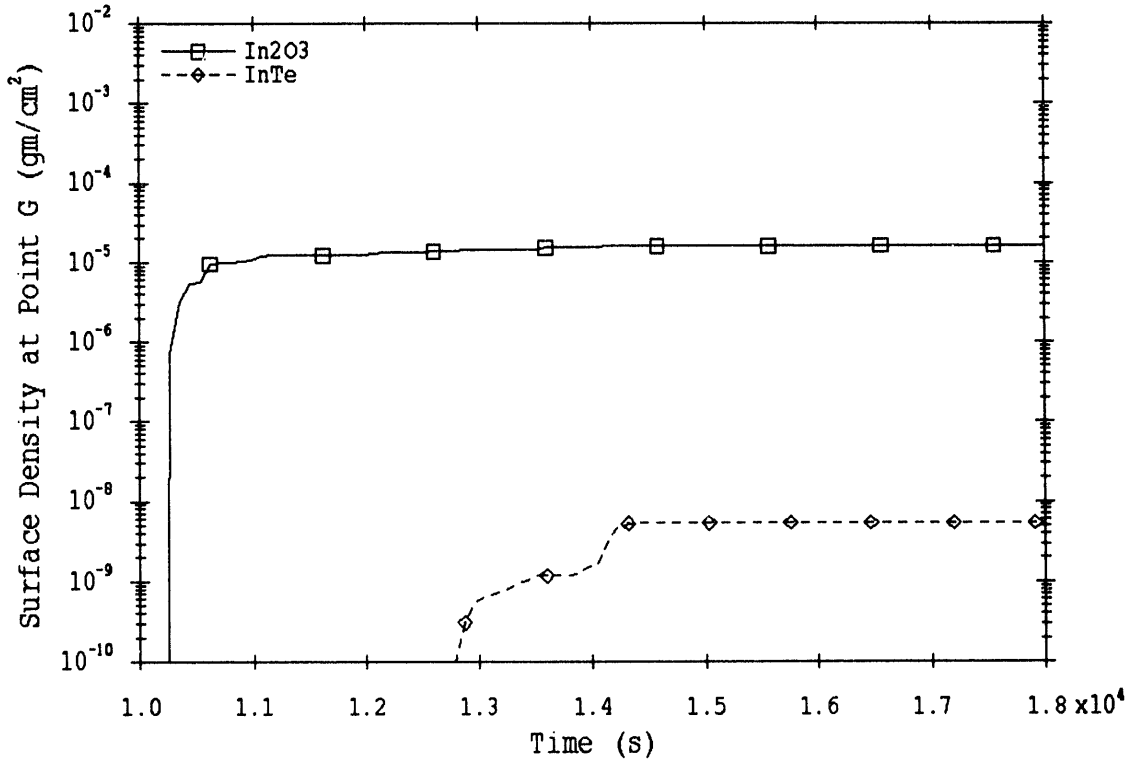

Figure 69. In surface deposit densities at point G in the FPT0 circuit.

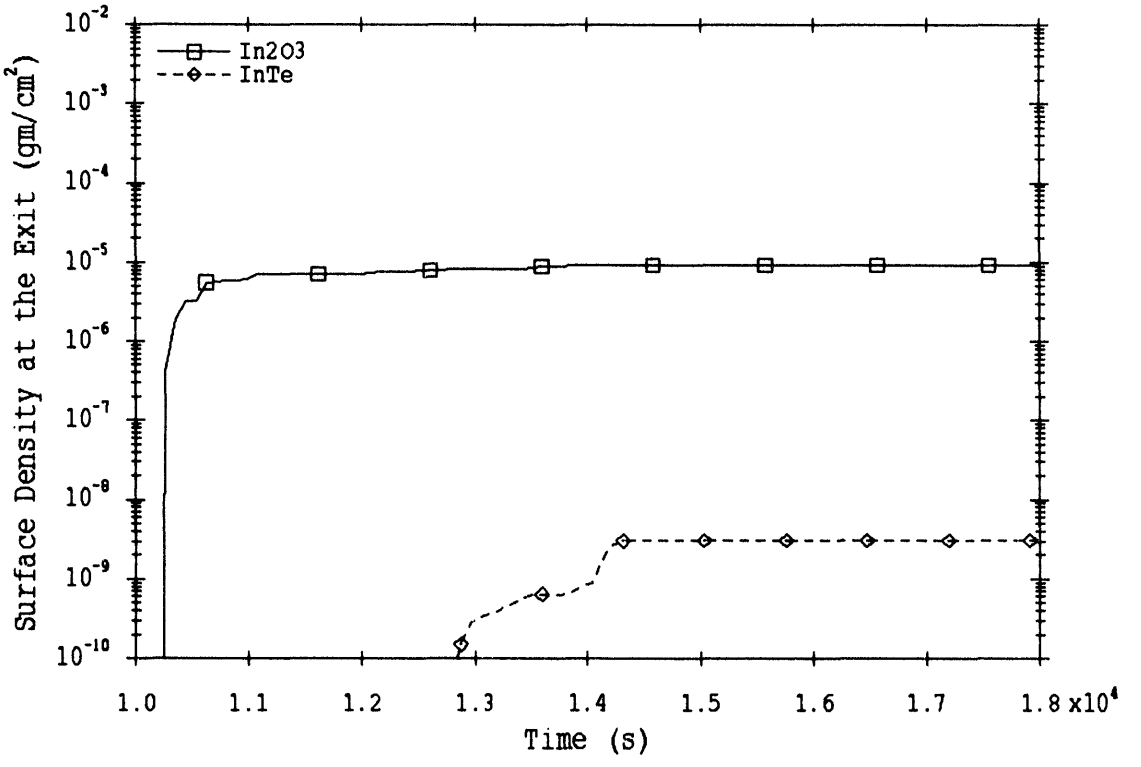

Figure 70. In surface deposit densities at the exit of the FPT0 circuit.

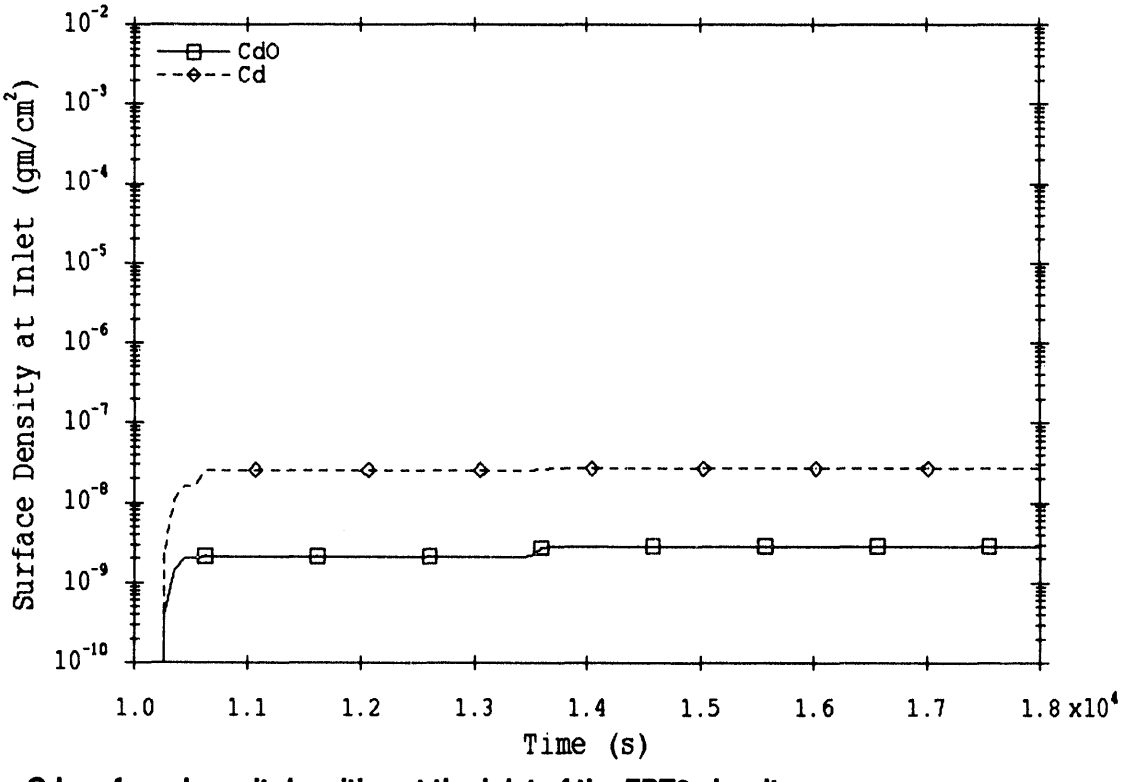

Figure 71. Cd surface deposit densities at the inlet of the FPT0 circuit.

both important at the inlet; In_2O_3 dominates throughout the rest of the circuit.

Cadmium deposit densities are shown in Figures 71 through 75. At the inlet, Cd(c) is the dominant species; at point C, Cd(c), CdTe(c), and CdO(c) are important; and at the steam generator and beyond, CdO(c) and Cd(c) dominate.

The overall retentions in the FPT0 primary circuit are summarized by element in Table 5. The masses released into the circuit are those predicted by CORSOR-M and match the values in Table 4. The masses released into containment and fractions retained in the circuit are those predicted by VICTORIA-92. As expected, all of the noble gases pass through the circuit and into containment. The other elements are retained between 32% and 51% in the circuit. In general, the elements forming less volatile species are retained at a higher fraction and those forming more volatile species are retained at a lower fraction. The predicted range of retentions is relatively narrow, less than a factor of two. This is because most of the deposition phenomena in FPT0 are governed by aerosol physics (primarily thermophoresis) and transport. If vapor condensation had been dominant for some of the elements, as it was in the FALCON-ISP experiments [10], the retentions would have been more varied. For example, measured retentions varied from 13% for B to 61% for Ag in FAL-ISP 1 and from 2% for B to 50% for I in FAL-ISP 2. VICTORIA predictions ranged from 16% to 49% and from 10% to 35% for these two tests, respectively.

Table 5: Summary of Retention in and Release from the FPT0 Primary Circuit

Element	Released from Core into Circuit (g) as predicted by CORSOR-M	Released from Circuit into Containment (g)	Retained in Circuit (%)
U	140	70	51
Cs	0.12	0.061	48
I	0.030	0.016	46
Te	0.040	0.020	50
Ba	0.049	0.024	51
Sr	0.0041	0.0020	51
Xe	0.28	0.28	0
Kr	0.027	0.027	0
Ag	3.9	2.3	41
In	0.50	0.31	38
Cd	10.	6.8	32
Sn	24.	12.	50
Zr	0.35	0.17	51
Fe	1.7	0.83	51
Cr	1.6	0.77	51
Mn	0.0019	0.0012	39
Ni	0.00013	0.000083	38

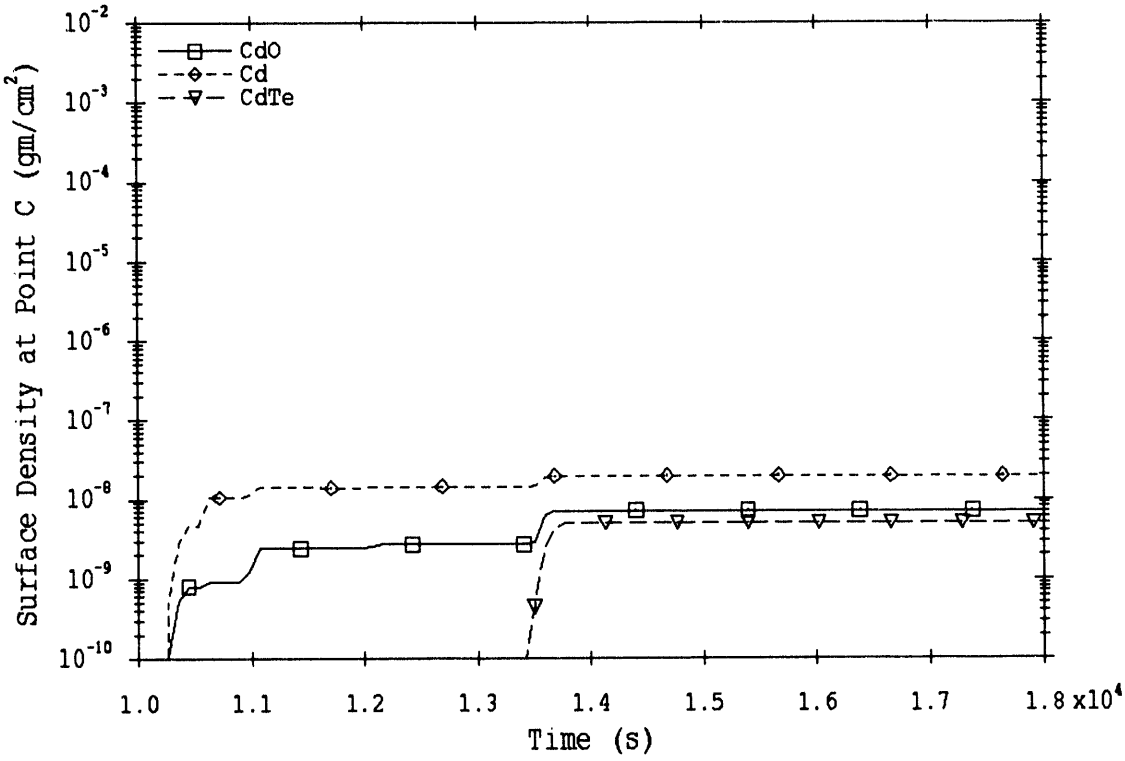

Figure 72. Cd surface deposit densities at point C in the FPT0 circuit.

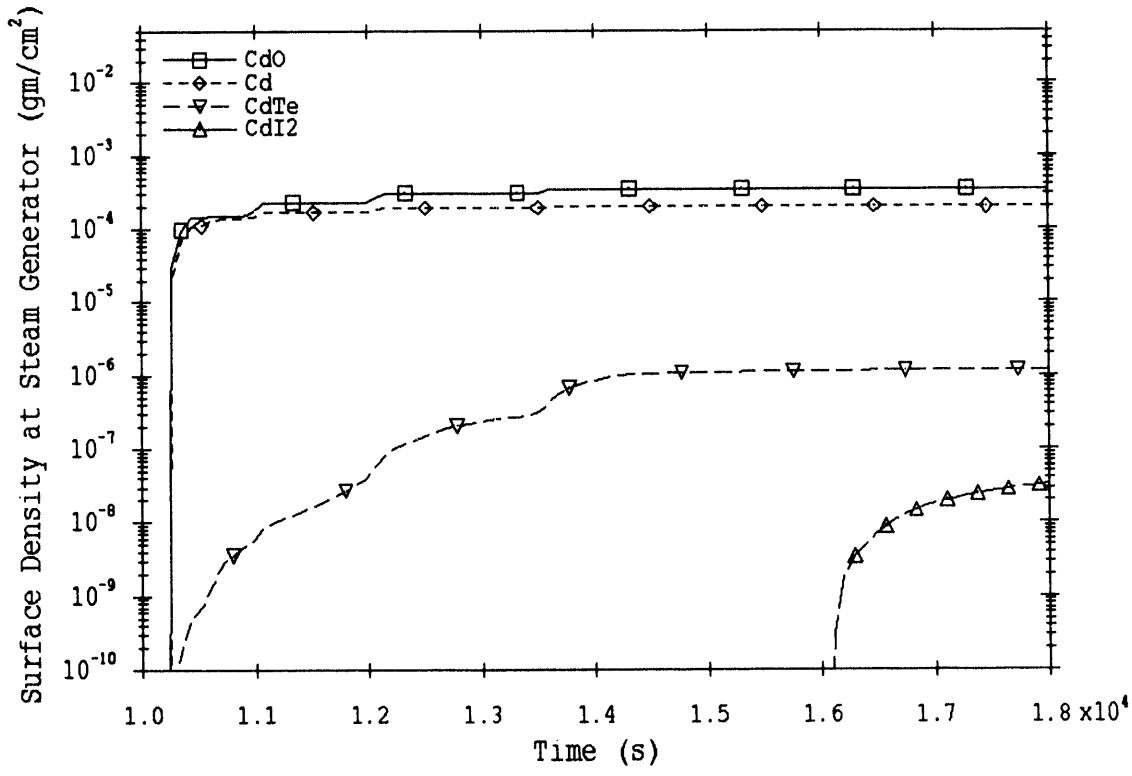

Figure 73. Cd surface deposit densities at the steam generator in the FPT0 circuit.

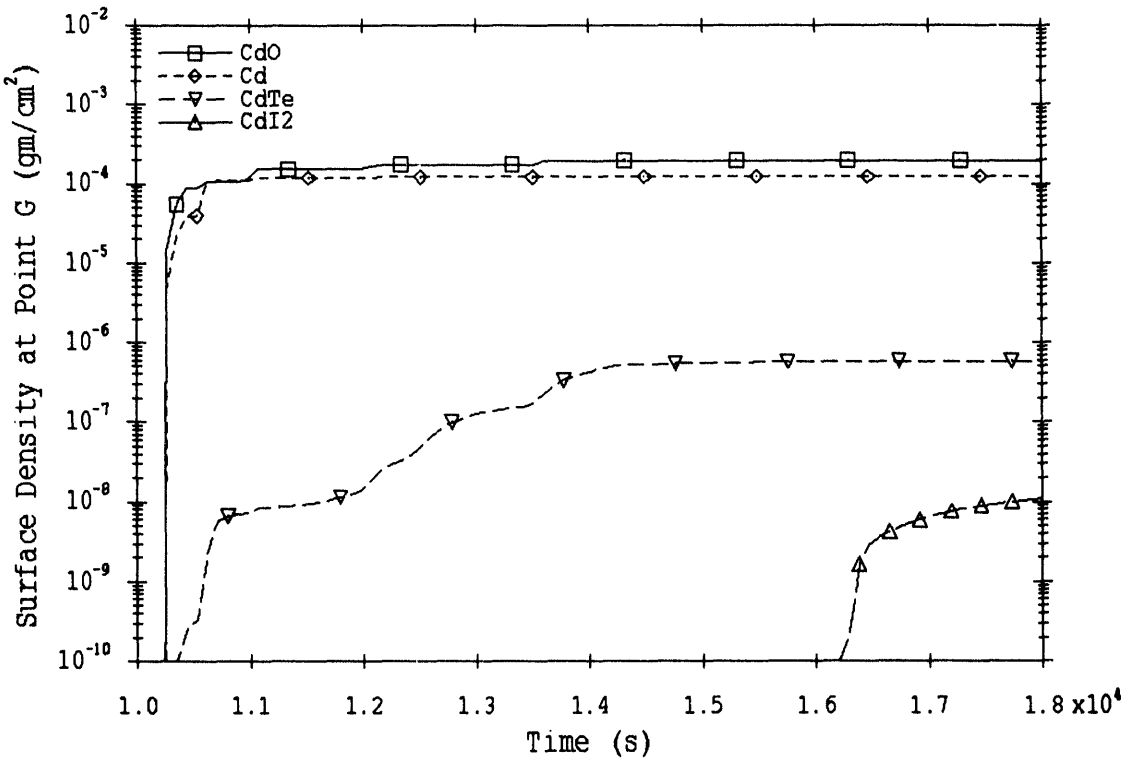

Figure 74. Cd surface deposit densities at point G in the FPT0 circuit.

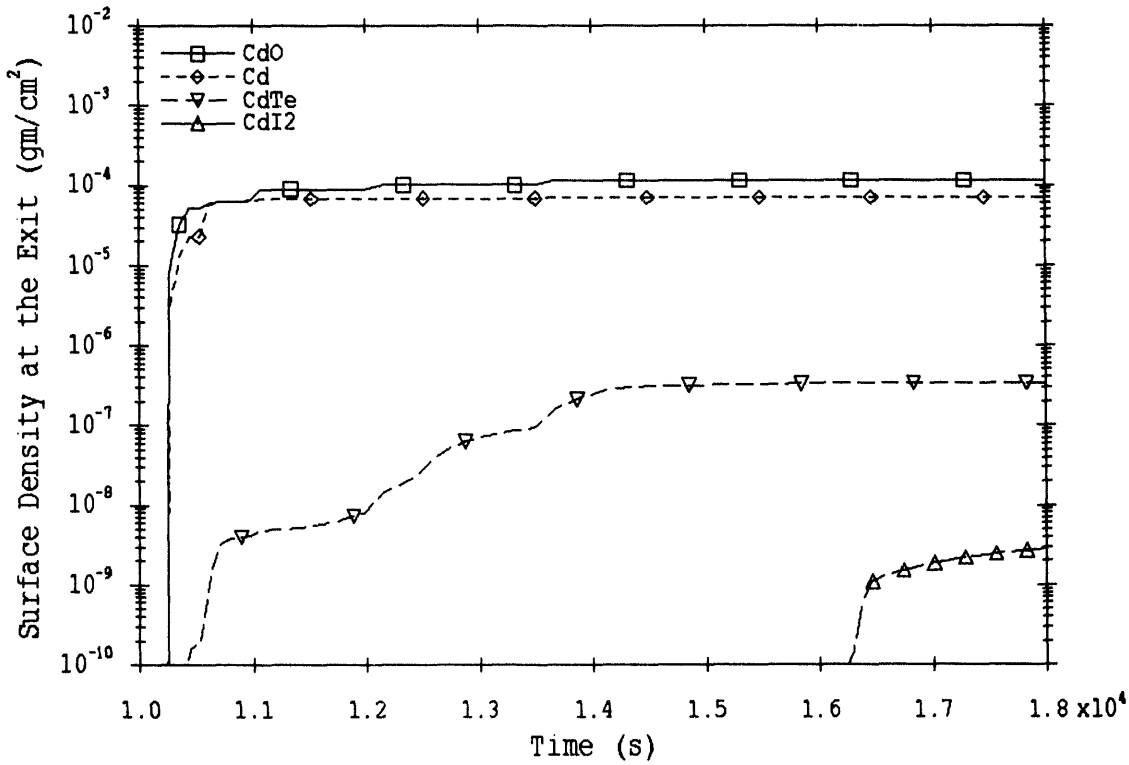

Figure 75. Cd surface deposit densities at the exit of the FPT0 circuit.

5.0 Conclusions

Analyses of the PHEBUS FPT0 fuel bundle and primary circuit have been performed with VICTORIA-92. Results for elemental releases from the fuel and control rods have been compared with ones provided by ISPRA using CORSOR-M with the Petti correlation [7]. Specific conclusions are drawn in the following two subsections.

5.1 FPT0 Fuel Bundle

The fission product releases predicted by VICTORIA-92 differ substantially from those predicted by CORSOR-M using the Petti correlation for release of the volatiles [7]. The VICTORIA-92 releases begin earlier in the transient. The predicted release fractions also differ. The most notable difference is for uranium. CORSOR-M predicts that U release will dominate not only the fission product releases but also those of the control rod elements; VICTORIA-92 predicts that U will be released in similar abundance as the control rod elements. The difference in the predictions is about two orders of magnitude. Most of the other differences are probably due to the low burn-up of the FPT0 fuel and to modeling differences in the treatment of melting of the fuel cladding and loss of the control rod alloy to colder regions of the reactor.

5.2 FPT0 Primary Circuit

A large quantity of predicted data has been presented for the FPT0 primary circuit. These include aerosol size distribution characteristics, the location and speciation of deposits, and the speciation of fission products in the circuit and of those entering containment. These data should be useful for calibration of aerosol instrumentation and for optimizing post-test chemical analyses.

VICTORIA-92 predicts that most of the uranium released from the fuel is deposited as UO_2. With time at ambient conditions, it should become further oxidized to form U_3O_8. Thus, post-test chemical analyses should detect U_3O_8 rather than UO_2 in the primary circuit.

Other detectable species in the primary circuit should include CsI, $Cs_2Zr_3O_7$, Te, CdTe, $BaUO_4$, $SrUO_4$, Ag, In_2O_3, In, CdO, and Cd. These species should be measured in post-test chemical analyses. VICTORIA-92 predictions show the portions of the circuit where each of these species should be relatively abundant. For most of the species, the steam generator tube is a region of high deposition. This is because the large temperature difference between the gas and steam-generator-tube surface should drive thermophoretic deposition there.

On-line sampling should be able to measure the aerosol size distributions during the test, especially between 13,000 and 16,000 s. Prior to this time, significant aerosols should be present only when the control rod bursts. One caveat is that CORSOR-M appears to predict unusually high releases of UO_2 from the fuel. If this prediction is in error, aerosol concentrations, sizes, and particle densities may be somewhat smaller than predicted. This uncertainty could be resolved by rerunning this calculation using VICTORIA-92 predictions of releases from the test section as input to the circuit.

The predictions indicate that revaporization will be an important phenomenon during the FPT0 test. Materials deposited in the early and middle part of the transient revaporize and flow into containment well after reactor shutdown. This should be observable during the test if on-line measurements are continued after reactor shutdown. Measurements of this kind should prove useful for assessment of the chemistry models in VICTORIA-92. Further, measurements of fission products in the primary circuit after reactor shutdown may prove to be one of the most useful to be made during FPT0. No other upcoming test offers the possibility to collect this type of revaporization data with a prototypical mix of elements. This opportunity should not be missed.

VICTORIA-92 predicts that chemical speciation for many of the elements changes dramatically along the primary circuit. In part, these changes in speciation are real and important. However, one weakness in VICTORIA-92 may call into question some of the predictions of speciation in the steam generator and cold leg. Below temperatures of about 800 K, the assumption of thermodynamic equilibrium is not valid. The circuit temperature falls well below 800 K in the steam generator and in the cold leg leading to containment. The effect

on the VICTORIA-92 predictions of imposing thermodynamic equilibrium in this part of the circuit is not known. In principle, speciation should be quickly "frozen" as temperatures fall below 800 K and only phase changes should continue to take place. This would probably lead to a larger set of species entering containment than is indicated here. It would be desirable to assess the effect of a "frozen chemistry" model on the FPT0 circuit analysis.

6.0 References

1. T. J. Heames, D. A. Williams, N. E. Bixler, A. J. Grimley, C. J. Wheatley, N. A. Johns, P. Domagala, L. W. Dickson, C. A. Alexander, I. Osborn-Lee, S. Zawadzki, J. Rest, A. Mason, R. Y. Lee, "VICTORIA: A Mechanistic Model of Radionuclide Behavior in the Reactor Coolant System Under Severe Accident Conditions," NUREG/CR-5545, SAND90-0756 Rev. 1, Sandia National Laboratories, Albuquerque, New Mexico, USA, December 1992.
2. I. Shepherd, F. Serre, M. C. Vicente, J. V. Lopez Montero, A. Ball, K. Trambauer, and K. Hocke, "PHEBUS-FPT0 Calculations for the Reference Scenario, Volume 1: The Bundle," EUR 14225 EN, Commission of the European Communities Joint Research Centre, 1992.
3. P. Dumaz, Y. Drossinos, and I. Drosik, "Fission Product Deposition and Revaporization Phenomena in Scenarios of Large Temperature Differences," Presented at the 1993 National Heat Transfer Conference, Atlanta, Georgia, August 8-11, 1993.
4. T. J. Heames, "VICTORIA-92 Analyses of Selected USNRC Fission Product Release Experiments," SAND94-0077, NUREG/CR-6175, Sandia National Laboratories, Albuquerque, NM, 87185, submitted for publication.
5. Hj. Matzke, "Gas Release Mechanisms in UO_2--A Critical Review," *Radiation Effects*, 53:219-242 (1980).
6. N. E. Bixler, T. J. Heames, and D. A. Powers, "VICTORIA Analysis of the PHEBUS FPT-0 Test," Presented at the Scientific Analysis Working Group (SAWG) Meeting, Ispra, Italy, January 21-22, 1992.
7. J. K. Hartwell, D. A. Petti, D. L. Hagrman, S. M. Jensen, and A. W. Cronenberg, "Fission Product Behavior During the PBF Severe Fuel Damage Test 1-1," NUREG/CR-4925, EGG-2462, Idaho National Engineering Laboratory, Idaho Falls, Idaho, USA, May 1987.
8. B. R. Bowsher, R. A. Jenkins, A. L. Nichols, N. A. Rowe, and J. A. Simpson, "Silver-Indium-Cadmium Control Rod Behavior During a Severe Accident," AEEW-R1991 UKAEA Winfrith, United Kingdom, 1986.
9. J. E. Brockmann, "Calibration of the On-Line Aerosol Monitor (OLAM) with Ammonium Chloride and Sodium Chloride Aerosols," SAND93-0046, Sandia National Laboratories, Albuquerque, New Mexico, USA, March 1993.
10. N. E. Bixler, "VICTORIA-92-01 Analyses of CSNI ISP 34 Tests 1 (Open) and 2 (Blind)," SAND93-2301, NUREG/CR-6131, Sandia National Laboratories, Albuquerque, NM, 87185, January, 1994.

DISTRIBUTION:

U. S. Nuclear Regulatory Commission (4)
Office of Nuclear Regulatory Regulation
Attn.: R. Barrett, OWFN
J. H. Flack, NLS324
L. Soffer, NLN324
A. C. Thadani, OWFN 8 E 2
Washington, D.C. 20555

U.S. Nuclear Regulatory Commission (10)
Office of Nuclear Regulatory Research
Attn.: E. S. Beckjord, NLS007
F. Eltawila, NLN344
N. Grossman, NLN344
T. L. King, NLN370
R. Y. Lee, NLN344
R. L. Palla, Jr., OWFN 10 E 4
A. M. Rubin, NLN344
B. W. Sheron, NLN369
T. P. Speis, NLS007
C. G. Tinkler, NLN344
Washington, D.C. 20555

U. S. Nuclear Regulatory Commission
Office of ACRS
Attn.: M. D. Houston, PHIL P-315
Washington, D.C. 20555

U. S. Nuclear Regulatory Commission
Division of Technical Information and Document Control
7920 Norfolk Avenue
Bethesda, MD 20014

U.S. Department of Energy (3)
Albuquerque Operations Office
P.O. Box 5400
Attn.: R. N. Holton
J. A. Morley
J. R. Roeder
Albuquerque, NM 87185

U.S. Department of Energy
Idaho Operations Office
785 DOE Place
Attn.: W. H. Rettig
Idaho Falls, ID 83401-1134

ABB/CE
1000 Prospect Mill Road
CEP 9612-2207
Attn.: R. Schneider
Winsor, CT 06095

Argonne National Laboratory
9700 South Cass Avenue
Attn.: B. Spencer
Argonne, IL 60439

Battelle Columbus Laboratory (2)
505 King Avenue
Attn.: C. Alexander
C. Ventresca
Columbus, OH 43201

Battelle Pacific Northwest Laboratory
Reactor Systems, Fuels & Matls. P8-35
P.O. Box 999
Attn.: F. E. Panisko
Richland, WA 99352

Brookhaven National Laboratory
130 BNL
Attn.: T. Pratt
Upton, NY 11973

Electric Power Research Institute
P.O. Box 10412
3412 Hillview Avenue
Attn.: M. Merilo
Palo Alto, CA 94303

Energy Research
6290 Montrose Rd.
Attn.: M. Khatib-Rahbar
Rockville, MD 20852

Fauske and Associates
16W070 West 83rd St.
Attn.: R. J. Hammersly
Burr Ridge, IL 60521

General Atomics
P. O. Box 85608
Attn.: S. Inamati
San Diego, CA 92138-5608

G. E. Knolls Atomic Power Lab
Box 1072
Attn.: J. Conine, D2-221
Schenectady, NY 12501

Idaho National Engineering Laboratory
EG&G Idaho, Inc.
Willow Creek Building, W-3
P.O. Box 1625
Attn.: C. M. Allison
Idaho Falls, ID 83415

International Technical Services
420 Lexington Avenue
Attn.: P. Abramson
New York, New York 10170

Los Alamos National Laboratory (3)
P.O. Box 1663
Attn.: F. Dearing
L. Trocki
B. Boyack
Los Alamos, NM 87545

Massachusetts Institute of Technology (2)
Nuclear Engineering Dept.
77 Massachusetts Avenue
Attn.: M. Kazimi
N. Todreas
Cambridge, MA 02139

Oak Ridge National Laboratory (7)
P.O. Box Y
Attn.: E. Beahm
T. Kress
R. Lorenz
M. Osborne
B. Patton
R. Taleyarkhan
A. L. Wright
Oak Ridge, TN 37830

PLG Inc.
191 Calle Magdalena
Suite 240
Attn.: D. Buttermer
Encunitas, CA 92024

Rensselaer Polytechnic Institute (2)
Department of Nuclear Engineering
and Engineering Physics
Attn.: R. T. Lahey Jr.
M. Podowski
Troy, NY 12180-3590

Rice University
Department of Chemistry
6100 Main Street
Attn.: J. L. Margrave
Houston, TX 77251

Risk Management Associates
2309 Dietz Farm Road, NW
Attn.: P. Bieniarz
Albuquerque, NM 87107

Stone and Webster
245 Summer Street
Attn.: J. Metcalf, MS 245-2
Boston, MA 02107

University of California, Berkeley (3)
Attn.: L. Brewer
D. Olander
S. Prussin
Berkeley, CA 94720

University of California, Los Angeles
Nuclear Energy Laboratory
405 Hilgaard Avenue
Attn.: I. Catton
Los Angeles, CA 90024

University of Maryland
Nuclear Engineering Department
Attn.: F. Munno
College Park, MD 20742

Westinghouse Bettis Atomic Laboratory
P.O. Box 79
Attn.: J. W. Wolfe
ZAP 34N
West Mifflin, PA 15122-0079

FOREIGN DISTRIBUTION:

AECL CANDU
Sheridan Park Research Community
2251 Speakman Avenue
Attn.: V. J. Nath
Mississauga, Ontario L5K 1B2
CANADA

AECL Research (4)
Chalk River Research Laboratories
Attn.: L. N. Carlucci
D. S. Cox
L. W. Dickson
R. S. Dickson
Chalk River, Ontario KOJ 1JO
CANADA

AECL Research (2)
Whiteshell Laboratories
Attn.: S. R. Mulpuru
L. A. Simpson
Pinawa, Manitoba R0E 1L0
CANADA

AERE Harwell (4)
Didcot
Attn.: R. G. J. Ball
N. E. Beatham
M. A. Mignanelli
A. L. Nichols
Oxfordshire OX11 ORA
UNITED KINGDOM

Cadarache Center for Nuclear Studies (5)
Attn.: B. Andre
P. Dumaz
J. Leveque
A. Meyer-Heine
F. Serre
F-13108 Saint Paul-Lez-Durance Cedex
FRANCE

Consejo de Seguridad Nuckan
SOR Angela de la Cruz No. 3
Attn.: J. Bagues
28056 Madrid
SPAIN

Consijo de Seguridad Nuclear
Justo Dorado 11
Attn.: J. A. Martinez
28040 Madrid
SPAIN

Committee on the Use of Atomic Energy for Peaceful Purposes
69 Shipchenski
Prokhod Blvd.
Attn.: Y. Yanev
1574, Sofia
BULGARIA

Director Research, Science Education CEC
Rue De La Loi 200
Attn.: B. Tolley
1049 Brussels
BELGIUM

Finnish Centre for Radiation and Nuclear Safety
Department of Nuclear Safety
P.O. Box 268
Attn.: R. Pollanen
SF-00101 Helsinki
FINLAND

ENEL - CRTN
Via Monfalcone 15
Attn.: E. Borioli
20132 Milan
ITALY

E. T. S. Ingenieros Industriales
Jost Gutierrez Abascal, 2
Attn.: A. Alonso
28006 Madrid
SPAIN

Hungarian Atomic Energy Commission
H-1374 Budapest, P.O. Box 565
Attn.: S. Elo
Budapest
HUNGARY

Institut de Protection et de Surete Nucleaire
CEN/FAR - B. P. No. 6
F-92265
Fontenay-aux-Roses
Attn.:M. LiVolant
Cedex
FRANCE

Institute of Nuclear Energy Research
P.O. Box 3
Attn.: Sen-I Chang
Lung-Tan
TAIWAN 325

Japan Atomic Energy Research Institute (2)
Tokai-mura
Naku-gun
Attn.: Y. Maruyama
J. Sugimoto
Ibaraki-ken, 319-11
JAPAN

JRC Ispra Establishment (6)
Thermodynamics and Radiation Physics
Attn.: J. Capitao
P. Fasoli-Stella
E. Hontanon
A. V. Jones
I. Shepherd
Y. Drossinos
1-201020 Ispra (Varese)
ITALY

Jozef Stefan Institute
Jamova 39
Attn.: B. Mavko
61111 Ljubljana
SLOVENIA

Kernforschungszentrum Karlsruhe (2)
P.O. Box 3640
Attn.: B. Kuczera
P. Hofmann
75 Karlsruhe
GERMANY

Korea Advanced Energy Research Institute
P.O. Box 7
Daeduk-Danji
Attn.: Hee-Dong Kim
Taejeon 305-353
KOREA

Netherlands Energy Research Foundation (5)
P.O. Box 1
Attn.: A. S. Booij
E. Cordfunke
M. E. Huntelaar
R. Konings
P. Stoop
1755 ZG Petten (NH)
THE NETHERLANDS

Nuclear Power Engineering Center
Fujitakanko Building
17-1, 3-Chrome, Toranomon, Minato-Ku
Attn.: Kenji Takumi
Tokyo, 105
JAPAN

Nuclear Electric (3)
Berkeley Nuclear Laboratory, Berkeley
Attn.: C. Chapman
J. Eccles
J. Gwyther
Gloucestershire GL13 9PB
UNITED KINGDOM

Nucleare e della Protezione Sanitaria (DISP)
Ente Nazionnle Energie Alternative (ENEA)
Viale Regina Margherita, 125
Casella Postale M. 2358
Attn.: G. Petrangeli
I-00100 Roma A. D.
ITALY

Nuclear Regulatory Authority
Slovak Republic
Bajkalska 27
Attn.: J. Misak
827 21 Bratislave
SLOVAK REPUBLIC

Nuclear Research Institute
Attn.: A. Rydl
250 68 Rez
CZECH REPUBLIC

Nuclear Safety Institute (3)
Russian Research Center KI
1 Kurchatov Square
Attn.: V. Asmolov
E. G. Basanski
V. Demin
123182 Moscow
RUSSIA

N. V. Kema
P.O. Box 9035
Attn.: P. Kloeg
6800 ET Arnhem
THE NETHERLANDS

Ontario Hydro (2)
700 University Avenue
Attn.: F. C. Iglesias
O. Akalin
Toronto, Ontario M5G 1X6
CANADA

Paul Scherrer Institute
Attn.: P. Hosemann
CH-5232 Villigen, PSI
SWITZERLAND

Polytechnical University of Madrid
Nuclear Engineering Department
Jose Gutierrez Abascal, 2
Attn.: A. Alonzo-Santos
28006 Madrid
SPAIN

Power Reactor Nuclear Fuel Development Corporation
(PNC)
9-13, 1-Chome
Akasaka
Attn.: A. Watanabe
Minato-Ku, Tokyo
JAPAN

Reactor Centrum Nederland
Attn.: K. J. Brinkman
1755 ZG Petten
THE NETHERLANDS

Research Centre Rossendorf Inc.
Forschungszentrum Rossendorf
Postfach 19
Attn.: Dr. H. Funke
DO-8051 Dresden
GERMANY

Royal Institute of Technology
Department of Nuclear Reactor Engineering
Attn.: K. M. Becker
S-10044 Stockholm
SWEDEN

State Office for Nuclear Safety
Slezska 9
Attn.: J. Stuller
120 00 Prague 2
CZECH REPUBLIC

Russian Accademy of Sciences
Nuclear Safety Institute
52, B. Tulskaya
Attn.: L. Bolshov
113191 Moscow
RUSSIA

Statens Karnkraftinspektion
P.O. Box 27106
Attn.: W. Frid
S-10252 Stockholm
SWEDEN

Swiss Federal Nuclear Safety Inspectorate
Attn.: S. Chakraborty
Ch-5232 Villigen - HSK
SWITZERLAND

UKAEA, Risley Nuclear Laboratories (4)
Risley, Warrington
Attn.: A. T. D. Butland
I. H. Dunbar
G. F. Holford
C. D. Wheatley
Cheshire WA3 4NE
UNITED KINGDOM

UKAEA, Winfrith Technology Centre (9)
Attn.: E. J. Allen
B. R. Bowsher
T. J. Haste
N. A. Johns
S. R. Kinnersly
J. N. Lillington
A. Mason
A. J. Smethurst
D. A. Williams
Dorchester Dorset DT2 8DH
UNITED KINGDOM

University of Stuttgart (2)
IKE
Pfaffenwaldring 31
Attn.: U. Bieder
N. Kourti
D-7000 Stuttgart 80
GERMANY

VATESI
Gediminis Prospect 36
Attn.: P Vaisnys
Vilnius
LITHUANIA

SANDIA DISTRIBUTION: (60)

MS0100 Document Processing for DOE/OSTI, 7613-2 (10)
MS0415 A. J. Grimley, 4111
MS0619 Technical Publications, 7151
MS0736 N. R. Ortiz, 6400
MS0739 K. Washington, 6429
MS0742 J. E. Kelly, 6414
MS0744 W. A. von Riesemann, 6403
MS0744 D. A. Powers, 6404
MS0745 S. L. Thompson, 6418
MS0745 R. C. Smith, 6418
MS0745 T. J. Tautges, 6418
MS0827 J. S. Rottler, 1511
MS0834 A. C. Ratzel, 1512
MS0835 R. D. Skocypec, 1513
MS0899 Technical Library, 7141 (5)
MS1137 M. D. Allen, 6422
MS1137 N. E. Bixler, 6422 (20)
MS1137 J. E. Brockmann, 6422
MS1137 R. M. Elrick, 6422
MS1137 C. M. Erickson, 6422
MS1137 T. J. Heames, 6422
MS1139 K. O. Reil, 6423
MS1139 R. C. Schmidt, 6423
MS1144 J. V. Walker, 6501
MS1145 S. A. Wright, 6514
MS1151 K. E. Boyack, 6515
MS1320 F. Gelbard, 6119
MS9211 Central Technical Files, 8523-2

DATE
FILMED
6/16/94

END